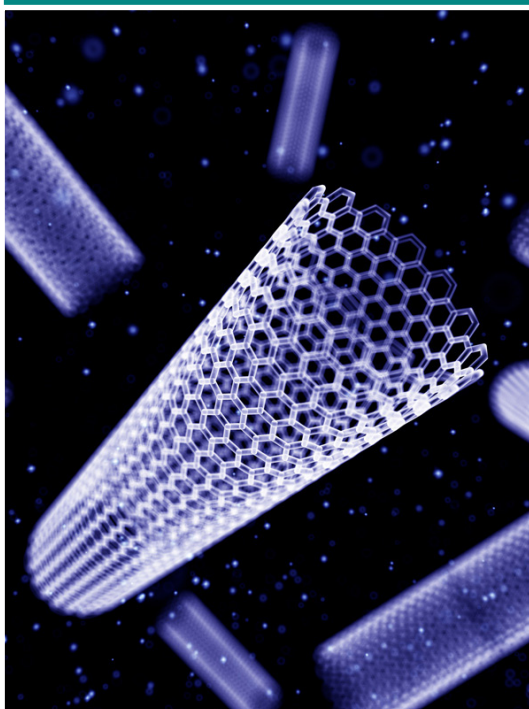


Conducting Polymer Nanocomposites for Supercapacitors

Subhash B. Kondawar



Conducting Polymer Nanocomposites for Supercapacitors

Subhash B. Kondawar



A Smithers Group Company

Shawbury, Shrewsbury, Shropshire, SY4 4NR, United Kingdom

Telephone: +44 (0)1939 250383 Fax: +44 (0)1939 251118

<http://www.polymer-books.com>

First Published in 2015 by

Smithers Rapra Technology Ltd

Shawbury, Shrewsbury, Shropshire, SY4 4NR, UK

©Smithers Information Ltd., 2015

All rights reserved. Except as permitted under current legislation no part of this publication may be photocopied, reproduced or distributed in any form or by any means or stored in a database or retrieval system, without the prior permission from the copyright holder.

A catalogue record for this book is available from the British Library.

Every effort has been made to contact copyright holders of any material reproduced within the text and the authors and publishers apologise if any have been overlooked.

ISBN: 978-191024-239-1 (Hardback)
978-191024-240-7 (ebook)

Typeset by Argil Services

Preface

During the past decade, nanotechnology has become an active field of research because of its tremendous potential for various applications. New and surprising properties often emerge if the size of many established, well-studied materials is reduced to the nanoscale or improved radically.

Conducting polymers are relatively new materials, studied extensively since discovery of the first conducting polymer (polyacetylene) in 1977. Conducting polymers are unique photonic and electronic functional materials owing to their high π -conjugated length, unusual conducting mechanism, and reversible redox doping/dedoping process. Typical examples of electronically conducting polymers are polyaniline, polypyrrole, polythiophene, and their derivatives. Conducting polymers and their composites have various promising applications: transistors, sensors, memories, actuators/artificial muscles, supercapacitors, and lithium ion batteries.

Numerous books are available on conducting polymers and composites. These books have their specialisations and limitations because the research scope of conducting polymers is so vast that it is difficult for an individual to have expertise in all fields. This book is intended to serve as a guide to understand the basics of conducting polymer technology as nanostructuring of conducting polymers and their composites emerges as a new field of research and development directed to the creation of new 'smart' materials for supercapacitors.

The book is divided into five chapters. Concepts of supercapacitors are explained in a straightforward and concise manner. The book

Conducting Polymer Nanocomposites for Supercapacitors

has a chemical-engineering orientation, so professionals working in polymer science may find this book suitable for their applied field of research. The book will provide such professionals an opportunity to learn about conducting polymers and nanocomposites, as well as the production and processing technology for supercapacitors. This book was written while referring to numerous journals and books to detail the most recent developments in supercapacitor electrodes based on conducting polymers.

Attention is focused mainly on the preparation of conducting polymer-based binary and ternary nanocomposites and their electrochemical performances for supercapacitor application. Nevertheless, this book will be a valuable reference for scientists, engineers, students and general readers interested in the investigation and exploitation of a fascinating new class of conducting polymer nanocomposites.

It is a great pleasure for me to thank my teachers, colleagues, friends, students, collaborators and family members without whose support in writing this book would not have been possible. Over the last 15 years, I have enjoyed researching conducting polymer nanocomposites with my collaborators and research students. I have worked in this fascinating field of polymer nanotechnology with my ex-research students, doctors Shubhangi Bompilwar, Vandana Khati, Arti Nandapure, Bharti Nandapure, Ajay Dahegaonkar, Shikha Agrawal, Milind Deshpande, Suyog Pethe and Shrikant Nimkar. The enthusiastic help I have received from my current research students, Ms. Bhavna Meshram, Mr. Ashish Mahajan, Ms. Pallavi Patil, Ms. Ritu Mahore, Ms. Hemlata Sharma, Mrs. Rajshri Anwane, Ms. Dipti Jamkar, Ms. Priyanka Virutkar, Ms. Monali Bhute, Mr. Anand More, Ms. Yogita Mahant, Ms. Manjusha Dandekar, Ms. Sangita Itankar, Ms. Prerna Modak, and many research project students enabled me to complete this book. Their frank opinions (and particularly their help in drawing) are gratefully acknowledged. I also thank the faculty and administrative staff of the Physics Department, Rashtrasant Tukadoji Maharaj Nagpur University (Nagpur, India) for their continuous help. I must also mention one of my collaborators, Dr. Devendra Burghate (Principal Shri Shivaji Science College, Nagpur) and my

Preface

research student, Ms. Ritu Mahore, who have been researching supercapacitors continuously for the last 5 years.

I also take this opportunity to thank my family for their constant moral support, especially while this book was being written.

Subhash B. Kondawar

Nagpur, India

September 2015

Conducting Polymer Nanocomposites for Supercapacitors

C contents

1	Supercapacitors	1
1.1	Introduction	1
1.2	Classification of Supercapacitors	9
1.2.1	Electrochemical Double-layer Capacitors	10
1.2.2	Pseudocapacitors.....	12
1.2.3	Hybrid Capacitors	12
1.2.3.1	Composite.....	13
1.2.3.2	Asymmetric.....	14
1.2.3.3	Battery-type	14
1.3	Challenges for Supercapacitors	15
1.4	Applications of Supercapacitors.....	16
1.4.1	Consumer Electronics	18
1.4.2	Buffer Power	18
1.4.3	Voltage Stabiliser.....	19
1.4.4	Energy Harvesting.....	19
1.4.5	Incorporation into Batteries	19
1.4.6	Street Lights	20
1.4.7	Military.....	20
1.4.8	Energy Recovery	21
1.4.9	Railways	21
1.4.10	Light-rails and Trams.....	21
1.4.11	Buses.....	23
1.4.12	Gondolas	24

Conducting Polymer Nanocomposites for Supercapacitors

1.4.13	Advantages and Disadvantages of Supercapacitors	24
2	Electrochemical Characterisations	29
2.1	Introduction	29
2.2	Equipment: Potentiostat	36
2.3	Cyclic Voltammetry	39
2.4	Galvanostatic Charge–Discharge	44
2.5	Electrochemical Impedance Spectroscopy	44
3	Conducting Polymers	51
3.1	Introduction	51
3.2	Doping of Polymers	53
3.3	Conduction Mechanism.....	55
3.4	Charge Transport	60
3.5	Nanostructure of Conductive Polymers	64
4	Nanocomposites.....	73
4.1	Introduction	73
4.2	Conducting Polymer Nanocomposites	74
4.3	Conducting Polymer Binary Nanocomposites for Supercapacitors	77
4.3.1	Particulate-reinforced Nanocomposites.....	79
4.3.2	Flake-reinforced Nanocomposites	87
4.3.3	Fibre-reinforced Nanocomposites	94
5	Ternary Nanocomposites for Supercapacitors.....	109
5.1	Metal Oxide-based Ternary Nanocomposites	109
5.1.1	Manganese Dioxide/Carbon Nanotube/ Polyaniline and Manganese Dioxide/ Carbon Nanotube/Polypyrrole Nanocomposites	110

5.1.2	Titanium Dioxide/Graphene/Polyaniline Ternary Nanocomposites	115
5.2	Ferrite-based Ternary Nanocomposites	118
5.2.1	Nickel ferrite/Graphene/Polyaniline Nanocomposites	119
5.2.2	Manganese Ferrite/Graphene/Polyaniline Nanocomposites	123
5.3	Graphene/Carbon Nanotubes/Polyaniline Ternary Nanocomposites	126
5.4	Polyaniline/Polypyrrole/Carbon Nanotubes Ternary Nanocomposites	130
	Abbreviations.....	143
	Index.....	147

Conducting Polymer Nanocomposites for Supercapacitors

1 Supercapacitors

1.1 Introduction

In response to the changing global landscape, energy has become a primary focus of the scientific community and major world powers. Limited energy supplies and environmental problems have forced researchers to search for cleaner energy-storage devices. Efforts have been made to develop flexible, lightweight and environmentally friendly energy-storage devices to meet urgent needs for sustainable and renewable power sources in the electronic industry. There has been great interest in developing and refining more efficient energy-storage devices.

One such device, the supercapacitor, has emerged with the potential to facilitate major advances in energy-storage. Supercapacitors have drawn intensive attention owing to their virtues of high power density, long life-cycle, short charging time, and safe operation for promising applications to resolve such problems [1].

Supercapacitors are designed to bridge the gap between batteries and capacitors to form fast-charging energy-storage devices of intermediate specific energy. Supercapacitors are important devices in energy-storage and conversion systems, and are used in electric vehicles, uninterruptible power supplies (UPS), as well as in memory protection of computer electronics and cellular devices.

A supercapacitor differs from a conventional capacitor in that it has a very high capacitance. A capacitor stores energy by means of a static charge as opposed to an electrochemical reaction. Applying a voltage differential on the positive and negative plates charges the capacitor.

Conducting Polymer Nanocomposites for Supercapacitors

Capacitors can be divided into three family types. The most basic type is the electrostatic capacitor, with a dry separator. This capacitor has a very low capacitance and is used to filter signals and tune radio frequencies (RF). The size ranges from a few picofarads to low microfarads. The next member is the electrolytic capacitor, which is used for the filtering, buffering and coupling of power. Rated in microfarads, this capacitor has several thousand times the storage capacity of the electrostatic capacitor, and uses a moist separator. The final type is the supercapacitor, rated in farads, which is thousands of times higher than the electrolytic capacitor.

A supercapacitor is ideal for energy-storage that undergoes frequent charge and discharge cycles at high current and short duration. In contrast to conventional capacitors, supercapacitors possess much higher energy density and do not have dielectrics, but instead use a phenomenon referred typically to as the 'electric double-layer'. In the double-layer, the effective thickness of the 'dielectric' is exceedingly thin and, because of the porous nature of carbon, the surface area is extremely high, which translates as very high capacitance. In general, if two different phases come into contact, positive and negative charges are set in array at the boundary. At every interface, an array of charged particles and induced charges are present. This array is known as the electric double-layer. The high capacitance of an electrochemical double-layer capacitor (EDLC) arises from the charge stored at the interface by the changing electric field between anodes and cathodes.

Conventional capacitors consist of two conducting electrodes separated by an insulating dielectric material. If a voltage is applied to a capacitor, opposite charges accumulate on the surfaces of each electrode. The charges are kept separate by the dielectric, thereby producing an electric field that allows the capacitor to store energy (Figure 1.1).

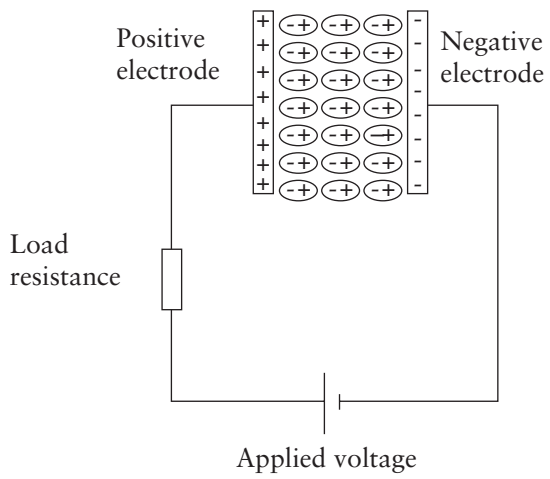


Figure 1.1 Conventional capacitor (schematic)

Capacitance C is defined as the ratio of stored (positive) charge Q to the applied voltage V :

$$C = \frac{Q}{V} \tag{1.1}$$

For a conventional capacitor, C is directly proportional to the surface area A of each electrode and inversely proportional to the distance D between the electrodes:

$$C = \epsilon_0 \epsilon_r \frac{A}{D} \tag{1.2}$$

The product of the first two factors on the right hand side of the Equation 1.2 is a constant of proportionality wherein ϵ_0 is the dielectric constant (or ‘permittivity’) of free space and ϵ_r is the dielectric constant of the insulating material between the electrodes.

The two primary attributes of a capacitor are its energy density and power density. For either measure, the density can be calculated as a quantity per unit mass or per unit volume. The energy E stored in a capacitor is directly proportional to its capacitance:

$$E = \frac{1}{2}CV^2 \quad (1.3)$$

In general, the power ‘P’ is the energy expended per unit time. However, to determine P for a capacitor, one must consider that capacitors are, in general, represented as a circuit in series with an external ‘load’ resistance ‘R’ (Figure 1.1).

The internal components of the capacitor (e.g., current collectors, electrodes, and dielectric material) also contribute to the resistance, which is measured in aggregate by a quantity known as the ‘equivalent series resistance’ (ESR). The voltage during discharge is determined by these resistances. If measured at matched impedance ($R = \text{ESR}$), the maximum power P_{\max} for a capacitor is given by:

$$P_{\max} = \frac{V^2}{4 \times \text{ESR}} \quad (1.4)$$

This relationship shows how the ESR can limit the maximum power of a capacitor.

Conventional capacitors have relatively high power densities, but relatively low energy densities when compared with electrochemical batteries and fuel cells. That is, a battery can store more total energy than a capacitor, but it cannot deliver it very quickly, which means its power density is low. Capacitors, on the other hand, store relatively less energy per unit mass or volume, but the electrical energy they store can be discharged rapidly to produce a lot of power, so their power density is usually high. Supercapacitors are governed by the same basic principles as conventional capacitors. However, they incorporate electrodes with much higher surface areas A and much thinner dielectrics that decrease the distance D between the electrodes.

Thus, from **Equations 1.2** and **1.3**, this phenomenon leads to an increase in capacitance and energy.

Furthermore, by maintaining the low ESR characteristic of conventional capacitors, supercapacitors can also achieve comparable power densities. In addition, supercapacitors have several advantages over electrochemical batteries and fuel cells: higher power density, shorter charging times, longer life-cycle and longer shelf-life [2]. **Figure 1.2** provides a schematic diagram of a supercapacitor, illustrating some of the physical features described above.

Supercapacitors do not contain a dielectric block. The electrical double-layers are formed in the electrolyte surrounding the particles, leading to effective separation of charge on the nanometre scale. The area of the electrical double-layer is dependent upon the surface area of the particles. High capacitances can be achieved due to the size of the electrode material particles in supercapacitor packages. In an electrical double-layer, each layer by itself is quite conductive, but the physics at the interface (where the layers are effectively in contact) means that no significant current can flow between the layers. However, the double-layer can withstand only a low voltage. The capacitance of these devices is proportional to the active electrode area, so increasing the surface area of the electrodes will increase the capacitance, thereby increasing the amount of energy that can be stored. The EDLC is ideal for energy-storage because it undergoes frequent charge and discharge cycles at high current and short duration.

A farad is a unit of capacitance named after the English physicist Michael Faraday. One farad stores one coulomb of electrical charge when 1 V is applied. The separator provides the electronic insulation between the electrode of opposite polarisation, and supports ionic conduction from one electrode to the other. The conductivity through the separator is proportional to its porosity (40–70%) and is represented by:

$$\sigma = \sigma_0 p^\alpha \quad (1.5)$$

Conducting Polymer Nanocomposites for Supercapacitors

Where σ_0 is the electrolyte conductance, p is the porosity and α is a power factor with $1.5 \leq \alpha \leq 2$.

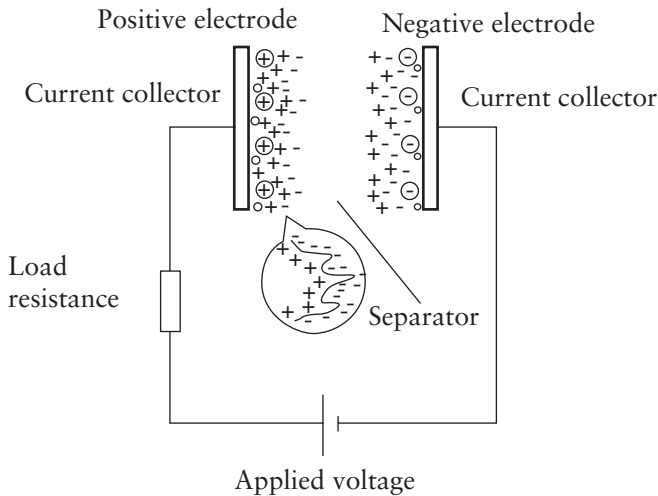


Figure 1.2 Supercapacitor (schematic)

Separator materials used in supercapacitors are based on cellulose or porous polypropylene. Electrode materials for supercapacitors are carbon [charcoal, aerogel, fibre, carbon nanotubes (CNT), graphene], metal oxide (rutenium oxide, manganese oxide, titanium dioxide) and conducting polymers (CP) [polyaniline, polypyrrole (Ppy), polythiophene].

The improvement in performance for a supercapacitor is shown in **Figure 1.3**. A graph between energy density and power density is termed a 'Ragone plot.' This type of graph presents the power densities of various energy-storage devices (measured along the vertical axis) *versus* their energy densities (measured along the horizontal axis). **Figure 1.3** reveals that supercapacitors occupy a

region between conventional capacitors and batteries. Despite having greater capacitances than conventional capacitors, supercapacitors have yet to match the energy densities of mid- to high-end batteries and fuel cells. Thus, much of the literature surveyed for this overview focuses on the development of improved types or classes of supercapacitors to make their energy densities more comparable with those of batteries.

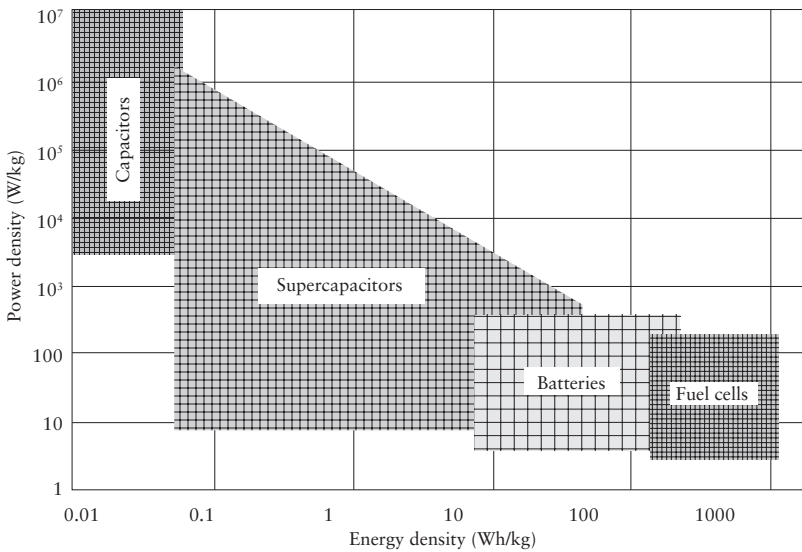


Figure 1.3 Ragone plot of energy devices

Compared with lithium-ion batteries, supercapacitors also exhibit higher specific power. Supercapacitors store electrical charge only at the electrode surface, rather than within the entire electrode, so they tend to have lower energy densities compared with batteries. The charge–discharge reaction is not limited by ionic conduction into the electrode bulk, therefore supercapacitors can be run at

high rates and provide high specific power. In addition, most supercapacitor materials do not participate in redox reactions, so there is little deterioration in the electrode, which has good cycle characteristics, and maintenance is unnecessary. Due to such differences, the corresponding electrochemical behaviour is also different. Supercapacitors have several advantages compared with batteries: high power density; short charge discharge time; high charge–discharge efficiency; long life-cycle; wide range of operating temperatures; environmental friendliness; safety [3–5].

Supercapacitors have the highest available capacitance values per unit volume and the greatest energy density of all capacitors. They can have capacitance values 10,000-times those of electrolytic capacitors; $\leq 12,000$ F at working voltages of 1.2 V. Supercapacitors bridge the gap between capacitors and rechargeable batteries. In terms of specific energy, as well as in terms of specific power, this gap covers several orders of magnitude. However, batteries still have about ten-times the capacity of supercapacitors [6]. Existing supercapacitors have energy densities that are $\approx 10\%$ of a conventional battery, but their power density is, in general, 10–100-times as great. This feature makes the charge-and-discharge cycles of supercapacitors much faster than those of batteries. In addition, supercapacitors can tolerate many more charge-and-discharge cycles than batteries. In these electrochemical capacitors, the electrolyte is the conductive connection between the two active electrodes. This setup distinguishes them from electrolytic capacitors, in which the electrolyte is the cathode and thus forms the second electrode. Supercapacitors are polarised and must operate with the correct polarity. Polarity is controlled by design with asymmetric electrodes or, for symmetric electrodes, by a potential applied during manufacture.

Supercapacitors support a broad spectrum of applications for power and energy requirements. In a conventional capacitor, energy is stored by moving charge carriers (typically electrons) from one metal plate to another. This charge separation creates a potential between the two plates that can be harnessed in an external circuit. The total energy-stored in this fashion increases with the amount of charge

stored and the potential between the plates. The amount of charge stored per unit voltage is essentially a function of the size, distance and material properties of the plates and the material between the plates (the dielectric), whereas the potential between the plates is limited by the breakdown in the field strength of the dielectric. The dielectric controls the voltage of the capacitor. Optimising the material leads to a higher energy density for a given size.

1.2 Classification of Supercapacitors

Supercapacitors are divided into three families (Figure 1.4) based on electrode design.

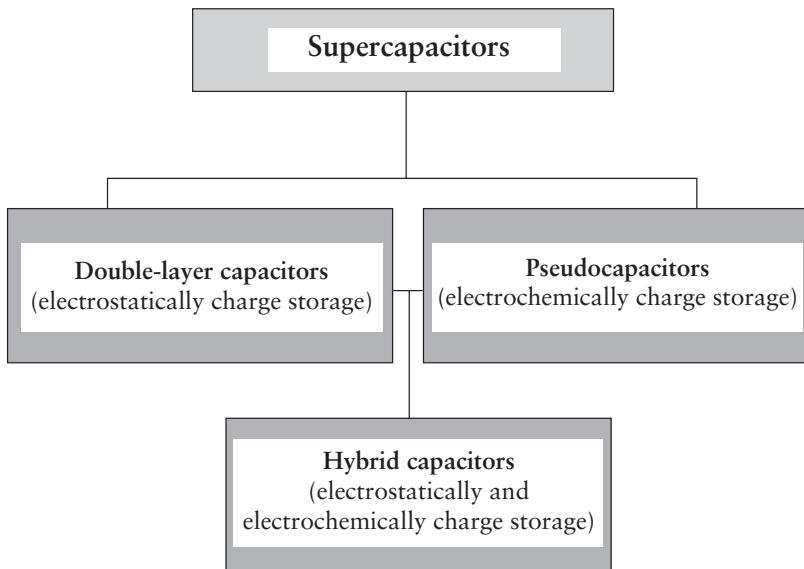


Figure 1.4 Classification of supercapacitors

- Double-layer capacitors – with carbon electrodes or derivatives with much higher static double-layer capacitance than ‘Faradaic pseudocapacitance’.
- Pseudocapacitors – with electrodes made of metal oxides or CP with much higher Faradaic pseudocapacitance than static double-layer capacitance.
- Hybrid capacitors – capacitors with special electrodes that exhibit significant double-layer capacitance and pseudocapacitance (e.g., lithium-ion capacitors).

1.2.1 Electrochemical Double-layer Capacitors

EDLC are constructed from two carbon-based electrodes, an electrolyte, and a separator (**Figure 1.2**). Like conventional capacitors, EDLC store charge electrostatically, or non-Faradaically, and there is no transfer of charge between electrode and electrolyte. EDLC utilise an electrochemical double-layer (EDL) of charge to store energy. As voltage is applied, charge accumulates on the electrode surfaces. Following the natural attraction of unlike charges, ions in the electrolyte solution diffuse across the separator into the pores of the electrode of opposite charge. However, the electrodes are engineered to prevent recombination of the ions. Thus, a double-layer of charge is produced at each electrode. These double-layers, coupled with an increase in surface area and a decrease in the distance between electrodes, allow EDLC to achieve higher energy densities than those observed in conventional capacitors. Because there is no transfer of charge between electrolyte and electrode, there are no changes in chemicals or composition associated with non-Faradaic processes. For this reason, charge storage in EDLC is highly reversible, which allows them to achieve very high cycling stabilities.

EDLC do not have a conventional dielectric. Instead of two plates separated by an intervening insulator, these capacitors use ‘virtual’ plates made of two layers of the same substrate. Their electrochemical

properties (electric double-layer) result in effective separation of charge despite the vanishingly thin (on the order of nanometres) physical separation of the layers. The lack of need for a bulky layer of dielectric and the porosity of the material used permits the packing of plates with much larger surface area into a given volume, resulting in high capacitances in small packages.

In an EDL, each layer is quite conductive, but the physics at the interface between them means that no significant current can flow between the layers. The double-layer can withstand only a low voltage, so higher voltages are achieved by matched series-connected individual EDLC, much like series-connected cells in higher-voltage batteries. EDLC have much higher power density than batteries. Power density combines the energy density with the speed at which the energy can be delivered to the load. Batteries (which are based on the movement of charge carriers in a liquid electrolyte) have relatively slow charge and discharge times. Capacitors can be charged or discharged at a rate that is typically limited by the heat tolerance of the electrodes. Existing EDLC have an energy density one-tenth that of a conventional battery but their power density is (in general) 10–100-times as great. This phenomenon makes them most suited to an ‘intermediary’ role between electrochemical batteries and electrostatic capacitors whereby neither sustained energy release nor immediate power demands dominate.

In general, EDLC operate with stable performance characteristics many charge–discharge cycles ($\leq 10^6$ cycles). On the other hand, electrochemical batteries are, in general, limited to $\approx 10^3$ cycles. Because of their cycling stability, EDLC are well suited for applications that involve non-user serviceable locations, such as deep-sea or mountain environments. The performance characteristics of an EDLC can be adjusted by changing the nature of its electrolyte. An EDLC can utilise an aqueous or organic electrolyte. Aqueous electrolytes (e.g., sulfuric acid, potassium hydroxide) in general have lower ESR and lower requirements for minimum pore size compared with organic electrolytes (e.g., acetonitrile). However, aqueous electrolytes also have lower breakdown voltages. Therefore, in choosing between

an aqueous or organic electrolyte, one must consider the trade-offs between capacitance, ESR, and voltage [7]. Because of these trade-offs, the choice of electrolyte is often dependent upon the intended application of the supercapacitor. The nature of the electrolyte is of great importance in supercapacitor design, but the subclasses of EDLC are distinguished primarily by the form of carbon they use as an electrode material. Carbon electrode materials, in general, have a higher surface area, lower cost, and more established fabrication methods than other materials (e.g., CP, metal oxides). Different forms of carbon materials that can be used to store charge in EDLC electrodes are activated carbons, carbon aerogels and CNT.

1.2.2 Pseudocapacitors

In contrast to EDLC, which store charge electrostatically, pseudocapacitors store charge Faradaically through the transfer of charge between electrode and electrolyte. This charge-storage is accomplished through electrosorption, reduction–oxidation reactions, and intercalation processes [8–9]. These Faradaic processes can allow pseudocapacitors to achieve greater capacitances and energy densities than those achieved by EDLC [10]. Two electrode materials are used to store charge in pseudocapacitors: CP and metal oxides. Nanostructured metal oxides, which exhibit pseudocapacitance behaviour, are considered to be excellent materials for achieving high specific capacitance (SC).

1.2.3 Hybrid Capacitors

Hybrid capacitors are used to exploit the relative advantages and mitigate the relative disadvantages of EDLC and pseudocapacitors to realise better performance characteristics. Utilising Faradaic and non-Faradaic processes to store charge, hybrid capacitors have achieved energy and power densities greater than those seen for EDLC without the sacrifices in cycling stability and affordability that have limited the success of pseudocapacitors. Research has focused on three types

of hybrid capacitors distinguished by their electrode configuration: composite, asymmetric and battery-type.

1.2.3.1 Composite

Composite electrodes integrate carbon-based materials with CP or metal-oxide materials and incorporate physical and chemical mechanisms of charge storage together in a single electrode. Carbon-based materials facilitate a capacitive double-layer of charge and also provide a high-surface-area backbone that increases the contact between deposited pseudocapacitive materials and electrolyte. Pseudocapacitive materials can further increase the capacitance of the composite electrode through Faradaic reactions [11]. Composite electrodes constructed from CNT and Ppy (a CP) have been particularly successful. Several experiments have demonstrated that this electrode can achieve higher capacitances than a pure CNT or pure Ppy polymer-based electrode [12]. This is attributed to the accessibility of the entangled mat structure, which allows a uniform coating of Ppy and a three-dimensional (3D) distribution of charge. Moreover, the structural integrity of the entangled mat has been shown to limit the mechanical stress caused by the insertion and removal of ions in the deposited Ppy. Therefore, unlike CP, these composites can achieve a cycling stability comparable with that of EDLC.

Composite electrodes for hybrid-type supercapacitors are constructed from carbon-based material with incorporated or deposited pseudocapacitive-active materials such as metal oxides and CP. As of 2013, most research for supercapacitors has explored composite electrodes. CNT provide a backbone for homogeneous distribution of metal oxide or electrical CP, producing good pseudocapacitance and good double-layer capacitance. These electrodes achieve higher capacitances than those made from pure carbon, pure metal oxide or polymer-based electrodes. This feature is attributed to the accessibility of the tangled mat structure of nanotubes, which allows a uniform coating of pseudocapacitive materials and 3D distribution of charge.

1.2.3.2 Asymmetric

Asymmetric hybrids combine Faradaic and non-Faradaic processes by coupling an EDLC electrode with a pseudocapacitor electrode. In particular, coupling of an activated carbon-negative electrode with a CP-positive electrode has received a great deal of attention [13–14]. As discussed in Section 1.2.1, lack of an efficient, negatively charged CP material has limited the success of CP pseudocapacitors. Implementation of a negatively charged, activated carbon electrode attempts to circumvent this problem. CP electrodes, in general, have higher capacitances and lower resistances than those seen for activated carbon electrodes, but they also have lower maximum voltages and lower cycling stability. Asymmetric hybrid capacitors that couple these two electrodes mitigate the extent of this trade-off to achieve higher energy and power densities than comparable EDLC. Also, they have better cycling stability than comparable pseudocapacitors.

1.2.3.3 Battery-type

Like asymmetric hybrids, battery-type hybrids couple two different electrodes. However, battery-type hybrids are unique in coupling a supercapacitor electrode with a battery electrode. This specialised configuration reflects the demand for higher-energy supercapacitors and higher-power batteries, combining the energy characteristics of batteries with the power, life-cycle, and recharging times of supercapacitors. Research has focused primarily on using nickel hydroxide, lead dioxide, and lithium titanium oxide as one electrode and activated carbon as the other [15–19]. There are less experimental data on battery-type hybrids than for other types of supercapacitors, but available data suggest that these hybrids can bridge the gap between supercapacitors and batteries. Despite promising results, the general consensus is that more research will be necessary to determine the full potential of battery-type hybrids.

1.3 Challenges for Supercapacitors

Supercapacitors have many advantages over batteries and fuel cells. Nevertheless, they also face challenges at the current stage of technology: (i) low energy density; (ii) high cost; (iii) high self-discharging rate; and (iv) industrial standards required for commercialisation. This type of supercapacitor is available commercially, but establishment of some general industrial standards (e.g., performance, electrode structure, thickness of the electrode layer, porosity) is necessary. Due to the variety of applications and limited number of commercial products, searching out generally available industrial standards has not been possible. Therefore, putting effort on establishment of standards for different applications is necessary.

In some ways, similar to the challenges faced by portable electronic devices, hybrid electric vehicles (HEV) require a high-power energy source. Oversized battery systems have been used to meet power demands, but difficulties arise in managing the heat generated from exothermic reactions and resistances, as well as having to adopt a predictable low life-cycle. By reducing the size of the battery and/or the major energy supplier, supercapacitors can also help to efficiently meet the irregular stop-and-go power requirements of HEV in urban settings. Serving to capture the break energy from these intervals, their fast recharge periods and high cycle efficiency (>95%) are well-suited to development of the fuel efficiency of HEV. A review [20] supported supercapacitor use in HEV by comparing current high-power lithium-ion batteries and supercapacitors to estimate the relevant energies captured and available for immediate use. Contrary to the conventional perspective, in a charge time of ≤ 10 s, supercapacitors possess roughly twice the energy density compared with high-power batteries, and do not need a heat-management system with high rate cycling. Other transport systems that stand to gain in energy efficiency through supercapacitor incorporation include buses, trams, and trains.

The valuable contributions made by supercapacitors are becoming

increasingly apparent as societal and technological trends continue to focus on employment of alternative and ecologically mindful energy generation and storage systems. In particular, with industrial and governmental regulations continuing to press for ‘green energy’ and ‘green product’ solutions, supercapacitors have an advantage over batteries with respect to a longer lifespan and material recyclability. Nevertheless, challenges related to their low energy density and high costs deter consumer investment and inhibit their market strength.

Two concurrent strategies to circumvent this problem have focused on developing ionic liquid electrolytes as safe, stable options with a broad operating voltage (>3 V) and development of electrode materials to enhance capacitive charge-storage. The latter, in particular, has elicited developments ranging from ‘sub-nanopores’ for modelling to the enhanced performances resulting from nanocomposite electrodes and hybrid system designs [21]. Research efforts to optimise hybrid materials, EDLC, and supercapacitance systems are expected to enable combination of rapid capacitive charging with high-energy density. Research into combination of carbon with redox materials (metal oxides) to develop and increase capacitive ability appears beneficial. However, understanding the main effects of pore-size distribution with stability and effective use of materials remain necessary. Also, production methods remain equally important for any practical purpose if a simple, direct procedure is required for commercialisation.

1.4 Applications of Supercapacitors

Supercapacitors occupy a position between conventional batteries and conventional capacitors. Typically, they are used in applications in which batteries have shortfalls in high power and life, and if conventional capacitors cannot be used because of a lack of energy. EDLC offer high-power density along with adequate energy density for most short-term high-power applications. Many users compare EDLC with other energy-storage devices, including batteries and conventional capacitor technology.

Each product has its own advantages and disadvantages compared with other technologies. Several applications for which supercapacitors are currently employed make use of their high pulse power to supply energy in very short time periods (milliseconds to seconds). Serving as a power source against power disturbances or low energy for extended periods of time, they have been incorporated into products ranging from cameras, computers, and mobile phones to energy-generator systems used to avoid costly system shutdowns and production losses. The benefits to support their use over secondary-batteries are validated by faster charge times and a considerably longer life-cycle that endures a negligible loss in performance with time.

Isolated use of supercapacitors in domestic electronics has also been successful, with power tools marketed at the 'average' homeowner. Such domestic electronics are designed for expected infrequent and short-period use that is well addressed by supercapacitors because they have a 90-s recharge time and seemingly unlimited life-cycle. The dependability of supercapacitor technology has been supported by their use in the emergency doors of the Airbus™ and electromechanical actuators for engine ignition. Systems that integrate supercapacitors and batteries for synchronous use in a hybrid design complement these two energy devices by developing their strengths. Portable energy systems can be promoted from this design by reducing battery size to address small average load demands, whereas short, infrequent high-power pulses are met by the supercapacitor. In addition, reducing average energy demands can conversely raise the lifespan of the battery. Such systems aid producers of portable electronics and mobile telecommunications in their quest to miniaturise their products [22].

Nowadays, industrial and commercial supercapacitors are accessible in several countries (e.g., Japan, Russia, USA) and most capacitors are EDLC. Eaton (Cleveland, OH), Maxwell Technologies (San Diego, CA), Evans Capacitor Company (East Providence RI), and the Los Alamos National Laboratory (Los Alamos, NM) in the USA have undertaken a considerable amount of work on supercapacitors. Industrial and commercial companies such as Maxwell Technologies

[23] and Panasonic (Osaka, Japan) [24] manufacture common electrochemical supercapacitors using symmetric activated carbon electrode materials and an acetonitrile electrolyte.

China is experimenting with a new form of electric bus (Capabus™). It runs without powerlines using power stored in large onboard EDLC, which are recharged rapidly whenever the bus is at a bus stop (under ‘electric umbrellas’), and fully charged in the terminus. A few prototypes were tested in Shanghai in early 2005. In 2001 and 2002, VAG (public-transport operator in Nuremberg, Germany) tested a hybrid bus that uses a diesel-electric battery drive system with EDLC. Since 2003, Mannheim Stadtbahn (Mannheim, Germany) has operated a light-rail vehicle (LRV) that uses EDLC to store braking energy [25].

1.4.1 Consumer Electronics

In applications with fluctuating loads (e.g., laptop computers, portable media players, hand-held devices, photovoltaic systems), supercapacitors can stabilise the power supply. Supercapacitors deliver power for photographic flashes in digital cameras and for light-emitting diode (LED) life flashlights that can be charged in, for example, 90 s. As of 2013, portable speakers powered by supercapacitors have been offered on the market.

1.4.2 Buffer Power

Supercapacitors provide backup or emergency shutdown power to low-power equipment such as random access memories, micro-controllers and computer cards. They are the sole power source for low-energy applications such as automated meter-reading equipment or for event notification in industrial electronics. Supercapacitors ‘buffer’ power to and from rechargeable batteries, mitigating the effects of short power interruptions and high current peaks. Batteries are activated only during extended interruptions (e.g., if the mains

power or a fuel cell fails), which lengthens battery life. In UPS, supercapacitors replace much larger banks of electrolytic capacitors. This combination reduces the cost per cycle, saves on replacement and maintenance costs, enables the battery to be downsized, and extends battery life. A disadvantage is the need for a special circuit to reconcile the differing behaviours. Supercapacitors provide backup power for actuators in wind turbine pitch systems so that blade pitch can be adjusted even if the main supply fails.

1.4.3 Voltage Stabiliser

Supercapacitors can stabilise voltage for power lines. Wind and photovoltaic systems exhibit fluctuating supply evoked by gusting or clouds that supercapacitors can buffer within milliseconds. This action helps to stabilise grid voltage and frequency, balance the supply and demand of power, and manage real power or reactive power.

1.4.4 Energy Harvesting

Supercapacitors are suitable temporary energy-storage devices for energy-harvesting systems. In energy-harvesting systems, the energy is collected from ambient or renewable sources (e.g., mechanical movement, light or electromagnetic fields) and converted into electrical energy in an energy-storage device. For example, it has been demonstrated that energy collected from RF fields (using an RF antenna as an appropriate rectifier circuit) can be stored to a printed supercapacitor. Then, the harvested energy is used to power an application-specific integrated circuit for >10 h.

1.4.5 Incorporation into Batteries

The UltraBattery® is a hybrid rechargeable lead-acid battery and a supercapacitor invented by the national science organization in Australia: CSIRO. Its cell construction contains a standard lead-

acid-battery positive electrode, standard sulfuric acid electrolyte, and a specially prepared negative carbon-based electrode that stores electrical energy with double-layer capacitance. The supercapacitor electrode alters the chemistry of the battery and provides protection, at a high rate, against sulfation of lead-acid battery during charge, which is the typical failure mode of valve-regulated lead-acid cells used this way. The resulting cell performs with characteristics beyond those seen in a lead-acid cell or supercapacitor, with enhancement of charge and discharge rates, life-cycle, efficiency, and performance. UltraBattery® has been installed in kilowatt- and megawatt-scale applications in Australia, Japan and the USA in frequency regulation, solar smoothing and shifting, wind smoothing, and other applications.

1.4.6 Street Lights

Street lights combine a solar-cell power source with LED lamps and supercapacitors for energy-storage. Sado City (Niigata Prefecture, Japan) has street lights that combine a stand-alone power source with solar-cells and LED. Supercapacitors store the solar energy and supply two LED lamps, providing 15-W power consumption overnight. Supercapacitors can last >10 years and offer stable performance under various weather conditions, including temperatures from +40 °C to below -20 °C.

1.4.7 Military

The low internal resistance of supercapacitors supports applications that require short-term high currents. Among the earliest uses were motor startups (engine starting for cold diesel) for large engines in tanks and submarines. Supercapacitors buffer the battery, handling short current peaks and reducing cycling. Further military applications that require high power density are phased-array radar antennae, laser power supplies, military radio communications, avionic displays and instrumentation, backup power for airbag deployment, and global positioning system-guided missiles and projectiles.

1.4.8 Energy Recovery

A primary challenge for all types of transport is reducing energy consumption and reducing emissions of carbon dioxide. Recovery of braking energy (recuperation or regeneration) helps with both of these challenges, but requires components that can quickly store and release energy over long times with a high cycle rate. Supercapacitors fulfill these requirements and are used in many applications in all types of transportation.

1.4.9 Railways

Supercapacitors can be used to supplement batteries in starter systems in diesel railroad locomotives with diesel-electric transmission. The capacitors capture the braking energy of a full stop and deliver the peak current for starting the diesel engine and acceleration of the train and ensure the stabilisation of catenary voltage. Depending on the driving mode, up to 30% energy saving is possible by recovery of braking energy. Low maintenance and environmentally friendly materials encouraged the choice of supercapacitors.

1.4.10 Light-rails and Trams

Supercapacitors make it possible not only to reduce energy but to replace catenary overhead lines in historic city areas, thereby preserving the architectural heritage of the city. This approach can allow many new LRV city lines to replace overhead wires that are too expensive to route fully. In 2003, Mannheim adopted a prototype LRV using the Energy Saver™ system from Bombardier Transportation (Derby, UK) to store mechanical braking energy with a roof-mounted supercapacitor unit. This system contains several units, each comprising 192 capacitors with 2,700 F/2.7 V interconnected in three parallel lines. This circuit results in a 518 V system with energy content of 1.5 kWh. Starting this 'on-board-system' can provide the LRV with 600 kW, and can drive the vehicle

Conducting Polymer Nanocomposites for Supercapacitors

≤1 km without the catenary supply, thereby integrating the LRV into the urban environment by driving without catenary lines. Compared with conventional LRV or metro vehicles that return energy into the grid, onboard energy-storage saves ≤30% and reduces peak grid demand by ≤50%.

Supercapacitors are used to power the Paris T3 tram line on sections without catenary overhead wires and to recover energy during braking. In 2009, supercapacitors enabled LRV to operate in the historical city area of Heidelberg without catenary overhead wires, thereby preserving its architectural heritage. The SC equipment costs an additional €270,000 per vehicle, which was expected to be recovered over the first 15 years of operation. The supercapacitors are charged at ‘stopover stations’ when the vehicle is at a scheduled stop. This approach can allow many LRV city lines to serve catenary overhead wires that are too expensive to route fully. In April 2011, the German regional transport operator Rhein-Neckar (which is responsible for Heidelberg) ordered a further 11 units.

In 2009 in Paris, a tram on route T3 began operation with an energy-recovery system made by Alstom (Levallois-Perret, France) called ‘STEEM’. The system is fitted with 48 roof-mounted supercapacitors to store braking energy. STEEM provides tramways with a high level of energy autonomy by enabling them to run without catenary power on parts of its route, recharging while traveling on powered stopover stations. During tests, the trams used an average less energy of ≈16%.

In 2012, the tram operator Geneva Public Transport (Geneva, Switzerland) began tests of an LRV equipped with a prototype roof-mounted supercapacitor unit to recover braking energy. Siemens (Munich, Germany) is delivering supercapacitor-enhanced light-rail transport systems that include mobile storage. The metro line in South Island (Hong Kong, China) is to be equipped with two 2-MW energy-storage units that are expected to reduce energy consumption by 10%. In August 2012, the Zhuzhou Electric Locomotive Corporation (Zhuzhou, China) presented a prototype two-car light metro train equipped with a roof-mounted supercapacitor unit. The train can

travel ≤ 2 km without wires, recharging in 30 s at stations *via* a ground-mounted pickup. The supplier claims the trains can be used in 100 small and medium-sized Chinese cities. In 2012, the public transportation administration in Lyon, France, SYTRAL started tests of a ‘wayside regeneration’ system built by the Adetel Group (Ecully, France), which developed its own energy saver (‘NeoGreen’) for LRV, light-rail transport and metros.

Seven trams (‘street cars’) powered by supercapacitors were scheduled to go into operation in 2014 in Guangzhou, China. Supercapacitors are recharged in 30 s by a device positioned between the rails which can power the tram for ≤ 4 km.

1.4.11 Buses

The first hybrid bus with supercapacitors in Europe was built in 2001 in Nuremberg, Germany. It was the Ultracapbus™ (MAN, Augsburg, Germany) and was tested in real operation in 2001/2002. The test vehicle was equipped with a diesel-electric drive in combination with supercapacitors. The system was supplied with 8 Ultracap™ modules of 80 V, each containing 36 components. The system worked with 640 V and could be charged/discharged at 400 A. Its energy content was 0.4 kWh with a weight of 400 kg. Supercapacitors recaptured braking energy and delivered starting energy. Fuel consumption was reduced by 10–15% compared with conventional diesel vehicles. Other advantages included reduction of emissions of carbon dioxide, quiet and emissions-free engine starts, less vibration, and reduced maintenance costs. In 2002 in Lucerne (Switzerland), an electric bus fleet called TOHYCO-Rider™ was tested. Supercapacitors could be recharged *via* an inductive contactless high-speed power charger after every transportation cycle within 3–4 min.

In early 2005 in Shanghai (China), the Capabus™ was tested. Capabus™ runs without powerlines (catenary-free operation) using large onboard supercapacitors that partially recharge whenever the bus is at an electric umbrella, and charge fully in the terminus.

Conducting Polymer Nanocomposites for Supercapacitors

In 2006, two commercial bus routes began to use the Capabus™; one is on route 11 in Shanghai. It has been estimated that the supercapacitor bus was cheaper than a lithium-ion battery bus, and one of its buses had one-tenth the energy cost of a diesel bus with lifetime fuel savings of \$200,000. A hybrid electric bus called Tribrid™ was unveiled in 2008 by the University of Glamorgan (Glamorgan, Wales) for use as transport for its students. Tribrid™ is powered by hydrogen fuel or solar-cells, batteries and ultracapacitors.

1.4.12 Gondolas

In Zell am See (Austria), an aerial lift connects the city with Schmittenhöhe mountain. The gondolas sometimes run 24 h/day, using electricity for lights, door opening and communication. The only available time for recharging batteries at the stations is during the brief intervals of loading and unloading of guests, which is too short to recharge batteries. Supercapacitors offer a fast charge, greater number of cycles, and longer lifetime than batteries. Emirates Air Line™ (cable car), also known as the Thames Cable Car™, is a 1-km gondola line that crosses the Thames River from the Greenwich Peninsula to the Royal Docks. Cabins are equipped with an infotainment system powered by supercapacitors [25].

1.4.13 Advantages and Disadvantages of Supercapacitors

Each application must be evaluated based on its requirements. Some of the advantages and disadvantages of supercapacitors when considering their use are shown below.

- Advantages
 - *High energy-storage*: Compared with conventional capacitor technologies, EDLC possess orders of magnitude higher energy density. This phenomenon is a result of using a porous activated carbon electrode to achieve a high surface area.

- o *Low ESR*: Compared with batteries, EDLC have low internal resistance, thereby providing the capability of high power density.
- o *Performance at low temperature*: PowerBurst[®] ultracapacitors from the Tecate Group (San Diego, CA, USA), with their use of patented technology, can deliver energy down to -40 °C with minimal effects upon efficiency.
- o *Fast charge/discharge*: EDLC achieve charging and discharging through the absorption and release of ions and, coupled with their low ESR, high current charging and discharging is achievable without damage to parts.
- Disadvantages
 - o *Low voltage per cell*: EDLC cells have a typical voltage of 2.7 V. A higher voltage is needed for most applications, so cells must be connected in series.
 - o *Cannot be used in alternating current (AC) and high-frequency circuits*: Because of their time constant, EDLC are not suitable for use in AC or high-frequency circuits.

References

1. Z. Li, J. Wang, L. Niu, J. Sun, P. Gong, W. Hong, L. Ma and S. Yang, *Journal of Power Sources*, 2014, **245**, 224.
2. R. Kötz and M. Carlen, *Electrochimica Acta*, 2000, **45**, 15, 2483.
3. G. Wang, L. Zhang and J. Zhang, *Chemical Society Review*, 2012, **41**, 797.
4. Y. Zhang, H. Feng, X. Wu, L. Wang, A. Zhang, T. Xia, H. Dong, X. Li and L. Zhang, *International Journal of Hydrogen Energy*, 2009, **34**, 4889.

Conducting Polymer Nanocomposites for Supercapacitors

5. C.D. Lokhande, D.P. Dubal and O.S. Joo, *Current Applied Physics*, 2011, **11**, 255.
6. G.A. Snook, P. Kao and A.S. Best, *Journal of Power Sources*, 2011, **196**, 1.
7. E. Frackowiak and F. Beguin, *Carbon*, 2001, **39**, 6, 937.
8. B.E. Conway, *Journal of the Electrochemical Society*, 1991, **138**, 6, 1539.
9. B.E. Conway and V. Birss, *Journal of Power Sources*, 1997, **66**, 1, 1.
10. K.S. Ryu and K.M. Kim, *Journal of Power Sources*, 2002, **103**, 2, 305.
11. K. Jurewicz and S. Delpeux, *Chemical Physics Letters*, 2001, **347**, 1, 36.
12. E. Frackowiak and K. Jurewicz, *Journal of Power Sources*, 2001, **97**, 8, 822.
13. A. Laforgue and P. Simon, *Journal of the Electrochemical Society*, 2003, **150**, 5, 645.
14. M. Mastragostino and C. Arbizzani, *Solid State Ionics*, 2002, **148**, 3, 493.
15. H.Q. Li and L. Cheng, *Electrochemical and Solid State Letters*, 2005, **8**, 9, 433.
16. X. Wang and J.P. Zheng, *Journal of the Electrochemical Society*, 2004, **151**, 10, 1683.
17. A. Du Pasquier and I. Plitz, *Journal of Power Sources*, 2003, **115**, 1, 171.
18. W.G. Pell and B.E. Conway, *Journal of Power Sources*, 2004, **136**, 2, 334.

19. G.G. Amatucci and F. Badway, *Journal of the Electrochemical Society*, 2001, **148**, 8, 930.
20. A. Burke and M. Miller, *Journal of Power Sources*, 2011, **196**, 514.
21. A. Davies and A. Yu, *Canadian Journal of Chemical Engineering*, 2011, **89**, 1342.
22. J.R. Miller and P. Simon, *Science*, 2008, **321**, 651.
23. <http://www.maxwell.com>
24. <http://www.panasonic.com>
25. <http://www.zukunft-mobilitaet-net/10048/analyse/seilbahn-london-fahrpreis-kosten-kritik-olympia2012/>

Conducting Polymer Nanocomposites for Supercapacitors

2 Electrochemical Characterisations

2.1 Introduction

Electrochemical measurements are made in an electrochemical cell comprising two or more electrodes as well as the electronic circuitry for controlling and measuring the current and potential. Usually, ‘electrochemical polymerisation’ is carried out in a single-compartment electrochemical cell by adopting a standard three-electrode configuration. A typical ‘electrochemical bath’ comprises a monomer and supporting electrolyte dissolved in an appropriate solvent.

In this section, we introduce the basic components of electrochemical instrumentation. The simplest electrochemical cell uses two electrodes. The potential of one electrode is sensitive to the analyte concentration, and is called the ‘working electrode’ or ‘indicator electrode’. The second electrode, which is called the ‘counter electrode’, completes the electrical circuit and provides a reference potential against which the working electrode potential is measured. Ideally, the potential from the counter electrode remains constant so that any change in the overall cell potential can be assigned to the working electrode. If the counter electrode potential is not constant, it is replaced with two electrodes: a reference electrode (whose potential remains constant) and an auxiliary electrode (which completes the electrical circuit). The current and potential cannot be controlled simultaneously, so there are only three basic experimental designs. That is, it is possible to measure the: (i) potential when the current is zero; (ii) potential while controlling the current; and (iii) current while controlling the potential.

Each of these experimental designs uses a different type of instrument. Electrochemical instruments provide an automated, electronic means for controlling and measuring current and potential, and that they do so by using very different electronic circuitry. To measure the potential of an electrochemical cell under a condition of zero current, a potentiometer is used. A galvanostat allows control of the current flowing through an electrochemical cell. To monitor the potential of the working electrode (which changes as the composition of the electrochemical cell changes) an optional reference electrode and a high-impedance potentiometer can be included. A potentiostat allows control of the potential of the working electrode. The potential of the working electrode is measured relative to a constant-potential reference electrode that is connected to the working electrode through a high-impedance potentiometer (Figure 2.1). To set the working electrode potential, the slide-wire resistor of the high-impedance potentiometer (which is connected to the auxiliary electrode) is adjusted. If the working electrode potential begins to 'drift', the slide-wire resistor can be adjusted to return the potential to its initial value. Current flowing between the auxiliary electrode and working electrode is measured with an ammeter. Potentiostats include waveform generators that permit application of a time-dependent potential profile, such as a series of potential pulses, to the working electrode.

Electrochemical methods are employed to measure the interactions between an electrode and the solution in contact with the electrode. Such methods are classified broadly into 'static' and 'dynamic' methods.

In static methods, current is not allowed to flow through the analyte solution. Potentiometry (in which the potential of an electrochemical cell under static conditions is measured) is a very important quantitative electrochemical method.

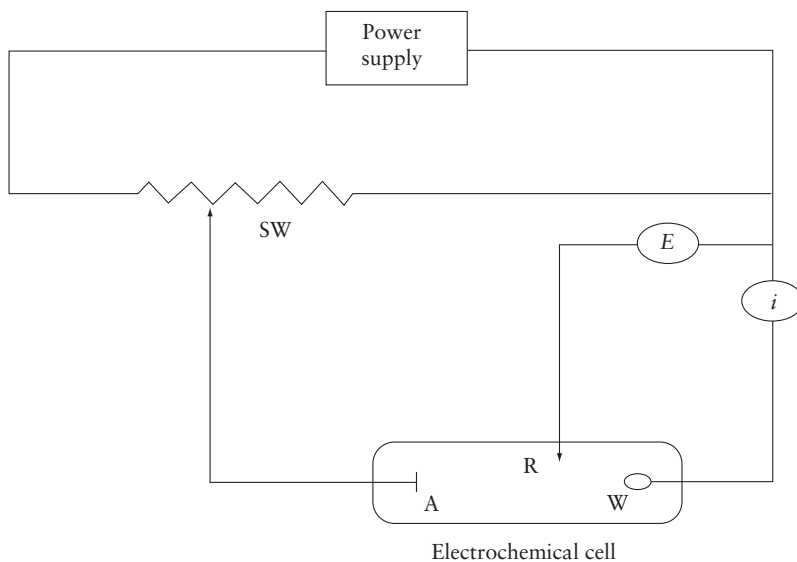


Figure 2.1 Manual potentiostat (schematic). W: Working electrode; A: auxiliary electrode; R: reference electrode; SW: slide-wire resistor; E: high-impedence potentiometer; and i : ammeter

In dynamic methods, current is allowed to flow through the analyte solution. Dynamic methods comprise the largest group of interfacial electrochemical methods. Coulometry (in which current is measured as a function of time) is a current-controlled (galvanostatic) method. Amperometry and voltammetry (in which current is measured as a function of potential) is a potential-controlled (potentiostatic) method. If current is measured at a constant potential, this is referred to as ‘amperometry’. If an electrical current is measured while controlled variations of the potential are being applied, this is named termed ‘voltammetry’. Advantages of a controlled-potential method include: high sensitivity; selectivity towards electroactive species; a wide, linear range; portable and low-cost instrumentation; a wide range of electrodes that allows assays of unusual environments. Extremely low limits of detection can be achieved with very small

sample volumes (5–20 μl), thereby allowing routine determination of analyte amounts of 10^{-13} to 10^{-15} mol.

Two types of process occur at electrodes. In the first type of process, charges (e.g., electrons) are transferred across the electrode–solution interface. Electron-transfer causes oxidation or reduction. Such reactions are governed by Faraday’s law (i.e., the amount of chemical reaction caused by the flow of current is proportional to the amount of electricity passed), so they are called ‘Faradaic processes’. Under some conditions, a given electrode–solution interface will show a range of potentials in which no charge-transfer reactions occur because such reactions are thermodynamically or kinetically unfavourable. The second process, non-Faradaic process, is where adsorption and desorption can occur and the structure of the electrode–solution interface can change with changing potential or solution composition. Charge does not cross the interface, but external currents can flow (at least transiently) when the potential, electrode area or solution composition changes.

The objective of a controlled potential electroanalytical experiment is to obtain a current response by monitoring the transfer of electrons during the redox process (**Equation 2.1**) of the analyte:



Where, O and R are the oxidised and reduced forms, respectively, of the redox couple. Such a reaction will occur in a potential region that makes electron-transfer thermodynamically and kinetically favourable. For a system controlled by the laws of thermodynamics, the potential of the electrode can be used to establish the relationship between the potential of an electrode and the concentrations of the two species O and R) involved in the redox reaction at that electrode according to the Nernst equation, **Equation 2.2**:

$$E = E^{\circ} + \frac{2.303RT}{nf} \log \frac{C_o}{C_R} \quad (2.2)$$

Where, E° is the standard potential for the redox reaction, R is the universal gas constant, T is the absolute temperature, n is the number of electrons transferred in the reaction, F is the Faraday constant, C_o is the concentration of the oxidised half of the couple and C_R is the concentration of the reduced half. If the potential applied to the electrode is changed, the ratio $\frac{C_o}{C_R}$ at the surface also changes so as to satisfy **Equation 2.2**. If the potential is made more negative, the ratio becomes larger (i.e., O is reduced). Conversely, if the potential is made more positive, the ratio becomes smaller (i.e., R is oxidised). The current resulting from the change in oxidation state of the electroactive species is termed the ‘Faradaic current’ because it obeys Faraday’s law. The Faradaic current is a direct measure of the rate of the redox reaction. The resulting current–potential plot, known as a ‘voltammogram’, displays the current signal *versus* the excitation potential. The potential at the working electrode determines if a Faradaic current is flowing, but the magnitude of the current is determined by the rate of the resulting oxidation or reduction reaction. Two factors contribute to the rate of the electrochemical reaction: the rate at which the reactants and products are transported to and from the electrode (‘mass transport’) and the rate at which electrons pass between the electrode and the reactants and products in solution. The net rate of a reaction (and hence the measured current) may be limited by mass transport of the reactant or by the rate of electron-transfer. The more ‘sluggish’ process is the rate-determining step.

There are three modes of mass transport that affect the rate at which reactants and products move toward or away from the electrode surface: diffusion, migration, and convection. Diffusion occurs whenever the concentration of an ion or molecule at the surface of the electrode is different from that in bulk solution. The region of solution over which diffusion occurs is called the ‘diffusion layer’. Convection occurs if the solution is mixed mechanically, thereby carrying reactants toward the electrode and removing products from the electrode. The most common form of convection is stirring the solution with a stir bar. Other methods include rotating the electrode

and incorporating the electrode into a flow-cell. The final mode of mass transport is migration, which occurs if a charged particle in solution is attracted to or repelled from an electrode that carries a surface charge. For example, if the electrode carries a positive charge, then an anion will move toward the electrode and a cation will move toward the bulk solution. Unlike diffusion and convection, migration affects the mass transport of only charged particles.

To understand how potential, concentration, and mass transfer act to limit current, recall of some concepts of physical chemistry is helpful. Fick's first law states that material diffuses from a region of high concentration to one of low concentration. The resulting flux (flux = moles of material diffusing per unit area per unit time) is given by **Equation 2.3**:

$$\text{Flux} = \frac{\text{moles}}{\text{area} \times \text{time}} = \frac{dN}{A dt} = -D \left(\frac{\partial C}{\partial x} \right) \quad (2.3)$$

Where, D is the diffusion coefficient for the species being transported to the electrode surface, and $\frac{\partial C}{\partial x}$ is the partial derivative of concentration of that species with respect to distance, as evaluated at the electrode surface. This partial derivative is the slope of a concentration (C) *versus* distance (x) curve, whereby the surface of the electrode is taken as $x = 0$. In electrochemistry, the flux is converted readily into current by invoking Faraday's law, which states that the number of moles of a species undergoing oxidation or reduction is related to the charge passed for that oxidation or reduction by the Faraday constant, **Equation 2.4**:

$$Q = nFN \quad (2.4)$$

Current is the flow rate of electrons (i.e., the derivative of charge with respect to time). Hence, it can be shown readily that, for the case of transport of analyte toward the surface, **Equation 2.5** holds:

$$i = \frac{dQ}{dt} = -nf \frac{dN}{dt} = -nf(\text{Flux}) = nFAD \frac{\partial C(x, t)}{\partial x} \quad (2.5)$$

This is the fundamental relationship used to calculate the current in any amperometric and voltammetric experiment. For **Equation 2.5** to be valid, convection and migration must not interfere with formation of a diffusion layer. Migration can be eliminated by adding a high concentration of an inert supporting electrolyte. Because ions of similar charge are equally attracted to or repelled from the surface of the electrode, each has an equal probability of migrating. A large excess of an inert electrolyte ensures that few reactants or products experience migration. Elimination of convection can be achieved by not stirring the solution. However, there are experimental designs in which convection cannot be avoided because the solution must be stirred or because an electrochemical flow cell is being used. Fortunately, the dynamics of a fluid moving past an electrode results in a small diffusion layer, typically 1–10 mm in thickness, in which the rate of mass transport by convection drops to zero.

The rate of mass transport is one factor influencing the current in voltammetry. The ease with which the electrons move between the electrode and the species reacting at the electrode also affects the current. When the kinetics of electron-transfer is fast, the redox reaction is at equilibrium. Under these conditions, the redox reaction is electrochemically reversible and the Nernst equation (**Equation 2.2**) applies. If the kinetics of electron-transfer is sufficiently slow, the concentration of reactants and products at the electrode surface (and thus the magnitude of the Faradaic current) are not what is predicted by the Nernst equation (**Equation 2.2**). In this case, the system is electrochemically irreversible.

In voltammetry, a time-dependent potential excitation signal is applied to the working electrode, thereby changing its potential relative to the fixed potential of the reference electrode, and the current that flows between the working and auxiliary electrodes is measured. The auxiliary electrode is usually a platinum wire, and the reference electrode is usually a standard calomel electrode or a silver/silver chloride electrode. For the working electrode, several materials can be chosen, including mercury, platinum, gold, silver and carbon [1–3].

2.2 Equipment: Potentiostat

A standard potentiostat used in a typical electrochemical setup is shown conceptually in **Figure 2.2**. A potentiostat is an electronic device used to maintain electrochemical stability in the sensor and to convert the sensor output into an analogue signal. It consists of three electrodes immersed in an electrolyte: the working electrode at which the reaction of interest (oxidation/reduction) occurs and to which biomolecular probes can be attached; a reference electrode to hold the electrolyte at a known potential; and a counter electrode.

The reference electrode takes up a stable potential: current does not flow through it. The potential of the working electrode is measured relative to it. The only role of a reference electrode is to act as a reference for measuring and controlling the working electrode potential, and at no point does it pass any current. On the other hand, the counter electrode passes all the current needed to balance the current observed at the working electrode. For electrochemical investigations, setups with three electrodes are preferred over those involving two electrodes due to the reduction in uncompensated resistance.

A typical electrochemical cell consists of the sample dissolved in a solvent, an ionic electrolyte, and three (or sometimes two) electrodes (**Figure 2.3**). Cells (i.e., sample holders) come in various sizes, shapes, and materials. The type used is dependent upon the amount and type of sample, the method, and the analytical data to be obtained. The material of the cell (glass, Teflon™, polyethylene) is selected to minimise reaction with the sample. In most cases, the reference electrode should be as close as possible to the working electrode. In some cases, to avoid contamination, it may be necessary to place the reference electrode in a separate compartment. The unique requirements for each of the voltammetric methods are described under the individual methods.

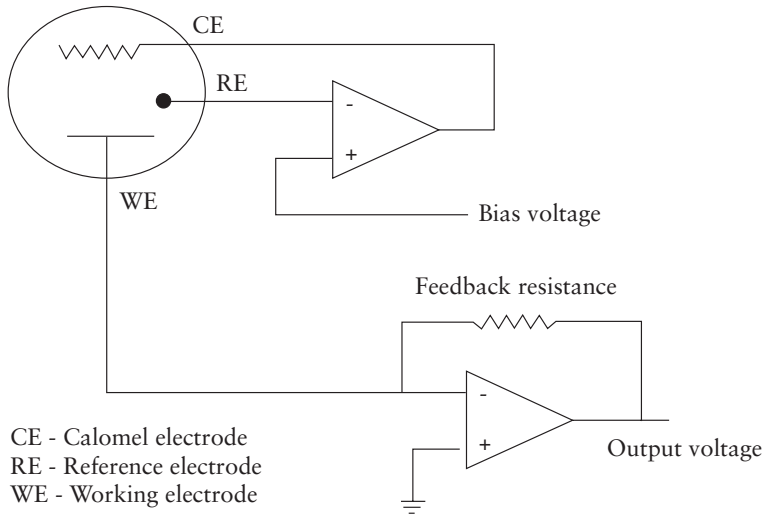


Figure 2.2 Block diagram of a three-electrode electrochemical cell and potentiostat circuit

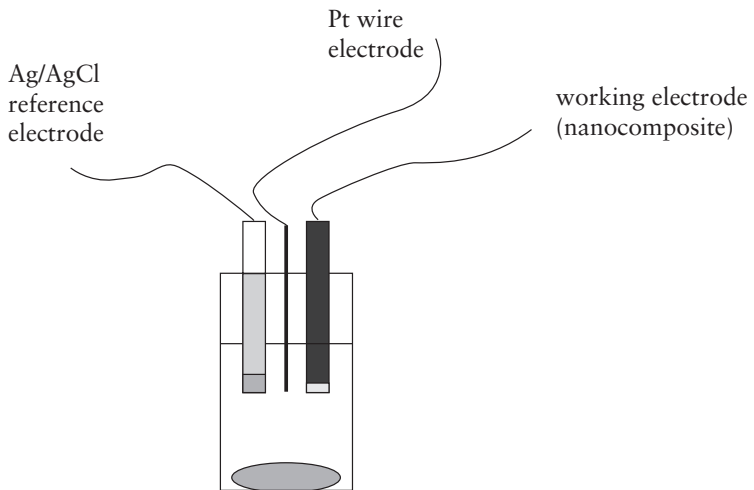


Figure 2.3 Typical three-electrode electrochemical cell

Reference electrodes: The reference electrode should provide a reversible half-reaction with Nernstian behaviour, be constant over time, and be easy to assemble and maintain. The most commonly used reference electrodes for aqueous solutions are the calomel electrode (with potential determined by the reaction $\text{Hg}_2\text{Cl}_2(\text{s}) + 2\text{e}^- \rightarrow 2\text{Hg}(\text{l}) + 2\text{Cl}^-$) and the silver/silver chloride electrode (with potential determined by the reaction $\text{AgCl}(\text{s}) + \text{e}^- \rightarrow \text{Ag}(\text{s}) + \text{Cl}^-$). These electrodes are available commercially in various sizes and shapes.

Counter electrodes: In most voltammetric methods, analytical reactions at the electrode surfaces occur over very short time periods and rarely produce appreciable changes in bulk concentrations of R or O. Thus, isolation of the counter electrode from the sample is not usually necessary. Usually, the counter electrode consists of a thin platinum wire, though gold (and sometimes graphite) have also been used.

Working electrodes are of various geometries and materials, ranging from small drops of mercury to flat platinum discs. Other commonly used electrode materials are gold, platinum and glassy carbon.

Electrochemical characterisation of supercapacitors is often carried out using cyclic voltammetry (CV), galvanostatic charge–discharge (GCD), and electrochemical impedance spectroscopy (EIS). These methods are not complimentary to each other in the context of supercapacitor design, instead each one of them has individual merits. For example, to obtain reliable preliminary estimates of specific capacitance (SC), GCD studies using a three-electrode (working, reference and counter electrodes) assembly in a suitable medium are carried out. On the other hand, CV provides information regarding the reversible nature of the electrode in a suitable electrolyte and the effect of the scan rate on the SC. The EIS not only yields accurate estimates of SC but also gives insights into the synergistic effect of each interfacial parameter. SC values are dependent upon operating variables (scan rate in CV, current density in GCD experiments, and potential in EIS). In reality, the actual capacitances are significantly

lower if two electrode assemblies are employed. Hence, fabrication of suitable devices and testing under appropriate discharge conditions are the criteria for judging the efficiency and stability of a supercapacitor. Magnitude of SC is an essential criterion in supercapacitor design, but power density, energy density, number of charge–discharge cycles, and time constants are equally crucial. The three-electrode assembly employed in such studies overestimates the SC significantly, so the correct value should be ascertained from GCD experiments pertaining to two electrodes [4]. However, investigations using a three-electrode assembly are prerequisites for the preliminary choice of materials and electrolytes.

2.3 Cyclic Voltammetry

CV is employed customarily for investigations of electron-transfer processes in diverse contexts. However, in analyses of supercapacitors, they are useful for: (i) ascertaining the stability of the electrode; (ii) choosing the appropriate electrolyte; and (iii) establishing the electrolyte concentrations. The potential window must be large in cyclic voltammetric experiments. Hence, organic electrolytes are preferred because aqueous electrolytes restrict the magnitude of the potential window to ≈ 1 V. Cyclic voltammograms are rectangular in shape for two-electrode assemblies, whereas those for three-electrode assemblies exhibit features depicted schematically in **Figure 2.4**. In cyclic voltammograms in a three-electrode system, E_p^a , E_p^c , i_p^a and i_p^c represent the peak anodic, cathodic current and peak anodic and cathodic voltage, respectively.

The SC (in Fg^{-1}) from CV is estimated from:

$$C = \frac{i}{v m} \quad (2.6)$$

Where i denotes the current and m is the mass loading, v being the scan rate. If ‘ m ’ in **Equation 2.6** is replaced by the area (A) of the electrode, capacitance per unit area is obtained (F cm^{-2}). As seen from **Equation 2.6**, the SC is dependent upon the scan rate, and the

latter is an experimental ‘control variable’. In a CV experiment, the working electrode potential is ramped linearly *versus* time. Unlike in linear-sweep voltammetry, after the set potential is reached in a CV experiment, the working electrode potential is ramped in the opposite direction to return to the initial potential. These cycles of ramps in potential may be repeated as many times as desired. The current at the working electrode is plotted *versus* the applied voltage (i.e., the working electrode potential) to give the cyclic voltammogram trace. CV is, in general, used to study the electrochemical properties of analytes in solution.

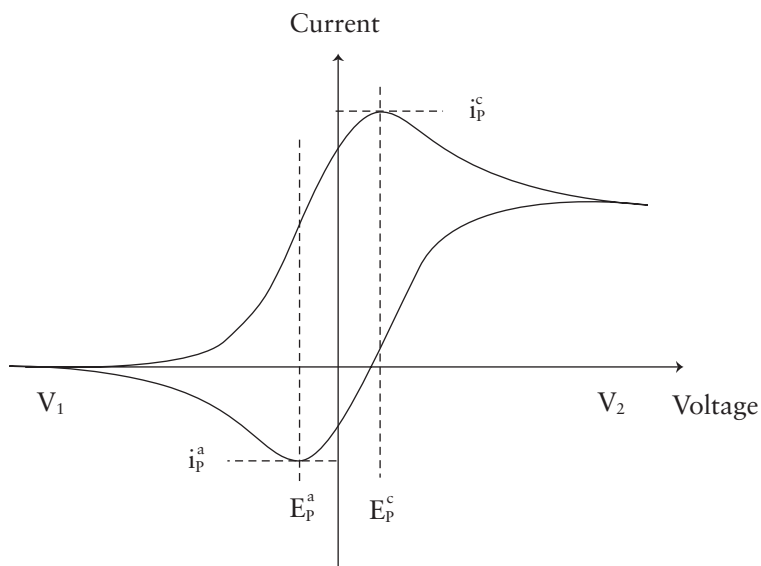


Figure 2.4 Typical cyclic voltammogram

In CV, the electrode potential ramps linearly *versus* time in cyclical phases (Figure 2.5). The rate of voltage change over time during each of these phases is known as the scan rate (V/s) of the experiment.

A potential is applied between the working electrode and reference electrode while the current is measured between the working electrode and counter electrode. These data are plotted as current (i) versus applied potential (E , often referred to as just ‘potential’). In **Figure 2.5**, during the initial forward scan (t_0 to t_1) an increasingly reducing potential is applied. Thus, the cathodic current will (at least initially) increase over this time period assuming that there are reducible analytes in the system. At some point after the reduction potential of the analyte is reached, the cathodic current will decrease as the concentration of reducible analyte is depleted. If the redox couple is reversible then, during the reverse scan (t_1 to t_2), the reduced analyte will start to be re-oxidised, giving rise to a current of reverse polarity (anodic current) compared with before. The more reversible the redox couple is, the more similar the oxidation peak will be in shape to the reduction peak. Hence, CV data can provide information about redox potentials and rates of electrochemical reactions. For instance, if electron-transfer at the surface of the working electrode is fast and current is limited by diffusion of analyte species to the electrode surface, then the peak current will be proportional to the square root of the scan rate.

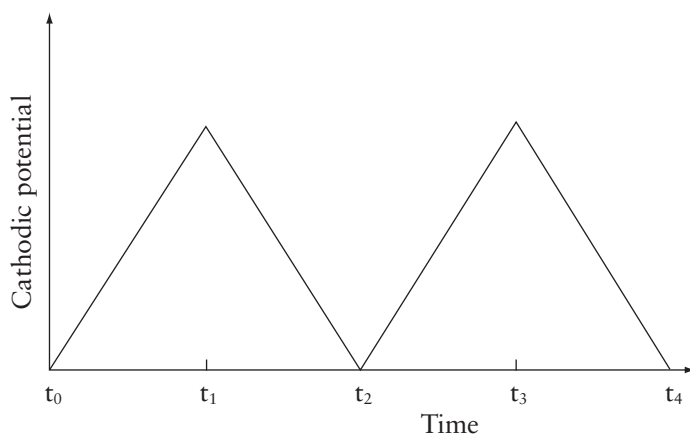


Figure 2.5 CV waveform

The utility of CV is highly dependent on the analyte being studied. Most importantly, the analyte must be redox active within the potential window to be scanned. It is also highly desirable for the analyte to display a reversible CV wave, which is observed when all of the initial analyte can be recovered after a forward-and-reverse scan cycle. Even reversible couples contain polarisation over potential, and thus display a hysteresis between the reduction (E_p^c) and oxidation peak (E_p^a) potentials. This over-potential emerges from a combination of analyte diffusion rates and the intrinsic activation barrier of transferring electrons from the electrode to an analyte. Reversible couples have a ratio of peak currents at analyte oxidation (i_p^a) and reduction (i_p^c) that is near unity ($i_p^a/i_p^c = 1$). Even with a reversible couple, this ratio can be perturbed away from unity in the presence of a subsequent chemical reaction that is triggered by electron-transfer, a stripping wave, or a nucleation event. If a reversible peak is observed, thermodynamic information in the form of a half-cell potential $E_{1/2}^0$ can be determined. If waves are semi-reversible (i_p^a/i_p^c is close but not equal to 1) it may be possible to determine even more specific information. If waves are non-reversible it is, in general, not possible to determine the thermodynamic potential $E_{1/2}^0$ with CV (when it is possible the system usually contains equal quantities of the analyte in both oxidation states). The redox couple could be irreversible because of a subsequent chemical process; a common example of this phenomenon is a transition metal complex changing its coordination sphere geometry after an electron is transferred to or from it. If this is the case, then higher scan rates may show a reversible wave because the electron-transfer cycles may occur faster than the geometry change can. It is also possible that the wave is irreversible due to a physical process that takes the analyte products out of solution.

A standard CV experiment uses a reference electrode, working electrode, and counter electrode. This combination is sometimes referred to as a 'three-electrode setup' [5–7]. An electrolyte is usually added to the sample solution to ensure sufficient conductivity. The solvent, electrolyte, and material composition of the working electrode determine the potential range that can be accessed during

the experiment. The electrodes are immobile and sit in unstirred solutions during CV. This 'still' solution method gives rise to CV characteristic diffusion-controlled peaks. This method also allows a portion of the analyte to remain after reduction or oxidation so that it may display further redox activity. Stirring the solution between CV traces is important to supply the electrode surface with fresh analyte for each new experiment. The solubility of an analyte can change drastically with its overall charge; as such, it is common for reduced or oxidised analyte species to precipitate out onto the electrode. This layering of analyte can insulate the electrode surface, display its own redox activity in subsequent scans, or otherwise alter the electrode surface in a way that affects CV measurements. Hence, it is often necessary to clean the electrodes between scans.

Common materials for the working electrode include glassy carbon, platinum, and gold. These electrodes are, in general, encased in a rod of inert insulator with a disc exposed at one end. A regular working electrode has a radius within one order of magnitude of 1 mm.

Having a controlled surface area with a well-defined shape is necessary for interpretation of CV results. To run CV experiments at very high scan rates, a regular working electrode is insufficient. High scan rates create peaks with large currents and increased resistances, which result in distortions. 'Ultra-microelectrodes' can be used to minimise the current and resistance. The counter electrode (also known as the 'auxiliary electrode' or 'second electrode') can be any material that conducts current readily and which does not react with the bulk solution. Reactions occurring at the counter electrode surface are unimportant as long as it continues to conduct current well. To maintain the observed current, the counter electrode will often oxidise or reduce the solvent or bulk electrolyte.

CV has become an important and widely used electroanalytical method in several areas of chemistry. It is often used to study various redox processes, as well as to determine: the stability of reaction products; intermediates in redox reactions; reaction and electron-transfer kinetics; the reversibility of a reaction. CV can also be used

to determine the electron stoichiometry of a system, the diffusion coefficient of an analyte, and the formal reduction potential of an analyte, which can be used as identification tools. In addition, because concentration is proportional to current in a reversible, Nernstian system, the concentration of an unknown solution can be determined by generating a calibration curve of current *versus* concentration.

2.4 Galvanostatic Charge–Discharge

In GCD experiments, a constant current density is applied and the potential *versus* time response is recorded, and the SC is evaluated using Equation 2.7:

$$C = \frac{I\Delta t}{\Delta Vm} \quad (2.7)$$

Where, I indicates the current, Δt denotes the discharge time, ΔV is the potential range, and m is the mass of the active material. Current density and time of discharge are parameters to be chosen such that the maximum number of charge–discharge cycles arises without significant decreases in the SC. The SC for conducting polymer (CP) polypyrrole (Ppy) and polyaniline (PANI)-based systems employing three-electrode assemblies on various electrodes made of nickel, stainless steel (SS), indium tin oxide, carbon, graphite, glassy carbon, gold, platinum, aluminium, and titanium have been reported [8–24]. The number of charge–discharge cycles obtainable from galvanostatic experiments is dependent upon the magnitude of current, whereas the SC, in general, decreases with increase in the number of cycles. In the case of PANI and Ppy nanocomposites, the commonly used electrodes are made of SS, nickel and graphite.

2.5 Electrochemical Impedance Spectroscopy

EIS is a powerful diagnostic tool that can be used to characterise the performance of supercapacitors. EIS is useful for the research

and development of new materials and electrode structures, as well as for product verification and quality assurance in manufacturing operations. Analyses of CP-based supercapacitors almost invariably employs impedance analyses so as to delineate the influence of different system components. Representation of impedance data can be carried out using: (i) Nyquist plot, *viz.* the imaginary *versus* real part of the impedance ($-Z''$ *versus* Z'); (ii) Bode' phase angle plot (θ *versus* $\log \omega$); (iii) Bode' magnitude plot ($|Z|$ *versus* $\log \omega$). However, for estimation of the SC, variation of the imaginary part of the impedance ($-Z''$) with the reciprocal frequency ($1/f$) is constructed to calculate the slope [25] according to **Equation 2.8**:

$$\frac{d(-Z'')}{d(1/f)} = \frac{1}{2\pi C} \quad (2.8)$$

Where, f denotes the frequency. By dividing the C value obtained from **Equation 2.8** by the mass of the deposited species, the SC per unit mass arises. **Equation 2.8** is satisfactory for estimating the SC, and has been employed hitherto, but the power of EIS will be lost if all the system parameters (double-layer capacitance, various resistances, exchange current density, and Warburg impedance) essential for comprehending the electrochemical behaviour are not reported. Hence, construction of appropriate equivalent circuits for deducing the system parameters becomes important. Composites of CP and metal oxides/carbon-based materials exhibit very low equivalent series resistance values and hence yield high SC. Thus, development of supercapacitors involving metal oxides/carbon materials and CP composites is poised for phenomenal growth during the coming years on account of interesting scientific and technological possibilities.

To measure electrochemical impedance, an alternating current (AC) potential is applied to an electrochemical cell and the current through the cell is measured. If the applied potential is sinusoidal, the response is an AC current signal containing the excitation frequency and its harmonics. The electrochemical response is measured and interpreted in terms of an equivalent circuit (a circuit composed of electrical components with the same frequency response as the

electrochemical reactions). In electrochemistry, the ‘imaginary impedance’ is almost always capacitive and, therefore, negative. In this work, EIS applications to characterise polymeric thin films are presented. An ideal Nyquist plot for a polymer-coated metal electrode in an electrolyte solution is a purely charge-transfer control system in which charge transfer resistance can be derived from the diameter of the semicircle. The two semicircles at the highest frequencies induced by the process at metal/polymer and polymer/solution interfaces are, in practice, not always detectable. If diffusion and kinetic control are involved, a more complex Nyquist plot will result. The circular portion corresponds to the charge-transfer control, and the linear portion corresponds to diffusion control. EIS spectra of CP are quite complex and incompletely understood because of numerous processes taking place simultaneously during recharge of the polymer layer. However, several models describing the impedance spectra for a particular type of polymer layer have been proposed. In this work, a generalised transmission line circuit model is applied describing the capacitive effects in the low-frequency range through chemical processes. The transmission line model predicts the impedance features of a polymer system in terms of Nyquist plots based on mathematical approaches and yields fairly accurate ionic and electronic conductivities. A combination of EIS with a commonly used method such as CV can, therefore, provide a powerful tool to understand the properties of CP-based nanocomposites and thus enable development of such nanomaterials for specific applications. The low-frequency capacitance values characterising the redox capacitance of a polymer film can be obtained using **Equation 2.9**:

$$C = \frac{1}{\omega Z''} = \frac{1}{2\pi f Z''} \quad (2.9)$$

Where f is the lowest frequency used to record the spectra and Z'' is the imaginary part of the impedance at that frequency. Electronic and ionic resistances of the CP composite film at different direct current potentials can be extracted from Nyquist plots [26–28].

References

1. O. Sheela, R. Mallika and J. Jayapandian, *Journal of Instrumentation Society India*, 2010, **38**, 44.
2. A. Bard and L. Faulkner in *Electrochemical Methods: Fundamentals and Applications*, John Wiley & Sons, New York, NY, USA, 2001.
3. J. Wang in *Analytical Electrochemistry*, John Wiley & Sons, New York, NY, USA, 2000.
4. V. Khomenko, E. Frackowiak and F. Beguin, *Electrochimica Acta*, 2005, **50**, 2499.
5. O. Koysuren, C. Du, N. Pan and G. Bayram, *Journal of Applied Polymer Science*, 2009, **113**, 1070.
6. Y. Yan, Q. Cheng, G. Wang and C. Li, *Journal of Power Sources*, 2011, **196**, 7835.
7. S. Dhibar, P. Bhattacharya, G. Hatui and C.K. Das, *Journal of Alloys and Compounds*, 2015, **625**, 64.
8. J. Li, M. Cui, Y. Lai, Z. Zhang, H. Lu, J. Fang and Y. Liu, *Synthetic Metals*, 2010, **160**, 1228.
9. H. Zhang, Q. Zhao, S. Zhou, N. Liu, X. Wang, J. Li and F. Wang, *Journal of Power Sources*, 2011, **196**, 10484.
10. H. Huang, M. Gan, L. Ma, L. Yu, H. Hu, F. Yang, Y. Li and C. Ge, *Journal of Alloys and Compounds*, 2015, **630**, 214.
11. P. Sivaraman, R.K. Kushwaha, K. Shashidahara, V.R. Hande, A.P. Thakur, A.B. Samui and M.M. Khandpekar, *Electrochimica Acta*, 2010, **55**, 2451.
12. Z. Lei, Z. Chen and X.S. Zaho, *Journal of Physical Chemistry C*, 2010, **114**, 19867.

13. K.S. Ryu, S.K. Jeong, J. Joo and K.M. Kim, *Journal of Physical Chemistry B*, 2007, **11**, 731.
14. K.S. Ryu, X. Wu, Y. Lee and S.H. Chang, *Journal of Applied Polymer Science*, 2003, **89**, 1300.
15. S. Palaniappan, S.B. Sydulu, T.L. Prasanna and P. Srinivas, *Journal of Applied Polymer Science*, 2011, **120**, 780.
16. J. Zhang, L.B. Kong, J.J. Cai, Y.C. Luo and L. Kang, *Electrochimica Acta*, 2010, **55**, 8067.
17. X. Wang, C. Yang, T. Wang and P. Liu, *Electrochimica Acta*, 2011, **58**, 193.
18. C. Yang and P. Liu, *Synthetic Metals*, 2010, **160**, 768.
19. Y. Han, L. Hao and X. Zhang, *Synthetic Metals*, 2010, **160**, 2336.
20. S. Sahoo, G. Karthikeyan, G.C. Nayak and C.K. Das, *Synthetic Metals*, 2011, **161**, 1713.
21. Y.Q. Han, B. Ding and X.G. Zhang, *Chinese Science Bulletin*, 2011, **56**, 2846.
22. B. Zhang, Y. Xu, Y. Zheng, L. Dai, M. Zhang, J. Yang, Y. Chen, X. Chen and J. Zhou, *Nanoscale Research Letters*, 2011, **6**, 431.
23. J. Zhang and X. Li, *Journal of Materials Chemistry*, 2011, **21**, 10965.
24. R.K. Sharma, A. Karakoti, S. Seal and L. Zhai, *Journal of Power Sources*, 2010, **195**, 1256.
25. D. Belanger, X. Ren, J. Davey, F. Uribe and S. Gottesdeld, *Journal of the Electrochemical Society*, 2000, **147**, 2923.

26. Z. Uygun and H. Uygun, *Sensors and Actuators B*, 2014, 202, 448.
27. V. Huang, S. Wu, M. Orazem, N. Pébère, B. Tribollet and V. Vivier, *Electrochimica Acta*, 2011, 56, 8048.
28. A. Bondarenko, *Analytica Chimica Acta*, 2012, 743, 41.

Conducting Polymer Nanocomposites for Supercapacitors

3 Conducting Polymers

3.1 Introduction

A polymer is a large molecule built-up by the repetition of small, simple chemical units. In some cases, the repetition is linear and in other cases it is branched or interconnected to form three-dimensional (3D) networks. The repeat unit of the polymer is usually equivalent (or nearly equivalent) to the monomer or starting material from which the polymer is formed. The length of the polymer chain is specified by the number of repeat units in the chain. This is called the 'degree of polymerisation'. The molecular weight of the polymer is the product of the molecular weight of the repeat unit and the degree of polymerisation. Therefore, polymers have high molecular weight. 'Polymer' is a generic name given to a vast number of materials of high molecular weight. Polymers can have different chemical structure, physical properties, mechanical behaviour and thermal characteristics. Polymers can be classified as 'natural', 'synthetic', 'organic', 'inorganic', 'thermoplastic', 'thermosetting', 'plastic', or 'fibre'.

Organic polymers that show a semiconducting nature with electrical conductivity identical to that of conductors are called as 'conductive polymers' or, more commonly, 'conducting polymers' (CP). The biggest advantage of CP is their processability, which is mainly by dispersion. They can offer high electrical conductivity but do not show similar mechanical properties to other polymers available commercially.

In most cases, polymers are insulators in their neutral state, and they

become conductive only after introduction of electron acceptors/donors by a process known as 'doping'. The conductivity of a polymer can be 'tuned' by chemical manipulation such as the nature of the dopant, the degree of doping, and blending with other polymers.

CP are rapidly becoming attractive for new applications because they are processable materials with good electrical/physical properties and low costs. Emergence of CP constitutes an important milestone in analytical science [1]. These materials, being conjugated systems, possess considerable electron availability, which provides them with a rigid structure and better capacity to be adsorbed onto metallic surfaces [2]. Most common forms of CP in their neutral state are insulators called 'conjugated polymers'. However, these neutral conjugated polymers can be converted into semi-conductive or conductive states through chemical or electrochemical redox reactions. To extend functions or to improve the performances of these polymers, CP are frequently doped with other functional materials to form composites. The general characteristics of these forms were reviewed recently [3].

Due to their unique conductive properties, CP are usually employed in important applications in chemistry, physics, electronics, optics, materials and biomedical science. Such applications have prompted the need for analytical methodologies to characterise and control the quality of these materials [4].

CP have highly delocalised π -electron systems with alternate single and double bonds in the polymer backbone. The π -conjugation of the polymer chain generates high energy-occupied molecular orbitals and low energy-unoccupied molecular orbitals, thereby leading to a system that can be oxidised or reduced readily. Unlike conventional polymers (which are electrical insulators), CP are semiconducting and can be doped into regions of metallic conductivity [5, 6]. This novel finding, at odds with what had been previously expected of polymers, yielded the 2000 Nobel Prize in Chemistry for Alan J. Heeger, Alan G. MacDiarmid and Hideki Shirakawa for the discovery and subsequent development of this new class of material.

Thanks to intense research efforts, there is now a large variety of CP, with polyacetylene (PA), polythiophene (PTH), polypyrrole (Ppy) and polyaniline (PANI) being four of the most studied and promising types. It has been shown that PA (which has the simplest polyconjugated system) can be made conductive by reaction with bromine (Br) or iodine (I) vapours. Spectroscopic studies have demonstrated without ambiguity that this reaction is redox in nature and consists of the transformation of neutral polymer chains into polycarbocations with simultaneous insertion of the corresponding number of Br_3^- or I_3^- anions between polymer chains to neutralise the positive charge generated on the polymer chain. This important discovery initiated extensive and systematic research of various aspects of the chemistry and physics of conjugated polymers in their neutral ('undoped') and charged (doped) states. Undoped conjugated polymers are semiconductors with band gaps ranging from 1 eV to 4 eV. Therefore their conductivities at room temperature are very low (typically $\leq 10^{-8}$ S/cm). However, doping can lead to an increase in the conductivity of polymer by many orders of magnitude [7].

3.2 Doping of Polymers

The concept of doping is unique and distinguishes CP from all other types of polymer [8]. During doping, an undoped conjugated polymer having small conductivity (typically 10^{-10} – 10^{-5} S/cm) is converted to a doped CP, which is in a 'metallic' conducting regime (1 – 10^4 S/cm). Controlled addition of known and usually small (<10%) non-stoichiometric quantities of chemical species can result in dramatic changes in the electronic, electrical, magnetic, optical, and structural properties of the polymers. By controllably adjusting doping, conductivity anywhere between that of the non-doped and fully doped form of the polymer can be obtained readily. The highest value reported to date has been obtained in I-doped PA ($>10^5$ S/cm) and the predicted theoretical limit is about 2×10^7 , more than one order of magnitude higher than that of copper. Conductivity of other conjugated polymers can reach $\leq 10^3$ S/cm. *Trans*-(CH)_x form of PA and the emeraldine base form of PANI are shown in **Figure 3.1** to

illustrate the increases in the electrical conductivity, by many orders of magnitude, that can be obtained by doping [9].

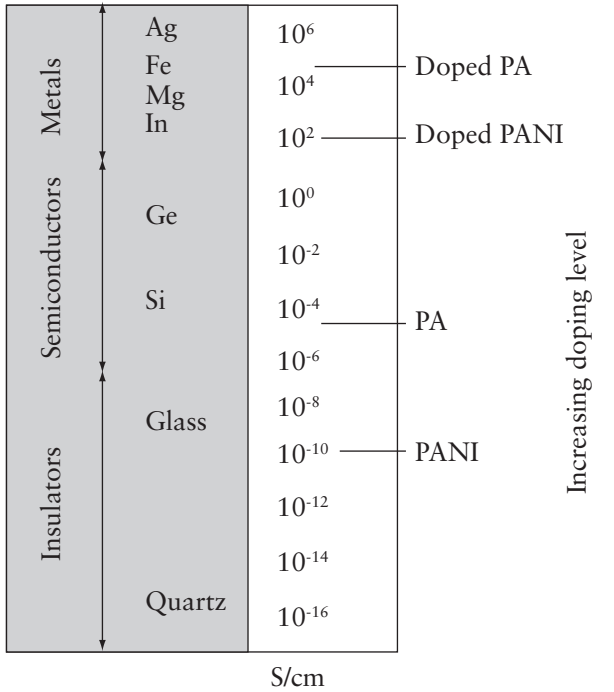


Figure 3.1 Conductivity of some metals, semiconductors, insulators and conjugated polymers

In the doped state, the backbone of CP comprises a delocalised π -system. In the undoped state, the polymer may have : a conjugated backbone, such as that seen in *trans*-(CH)_x (which is retained in a modified form after doping); a non-conjugated backbone, such as in PANI (leucoemeraldine base form), which becomes truly conjugated only after p-doping; a non-conjugated structure as in the emeraldine

base form of PANI, which becomes conjugated only after doping with a protonic acid. All CP and most of their derivatives shown in **Figure 3.2** undergo p- and/or n-redox doping by chemical and/or electrochemical processes during which the number of electrons associated with the polymer backbone changes. The molecules of the monomers of all these polymers have alternating double-single chemical bonds, so they form polymers that are π -conjugated.

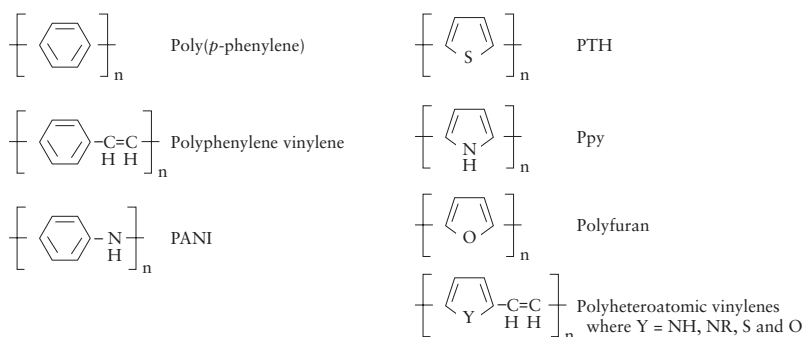


Figure 3.2 CP undergo redox doping

Charge injection onto conjugated, semiconducting macromolecular chains by doping leads to a wide variety of interesting and important phenomena. Reversible charge injection by doping can be accomplished in several ways: chemical doping by charge transfer, electrochemical doping, doping using acid–base chemistry, and photodoping.

3.3 Conduction Mechanism

CP are unusual in that they do not conduct electrons *via* the same mechanisms used to describe classical semiconductors. Hence, their

electronic properties cannot be explained by standard band theory. Electronic conductivity of CP results from mobile charge carriers introduced into the conjugated π -system through doping. To explain the electronic phenomena in these organic CP, new concepts involving solitons, polarons and bipolarons have been proposed by scholars of solid-state physics [10–12].

Electronic structures of π -conjugated polymers with degenerate and non-degenerate ground states are different. In π -conjugated polymers with degenerate ground states, solitons are the important and dominant charge-storage species. PA, $(\text{CH})_x$, is the only known polymer with a degenerate ground state due to its access to two possible configurations. The two structures differ from each other by the position of carbon–carbon single and double bonds. PA can exist in two isomeric forms (*cis* and *trans*) but the *trans*-acetylene form is thermodynamically more stable and the *cis*–*trans* isomerisation is irreversible. A soliton can also be viewed as an excitation of the radical from one potential well to another well of the same energy. A neutral soliton occurs in pristine *trans*-PA if a chain contains an odd number of conjugated carbons, in which case there remains an unpaired π -electron, a radical, which corresponds to a soliton. In a long chain, the spin density in a neutral soliton (or charge density in a charged soliton) is not localised on one carbon but instead spread over several carbon atoms, which gives the soliton a width. Starting from one side of the soliton, the double bonds become gradually longer and the single bonds shorter so that, arriving at the other side, the alternation has reversed completely. This phenomenon implies that the bond lengths equalise in the middle of a soliton. Presence of a soliton leads to the appearance of a localised electronic level at mid-gap that is half occupied in the case of a neutral soliton, and empty (doubly occupied) in the case of a positively (or negatively) charged soliton. Similarly, in n-type doping, neutral chains are chemically or electrochemically reduced to polycarbonium anions and, simultaneously, charge-compensating cations are inserted into the polymer matrix. In this case, negatively charged, spinless solitons are charge carriers.

Consider the structure of other CP such as poly(*p*-phenylene), Ppy, PTH and PANI. These polymers do not support soliton-like defects because the ground state energy of the quinoid form is substantially higher than that of the aromatic benzenoid structure. As a result, the charge defects on these polymers are different. As an example, consider the oxidation of Ppy (Figure 3.3).

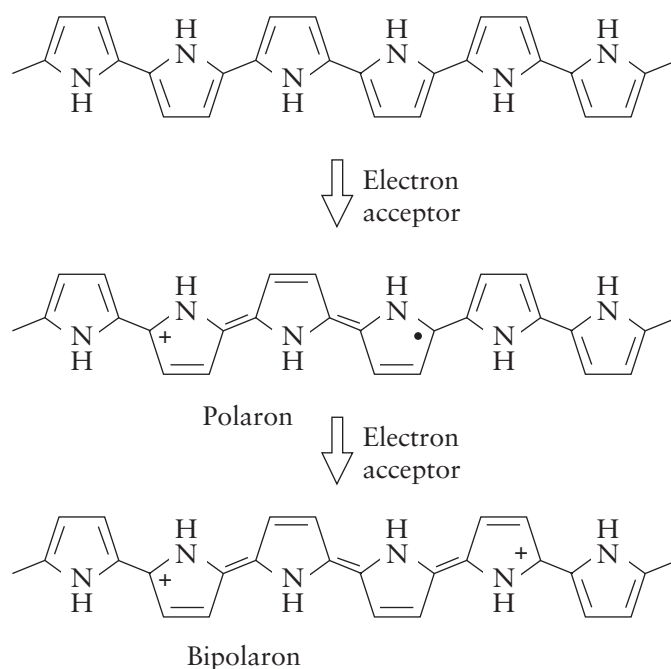


Figure 3.3 Formation of polarons and bipolarons on the π -conjugated backbone of Ppy

Removal of an electron from a pyrrole unit leads to formation of a polaron consisting of a tightly bound radical and cation. This binding arises from the increase in energy (of the defect) with increasing

radical–cation separation. This increase in energy is due (at least in part) to a loss of aromaticity. Calculations on Ppy and PTH suggest that two polarons in close proximity are unstable with respect to formation of a bipolaron. The two free radicals combine, leaving behind two cations separated by a quinoid section of the polymer chain. However, the higher energy of the quinoid section between them binds them together, resulting in correlated motion. The net effect is formation of a doubly charged defect acting like a single entity and delocalised over several rings (3–5), i.e., a bipolaron. Formation of bipolarons implies a net gain in free energy in forming a closed-shell defect from two open-shell structures. The quinoid form has a higher energy than the aromatic benzenoid form but its electron affinity is higher and the ionisation potential lower. This situation leads to formation of two localised states in the band gap. As doping is increased, additional states are created in the gap, and they finally evolve into two narrow bands. At low levels of doping, the defects are polarons, which tend to combine at higher doping levels to form bipolarons.

Let us now consider some peculiarities of the PANI system. In conventional CP [e.g., Ppy, PTH, PA and poly(*p*-phenylene)], oxidative doping results in removal of electrons from the bonding π -system. In contrast, in PANI, initial removal of electrons is from the non-bonding nitrogen lone pairs. Unlike other CP, the quinoid form is not simply an alternative resonance form. Its formation requires reduction and deprotonation so that it differs in chemical composition from the benzenoid form (Figure 3.4).

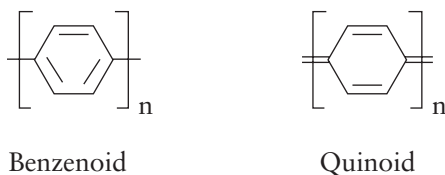


Figure 3.4 Benzenoid and quinoid forms of PANI

This peculiarity of the PANI structure makes doping by an acid–base reaction possible. In addition, the constituent parts of the polaron and bipolaron are very tightly bound owing to valence restrictions. Radical cations of the polaron are confined to a single aniline residue. The bipolaron is confined to, and identical with, a (doubly protonated) quinone–diimine unit. This narrow confinement can destabilise bipolarons with respect to polarons owing to the coulomb repulsion between the cations.

As indicated above, doping of PANI can be achieved *via* two routes. Doping by oxidation of the leucoemeraldine form of PANI results in the formation of radical cations, which may then be converted to bipolarons. Alternatively, protonation of the emeraldine base form leads to initial formation of bipolarons, which may rearrange with neutral amine units to form radical cations (**Figure 3.5**). The totally reduced leucoemeraldine state of PANI can be doped oxidatively to the conductive emeraldine state by chemical or electrochemical means. Progressive oxidative doping of leucoemeraldine base to the emeraldine salt and finally to pernigraniline by electrochemical means using cyclic voltammetry has been reported. Protonic doping involves doping of a conjugated polymer to its conducting regime without any change in the number of electrons associated with the polymer.

PANI was the first well-established example of this type of doping and was accomplished by treating the emeraldine base with aqueous protonic acids. For example, the emeraldine base can be doped by hydrochloric acid to yield the conducting emeraldine hydrochloride. The dication can form a resonance structure consisting of two separated polarons. The ability of PANI to exist in various forms *via* acid–base treatment and oxidation–reduction by chemical or electrochemical means has made PANI the most ‘tunable’ CP.

PANI finds a wide variety of applications in different fields. The completely reduced form of leucoemeraldine finds applications in electrochromic devices and in lithium–PANI batteries. Pernigraniline is used for non-linear optics. Emeraldine base comprising 50% reduced and 50% oxidised moieties is used in hydrochloric acid

sensors and for making thin films. Other applications of conducting PANI include: dissipation of electrostatic charge; electromagnetic interference (EMI) shielding; transparent packaging of electronic components; solar batteries; non-linear optical display devices; ‘smart’ fabrics; recording [13].

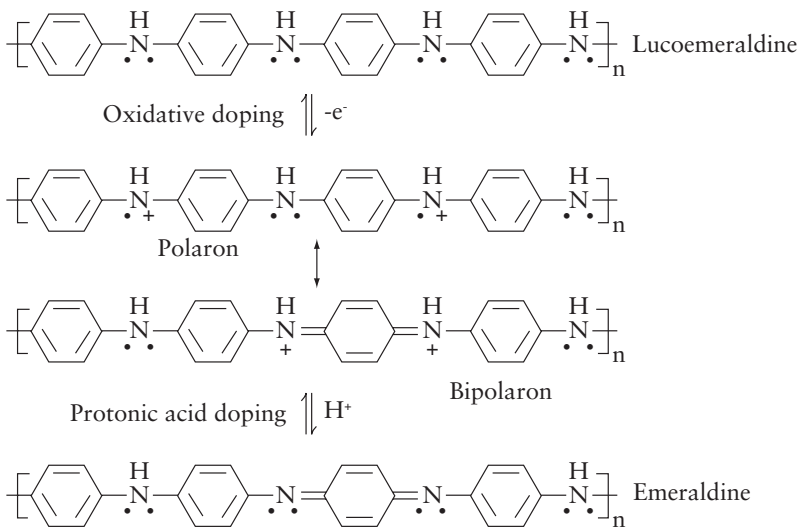


Figure 3.5 Oxidative and protonic-acid doping in PANI

3.4 Charge Transport

Transport mechanisms of intra- and intermolecular charge in CP can be differentiated. Charge can be delocalised along the polymer backbone but, without an efficient intermolecular tunneling or hopping mechanism (charge transport mechanisms where charge carriers tunnel or hop from molecule-to-molecule), conductivity

may remain low. In general, CP are refractory materials, so poor inter-particle contacts may further limit conductivity in compressed pellets [14]. Inhomogeneous doping may also lead to a dependence on doping level, which does not reflect intrinsic behaviour but derives instead from the microscopic topology of the granular dispersion. Conductivity of a dispersion of conducting particles in an insulating matrix shows percolation effects [15]. The composite shows a dramatic rise in conductivity above a threshold loading corresponding to formation of an 'infinite' network of particles in mutual contact. The complicating factor is that differential thermal expansion coefficients may lead to pseudo-temperature dependence. Soliton, polaron or bipolaron states can overlap in CP to form 'bands' of states [16]. In principle, a metallic state may result if such bands are partially filled. Overlap of bipolaron bands with the valence band and a regular array of polarons are examples of such metallic states with a finite density of states at the Fermi level.

Historically, the concept of a metallic state for the conductive form of PANI was marked by revolutionary change. One of the initial suggestions by MacDiarmid [17] was that the metallic state in PANI derives from a delocalised bipolaron defect. On the other hand, Epstein and coworkers [18] favoured a metallic state derived from a regular array of polarons. The observed temperature dependence for conductivity is not metallic, so they proposed a picture of metallic particles embedded in a dielectric medium. Conductivity of such a granular metal is determined by space charging limited tunneling (process of the limitation of charge carrier tunneling, through space charge created). In the case of CP, it has been observed that direct current electrical conductivity varies exponentially with absolute temperature. Temperature dependence of such conductivity has been described by Arrhenius-type **Equation 3.1**:

$$\sigma = \sigma_0 e^{\left(\frac{-E_g}{2kT}\right)} \quad (3.1)$$

Where:

σ : Electrical conductivity at temperature T ,

Conducting Polymer Nanocomposites for Supercapacitors

σ_0 : Pre-exponential conductivity,

E_g : Activation energy,

k : Boltzmann constant = 1.38×10^{-34} J/K, and

T : Absolute temperature.

The logarithmic form of **Equation 3.1** is written as **Equation 3.2**:

$$\log(\sigma) = \log(\sigma_0) - \frac{E_g}{2.303(2k)T} \quad (3.2)$$

Temperature dependence of electrical conductivity for CP was estimated in the range of applicability of an Arrhenius-type equation. Measured values were plotted as a function of the reciprocal of temperature. Conductivity increased with temperature but deviations at lower temperature were noted. Arrhenius behaviour can be regarded as a good approximation to band theory in relation to low temperature. The conduction mechanism in polymers could be explained by the well-known band structure. In general, organic polymers are insulators, so there are no mobile charge carriers to support conduction. However, appropriate charge carriers may be generated in organic polymers by partial oxidation or partial reduction. Several investigators [19–21] have suggested equations relevant to various modes for electrical conduction in composites. In Greave's equation, conductivity is a function of temperature in terms of the hopping conduction mechanism:

$$\sigma \sqrt{T} = e^{\left(\frac{-\beta}{\sqrt{T}}\right)} \quad (3.3)$$

Equation 3.3 represents a variable range hopping (VRH) conduction mechanism. In Matare's [20] **Equation 3.4**, conductivity is a function of temperature in terms of electrical conduction, including grain boundary barriers:

$$\sigma = A \sqrt{T} e^{\left(\frac{-E_g}{kT}\right)} \quad (3.4)$$

Zeller's equation [21] for tunneling conduction is expressed by **Equation 3.5**:

$$\sigma = \sigma_o e^{\left(\frac{-A}{\sqrt{T}}\right)} \quad (3.5)$$

Zuo [22] proposed a PANI salt as a 3D granular metal. However, Lundberg suggested the electron state of PANI salt to be localised and the conductivity to be due to quasi-one-dimensional (1D) VRH. According to Wang [23], PANI salts represent a class of quasi-1D-disordered conductors consisting of bundles of closely coupled chains in which electron states are 3D-extended. 3D metallic bundles correspond to crystalline regions of the polymer and are separated from one another by amorphous regions. For the quasi-1D VRH between bundles, **Equation 3.6** can be applied for conductivity along the chain:

$$\sigma_T = \sigma_o e^{\left(-\sqrt{\frac{T_o}{T}}\right)} \quad (3.6)$$

' T_o ' – the characteristic temperature – can be used to calculate transport parameters such as charge localisation length (α^1), most probable hopping distance (R) and charge hopping energy (w) using **Equations 3.7–3.9**:

$$T_o = \frac{8\alpha}{N(E_f)Zk} \quad (3.7)$$

$$R = \frac{\sqrt{T_o}}{4\alpha\sqrt{T}} \quad (3.8)$$

$$w = Zk\frac{T_o}{16} \quad (3.9)$$

Where, Z is the number of nearest neighbouring chains, k is the Boltzmann constant and $N(E_f)$ is the density of states of Fermi energy for both signs of spin.

3.5 Nanostructure of Conductive Polymers

Nanotechnology has become an active field of research during the past decade because of its tremendous potential for various applications. If the size of many established, well-studied materials is reduced to the nanoscale, radically improved or new surprising properties often emerge.

Intrinsically, CP have been studied extensively due to their intriguing electronic and redox properties and numerous potential applications in many fields since their discovery in 1977. To improve and extend their functions, fabrication of the nanostructures of CP has attracted considerable attention because of the emergence of nanotechnology. Unlike conventional polymers, which are electrical insulators, CP are semiconducting and can be doped into regions of metallic conductivity. Semiconducting and metallic polymers are the fourth generation of polymeric materials. Their electrical conductivities can be increased by many orders of magnitude that cover the entire insulator–semiconductor–metal range. Various CP (especially their nanostructures) have received special attention recently in the areas of nanoscience and nanotechnology due to their: special conduction mechanisms; unique electrical properties; reversible doping/dedoping process; controllable chemical and electrochemical properties; processability [24, 25]. By offering metal-like electrical and optical properties in addition to the inherent ease of processing and mechanical flexibility of polymers, innovative new devices and applications have been made possible by CP. Moreover, the morphology of such materials can be tuned at the nanoscale.

Nanostructure CP materials are of exceptional interest due to their potential applications in EMI shielding, sensors, actuators, transistors and displays. This nanostructuring of materials by designing their dimensions to be of the order of hundreds of nanometres or lower often yields novel properties. Combining these two sources of innovation – CP and nanostructuring – has been an area of intense study in recent years, yielding innovative applications. CP can be synthesised in various sizes and morphologies, with useful distinction

being drawn between bulk and nanostructure CP. Bulk granular CP can be obtained readily through conventional processing methods: by dissolving the monomer in a strong acid and then polymerising it through addition of an oxidant [26]. For tubular CP, the options are more varied, with several synthetic methods under active research and development [27]. Using an external template to form CP nanostructures is the most conceptually straightforward synthetic method of all the known template syntheses. Various CP nanostructures have been prepared by a template-free method [28].

Electrospinning is an effective approach to fabricate long polymer fibres with diameters from micrometres down to 100 nm or even a few nanometres using strong electrostatic forces. This process creates an even mat of uniform thickness without imparting a high degree of alignment to deposited fibres [29–31]. Electrospinning is useful for fabrication of polymeric nanofibres but, unfortunately, most CP have low solubility, making them difficult to electrospin in diameters <100 nm [32]. This problem can be overcome by using a polymer blend. However, this process reduces the electrical conductivity of the resulting composite nanofibre.

The most popular approaches, however, are based on self-assembly methods, which are favoured for their simplicity and high throughput. If nanostructures can be induced to self-assemble, there is no longer a need for external manipulation through templates, lithography or electrospinning.

With tremendous research efforts, there is now a large variety of CP, with PA, PTH, Ppy and PANI being the most studied and promising types. PANI exhibits high conductivity, excellent environmental stability, and is low-cost and straightforward to synthesise. It is also unique among CP in that it has a reversible and relatively simple acid–base doping–dedoping pathway, which is useful for tuning its electrical and optical properties. Arguably the most promising method for synthesising PANI nanostructures is self-assembly, which is very advantageous in its simplicity and volume. However, self-assembly is only partly understood, with several already established models such

as ‘micelle theory’ and ‘phenazine theory’ at odds with more recent discoveries (‘nanosheet curling’ and ‘nanoparticle agglomeration’), leading to a fragmented understanding of this important topic.

An expanded PANI nanostructure self-assembly model, the ‘multi-layer theory’, goes beyond the scope of existing theories, thereby accommodating more recent discoveries. The expanded synthesis framework is based on a multi-layered approach incorporating intrinsic morphologies. The three proposed intrinsic morphologies underpinning this model are nanofibrils, nanosheets and nanoparticles, and the forces driving their subsequent self-assembly interactions are mainly π - π stacking, hydrogen bonding and charge–charge repulsion from protonation, respectively. These interactions between the three intrinsic morphologies give rise to observed growth, agglomeration and curling behaviours that ultimately generate complex multi-layered nanostructures such as double-walled CP nanotubes. The challenges that motivate much of this research have to do with understanding (and ultimately controlling) the morphology and underlying structure of nanostructure CP.

Several methods, such as hard and soft templates, as well as physical methodologies, have been used to synthesise CP nanostructures. In the hard template method, a template membrane is usually required to guide the growth of the nanostructures within the pores or channels of the membrane as a hard-template. This method leads to completely controlled nanostructures in terms of morphology and diameter, and dominated by pores or channels. The hard template method is a general tool to prepare material nanostructures, including metal, semiconductor and CP, which can be synthesised by chemical or electrochemical means. The diameter of the nanostructure is controlled by the size of the pores or channels in the membrane, whereas the length and thickness of the nanostructure is usually adjusted by changing the polymerisation time. For this reason, the hard template method is the most commonly used and most efficient approach for preparing well controlled and highly oriented nanostructures.

One disadvantage of the hard template method is complications in the preparation process and post-preparation process that often destroy or disorder the formed nanostructures. Also, the quantity of nanostructures produced by this method is limited by the size of the template membrane, which thereby limits its applications in large-scale production of nanostructures.

In general, preparation of CP nanostructures by a hard template method is carried out by chemical or electrochemical polymerisation. Synthesis of a chemical hard template is accomplished by immersing a membrane in a solution of the desired monomer, dopant, and oxidant, and then allowing monomer polymerisation within the pores serving as 'nanoreactors'. By controlling the polymerisation time, different types of nanostructures can be produced. Short polymerisations lead to tubules with thin walls, whereas longer polymerisations can produce thick-walled tubules or even fibres. For synthesis of an electrochemical hard template, a metal film coated on one surface of the membrane is required to carry out electrochemical polymerisation of the desired polymer within the pores of the membrane. Compared with the chemical hard template method, the electrochemical hard template method is more complex and expensive, but it is more controllable through changing current density, applied potential, and polymerisation time. On the other hand, large mass synthesis by the electrochemical hard template method is impossible because of the limiting size of the membrane used as the template.

The porous membrane is the basic and most important part of the hard template method. A typical template synthesis based on a porous membrane is illustrated in **Figure 3.6**. In **Figure 3.6a**, the porous membrane is the hard template used to produce CP nanotubes and nanowires. The growth of the CP is guided within the pores or channels of the membrane, and then the template is removed after polymerization. In **Figure 3.6b**, nanofibres as the hard template are used to produce CP nanotubes. Nucleation and growth of CP take place on nanofibre templates, and then the nanofibres are dissolved or depolymerised to obtain nanotubes. In **Figure 3.6c**, colloidal particles as the hard template are used to produce nanoporous membranes. CP

monomers are polymerised in the voids between colloidal particles. If colloidal particles are removed, a 3D CP porous structure remains.

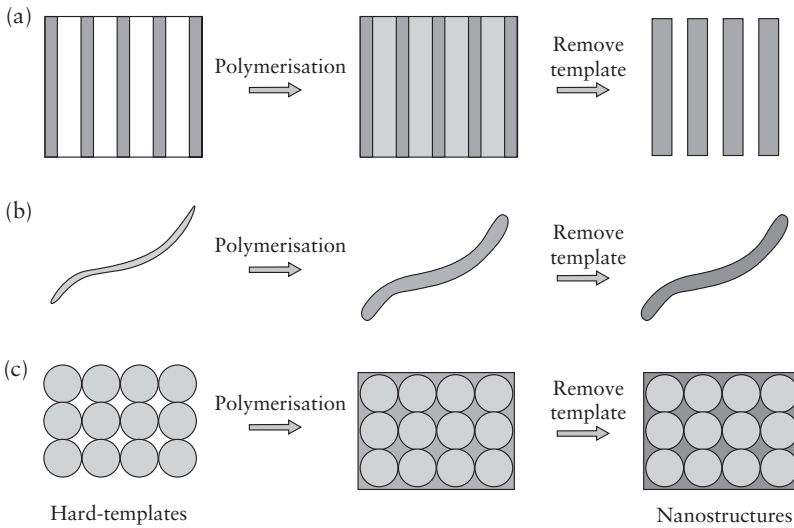


Figure 3.6 Hard-template synthesis of different CP nanostructures (schematic)

The soft template method is also called the ‘template free’ or ‘self-assembly’ method. It is another relatively simple, inexpensive, and powerful approach for fabricating CP nanostructures *via* self-assembly. Self-assembly is based on selective control of non-covalent interactions, such as hydrogen bonds, van der Waals forces, π - π stacking interaction, metal coordination, and dispersive forces as the driving forces of self-assembly. To date, surfactants, colloidal particles, structure-directing molecules, oligomers, soap bubbles and colloids as soft-templates, as well as interfacial polymerisation, have been employed to synthesise CP nanostructures.

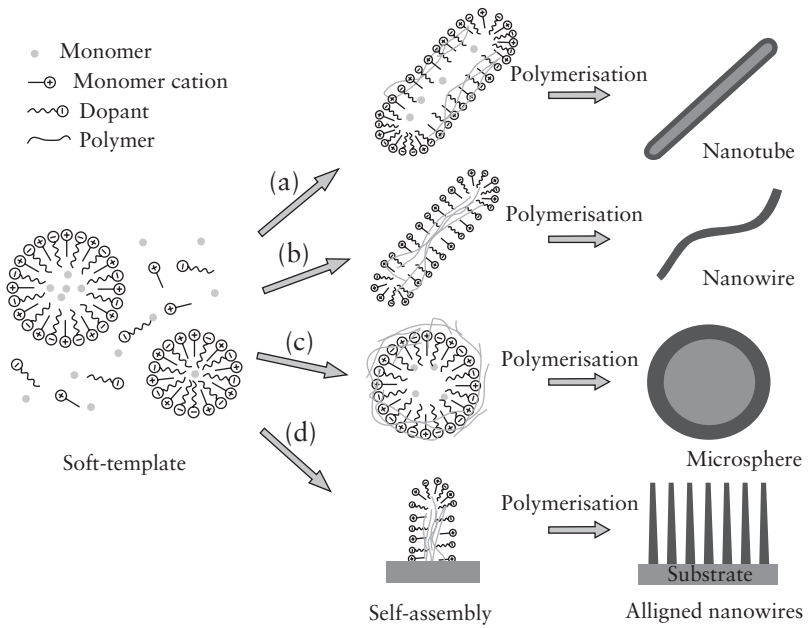


Figure 3.7 Mechanism of the soft-template synthesis of different CP nanostructures (schematic). a) Micelles act as soft-templates in nanotube formation. Micelles are formed by the self-assembly of dopants, and polymerisation is carried out on the surface of micelles; b) nanowires are formed by the protection of dopants. Polymerisation is carried out within micelles; c) monomer droplets act as soft-templates in microsphere formation; and d) polymerisation on the substrate produces aligned nanowire arrays. Nanowires are protected by dopants, and polymerisation is carried out preferentially on the tips of nanowires

Surfactants are a class of molecules that form thermodynamically stable aggregates of inherently nanoscale dimensions in solution and at interfaces. Surfactant self-assembly in a solution has been investigated by theoretical and experimental means owing to its importance in the synthesis of micro- or nanoscale structures with

controlled dimensions. The equilibrium size and shape of surfactant aggregates are controlled by the volume and length of the surfactant tail within the hydrophobic core of the aggregate and the effective area occupied by each surfactant head group at the surface of the aggregate. The favoured aggregate morphology of a surfactant in a solution is spherical, cylindrical, or a flat bilayer, depending on these parameters. The self-assembly ability of surfactants in a bulk solution, therefore, creates the possibility of surfactant micelles serving as soft-templates to form CP nanostructures (Figure 3.7).

References

1. M. Trojanowicz, *Microchimica Acta*, 2003, **143**, 75.
2. R.S. Jadhav, D.G. Hundiwale and P.P. Mahulikar, *Journal of Coating Technology Research*, 2010, **7**, 449.
3. R. Holze, *Journal of Applied Electrochemistry*, 2009, **39**, 953.
4. J. Jang, *Emissive Materials Nanomaterials*, 2006, **199**, 189.
5. J. Stejskal, *Polymer International*, 2009, **58**, 872.
6. C. Laslauer, Z. Zujovica and J.T. Sejdica, *Progress in Polymer Science*, 2010, **35**, 1403.
7. T.A. Skotheim, R.L. Elsenbaumer and J.R. Reynolds in *Handbook of Conducting Polymers*, 2nd Edition, Marcel Dekker, New York, NY, USA, 1998.
8. T.M. Swager, *Chemical Research Toxicology*, 2002, **15**, 125.
9. A. MacDiarmid, *Synthetic Metals*, 2002, **125**, 11.
10. A.J. Heeger, *Chemical Society Review*, 2010, **39**, 2354.

11. A.R. Bishop, D.K. Campbell and K. Fesser, *Molecular Crystal Liquid Crystal*, 1981, 77, 253.
12. J.L. Bredas, B. Themans, J.M. Andre, R.R. Chance and R. Silbey, *Synthetic Metals*, 1984, 9, 265.
13. R.H. Baughman and L.W. Shacklette, *Synthetic Metals*, 1987, 17, 173.
14. G. Wegner, *Angewandte Chemie International Edition*, 1981, 20, 361.
15. B. Horovitz, *Physical Review Letters*, 1985, 55, 1429.
16. S. Kivelson and A.J. Heeger, *Physical Review Letters*, 1985, 55, 308.
17. J.C. Chance and A.G. MacDiarmid, *Synthetic Metals*, 1986, 13, 193.
18. A.J. Epstein, J.M. Ginder, F. Zhuo, R.W. Gibelow, H.S. Woo, D.B. Tanner, A.F. Richter, W.S. Huang and A.G. MacDiarmid, *Synthetic Metals*, 1987, 18, 303.
19. N.F. Mott, *Journal of Non Crystalline Solids*, 1980, 1, 1.
20. M. F Matare, *Journal of Applied Physics*, 1984, 56, 2605.
21. H.R. Zeller, *Physical Review Letters*, 1972, 28, 1452.
22. F. Zuo, M. Angelopoulos, A.G. MacDiarmid and A.J. Epstein, *Physical Review*, 1987, 26, 475.
23. Z.H. Wang, E.M. Scherr, A.G. MacDiarmid and A.J. Epstein, *Physical Review*, 1995, 62, 976.
24. Y.Z. Long, *Progress in Polymer Science*, 2011, 36, 1415.
25. J.S. Im, J.G. Kim, S. Lee and Y.S. Lee, *Colloids and Surfaces A: Physicochemical Engineering Aspects*, 2010, 364, 151.

26. E.T. Kang, K.G. Neoh and K.L. Tan, *Progress in Polymer Science*, 1998, **23**, 277
27. *Conjugated Polymers: Theory, Synthesis, Properties and Characterization*, 3rd Edition, Eds., T.A. Skotheim and J.R. Reynolds, CRC Press, Cleveland, OH, USA, 2006.
28. D.H. Reneker and I. Chun, *Nanotechnology*, 1996, **7**, 216.
29. S.J. Kim, S.M. Yun and Y.S. Lee, *Journal of Industrial Engineering Chemistry*, 2010, **16**, 273.
30. J.S. Im, J.S. Jang and Y.S. Lee, *Journal of Industrial Engineering Chemistry*, 2009, **15**, 914.
31. J.S. Im, S.J. Park and Y.S. Lee, *International Journal of Hydrogen Energy*, 2009, **34**, 1423.
32. H.J. Ding, Y.J. Long, J.Y. Shen and M.X. Wan, *Journal of Physical Chemistry B*, 2010, **114**, 115.

4 Nanocomposites

4.1 Introduction

A ‘composite’ is a material composed of two or more different materials with the properties of the resultant material being superior to the properties of the individual materials that comprise the composite. A composite is a structural material that consists of the combination of two or more constituents [1]. In these constituents, one of them is called the ‘reinforcing phase’ and the other (in which it is embedded) is termed the ‘matrix phase’. The material in the reinforcing phase may be in a fibre, particle or flake. The materials in the matrix phase are, in general, continuous (e.g., epoxy reinforced with graphite fibres, nanoparticle-reinforced polymers). Overall, composites are more efficient, possess the advantages of their constituents, and have improved strength, stiffness, thermal conductivity, and corrosion resistance.

Composites are classified by the geometry of the reinforcement (particulate, flake and fibre) or by the type of matrix (polymer, metal, ceramic) (**Figure 4.1**).

In a composite, even if one of the constituents is in the nano-size range, then it is called a ‘nanocomposite’. If the nano-sized particulate/flake/fibre is reinforced with a polymer matrix, then it is called a ‘polymer nanocomposite’. A polymer nanocomposite is a multi-phase solid material in which one of the phases has one, two- or three-dimensions that is <100 nanometres (nm) in different polymer matrices.

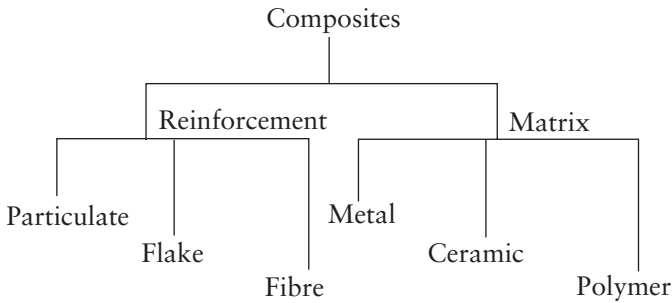


Figure 4.1 Classification of composites

Nanocomposites are suitable for applications as high-performance composites, where good dispersion of the filler can be achieved and the properties of the nanoscale filler are substantially different or better than those of the matrix. If the polymer is conducting, it is called a ‘conducting polymer’ (CP)-nanocomposite. A ‘CP binary nanocomposite’ is a structural material that combines two constituents, with one of them in the reinforcing phase (nano-sized particulate/flake/fibre) and the other (in which the reinforcing phase is embedded) in the CP matrix phase. A ‘CP ternary nanocomposite’ is a structural material that combines three constituents, with two of them in the reinforcing phase (nano-sized particulate/flake/fibre) embedded in a CP matrix phase.

4.2 Conducting Polymer Nanocomposites

In the area of nanotechnology, CP matrix-based nanocomposites have generated considerable attention recently. CP provide tremendous scope for tuning of their electrical conductivity from semiconducting to metallic regimes. CP conductivity can be ‘tuned’ by electrical manipulation of the polymer backbone by the nature of the dopant, by the degree of doping, by blending with other polymers (‘co-polymers’), and by creating composites with inorganic materials.

If CP are taken in a composite form, their properties are altered from those of basic materials. It has been shown that the conductivity of these heterogeneous systems is dependent upon several factors, such as the concentration of the conducting fillers, their shape, size, and orientation, as well as interactions between filler molecules and the host matrix. Polymeric materials are, in general, thermal insulators, so nanoscale fillers with superior thermal transport characteristics are incorporated into polymeric matrices to prepare nanocomposites that exhibit a good combination of processability and thermal conductivity [2]. The geometric shape of the dispersant governs the ability of conductive network formation, which results in a large increase in conductivity. Also, dispersant–matrix interactions and the physical properties of the matrix influence agglomeration of the dispersant phase, which affects the properties of composites. Using natural reagents and polymers such as carbohydrates, lipids, and proteins in nature makes strong composites such as bones, shells, and wood. These are examples of nanocomposites, made by mixing two phases such as particles, layers or fibres, in which at least one of the phases is in the size range 1–100 nm.

A nanocomposite is defined as a material with more than one solid phase, metal, ceramic, or polymer, compositionally or structurally, in which at least one-dimension falls in the nanometre range. Many binary nanocomposite materials are composed of just two phases; one is termed the ‘matrix’, which is continuous and surrounds the other phase, which is often called the ‘dispersed phase’. Properties of nanocomposites are a function of the properties of the constituent phases, their relative amounts, and the geometry of the dispersed phase. There have been great efforts to fabricate nanocomposite to obtain unique physical properties because these properties become increasingly dependent upon size at low dimensions.

Combination of the nanomaterial with a polymer is very attractive not only to reinforce the polymer but also to introduce new electronic properties based on morphological modification or electronic interactions between the two components. Properties of a nanocomposite are influenced greatly by the size scale of its component

phases and the degree of mixing between the two phases. Depending on the nature of the components used and the method of preparation, significant differences in composite properties can be obtained. Nanocomposites of CP have been prepared by various methods, such as colloidal dispersions [3], electrochemical encapsulation [4], coating of inorganic polymers, and *in situ* polymerisation with nanoparticles [5], and have opened new avenues for material syntheses. Combination of magnetic nanoparticles with CP leads to formation of ferromagnetic CP-nanocomposites possessing a unique combination of electrical and magnetic properties.

The feasibility of CP as materials for supercapacitors was demonstrated first by Rudge and co-workers [6]. Subsequently, a variety of such polymers has been investigated and, among them, polyaniline (PANI), polypyrrole (Ppy), polythiophene (PTH) and their substituted monomers are important. Prerequisites for CP-based supercapacitors are environmental stability, facile doping, dedoping and ease of fabrication.

In the chemical synthesis of PANI and Ppy pertaining to their feasibility as supercapacitors, various dopants, initiators, templates and oxidants have been employed [7–11]. Soft templates include various surfactants, seeded growth, and biotemplates [12–17]. For stability and suitable adhesion upon electrodes, binders such as polytetrafluoroethylene, polyvinylidene fluoride, N-methyl pyrrolidone (NMP) and Nafion have been employed. A novel synthesis of PANI nanowires using dilute polymerisation on gold/chronium layers thermally etched on polyethylene terephthalate films leads to the design of microsupercapacitors [18]. PANI-nanocomposites and Ppy-nanocomposites with diverse forms of carbon and oxides have been synthesised using various oxidants such as iron(III) chloride, ammonium persulfate, potassium permanganate, potassium dichromate, iron(II) chloride, and iron(III) nitrate, under acidic conditions. The synthesised material can then be pressed into pellets or coated onto electrodes using appropriate binders. Several interesting morphologies arise in chemical syntheses of CP-nanocomposites if soft templates such as

Cetyltrimethylammonium bromide, dodecyl benzenesulfonic acid, dodecyl(trimethyl)azanium bromide, noctadecyl(trimethyl) ammonium, or sodium dodecyl sulfate are employed. Apart from carbon-based substrates, other electrodes commonly employed are nickel, stainless steel (SS), titanium, indium tin oxide, tantalum, glassy carbon, gold, platinum, and silver.

Conducting PANI is a promising CP due to its high conductivity, ease of preparation, good environmental stability, and large variety of applications [19, 20]. These properties make this polymer suitable for gas sensors [21], functional hybrids [22], as a pH-switching electrical-conducting biopolymer hybrid for sensor applications [23], as an electrically active redox biomaterial for sensor applications [24], and as a matrix for preparation of CP-nanocomposites [25, 26]. Therefore, there has been increasing interest in preparation of nanocomposites based on PANI. A literature review on CP-nanocomposites shows that PANI has been used for nanocomposite preparation [27, 28]. If nanostructure filler particles are magnetic in a polymer matrix, then such nanocomposites show enhanced magnetic and transport properties of the polymer [29].

4.3 Conducting Polymer Binary Nanocomposites for Supercapacitors

High power/energy density, flexibility, and long life-cycle of supercapacitors can be achieved using suitable active electrodes. To improve energy density without losing power density and long life-cycle for future applications, finding new active materials and composites is essential. To date, activated carbon, carbon aerogel, carbon nanotubes (CNT), graphene, PANI, Ppy, PTH, poly(3,4-ethylenedioxythiophene) (PEDOT), ruthenium(IV) oxide, manganese oxide, iron(III) oxide, vanadium(V) oxide, nickel(II) oxide, zinc oxide, manganese ferrite and nickel ferrite have been used as active electrodes. In these carbon-based supercapacitors, energy can be stored based on an electrical double-layer (EDL) mechanism. In the case of CP and metal oxides, 'pseudocapacitive' charge storage

is prominent. 'Pseudocapacitors' provide higher energy density than EDL capacitors due to fast surface redox reactions. Ruthenium(IV) oxide is a promising active material in this class that supplies higher energy density compared with other active materials, and exhibits higher specific capacitance (SC) of ≤ 737 F/g. But commercialisation of ruthenium(IV) oxide is quite difficult due to the high cost of the noble metal ruthenium.

For use of supercapacitors in a wide range of applications, development of low-cost active electrode materials is inevitable. CP like PANI, PPy and PTH are low cost and good materials for supercapacitor applications. Among CP, PANI has attracted much attention and extensive research has been carried out owing to its environmental stability, high electronic conductivity in the doped state, and multiple oxidation states. Moreover, the monomer of PANI is inexpensive and abundant in nature. However, PANI suffers from volumetric shrinkage during dedoping (discharge) processes, which leads to reductions in cycling stability.

To conquer this problem, researchers have focused on enhancement of the cyclic stability of CP by making composites with particulate reinforcement with metal oxides and ferrites, fibre reinforcement with CNT, or flake reinforcement with graphene. CP have been composited with any one of these materials constituting binary nanocomposites and any two of these materials constituting ternary nanocomposites. In this way, the capacitive performances of such advanced functional and hybrid materials have been improved by synergistic effects, particularly for supercapacitor applications.

In the rapidly developing field of electrochemical supercapacitors, an exhaustive critical review encompassing the following features is not possible: (i) choice of electrode materials (metals, metal oxides, CNT, graphene and related materials, metal-polymer composites); (ii) their structural characterisation using spectroscopic and microscopic studies; (iii) influence of ionic liquids on SC; (iv) fabrication of supercapacitor devices and their marketability/

cost effectiveness; (v) efficacy of hybrid supercapacitors; and (vi) theoretical modelling of supercapacitors.

Several reviews on electrochemical supercapacitors have appeared during recent years with different perspectives. Consequently, our *critique* covers the literature on electrochemical supercapacitors based on PANI and Ppy during 2006–2014 with particular emphasis on electrochemical syntheses and electrochemical characterisation. A *critique* of CP-based supercapacitors would not be complete without analysing nanocomposite-based materials. The latter have received considerable attention recently in view of their versatility, as well as their ability to provide higher power densities and faster charge–discharge responses. A major limitation of CP-based systems coated on metal substrates is the sluggish rate of ion transport during redox reactions. This weakness can be obviated by employing nanostructures of appropriate shapes.

4.3.1 Particulate-reinforced Nanocomposites

‘Particulate’ refers to nanoparticles which are zero-dimensional (0D) nanomaterials. Examples of 0D nanomaterials are quantum dots, nanoparticles of metals, and metal oxides. Here, we report the preparation of metal oxide nanoparticle-reinforced CP-nanocomposites.

The synthesis of CP binary nanocomposites by *in situ* polymerisation is shown as a flow chart in **Figure 4.2**. It shows the preparation of novel electrically conducting binary nanocomposite materials consisting of nickel oxide nanoparticles dispersed in PANI by *in situ* polymerisation using ammonium persulfate as an oxidant in an acidic medium [30]. The possible interaction of polymer and filler is shown in the form of the structure of PANI–nickel(II) oxide nanocomposites (**Figure 4.3**).

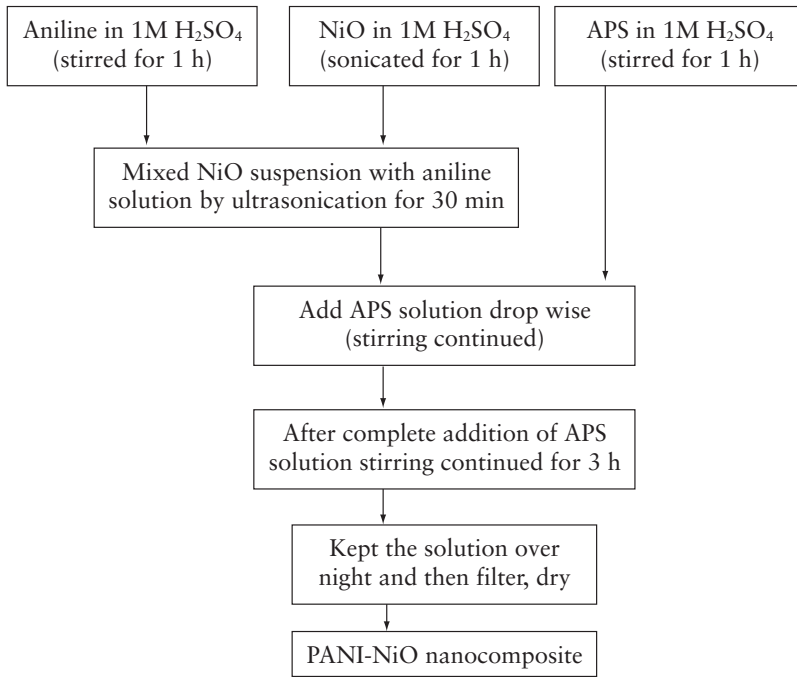


Figure 4.2 Flow chart for the synthesis of CP binary [PANI–nickel(II) oxide] nanocomposites

Song and co-workers prepared PANI–nickel(II) oxide nanoparticles, ‘nanobelts’ and nanotubes in the presence of sodium dodecyl benzenesulfonate that showed improved conductivity, thermal stability, and electrochemical stability [31–33]. Xu-Yuan Peng and co-workers studied electrochemical co-deposition of nickel(II) oxide and PANI, and showed the enhanced catalytic activities of the composite material [34]. Yanni Qi and co-workers demonstrated that the thermal stability and glass transition temperature of PANI–nickel(II) oxide composites increased with increasing nickel(II) oxide content in PANI [35].

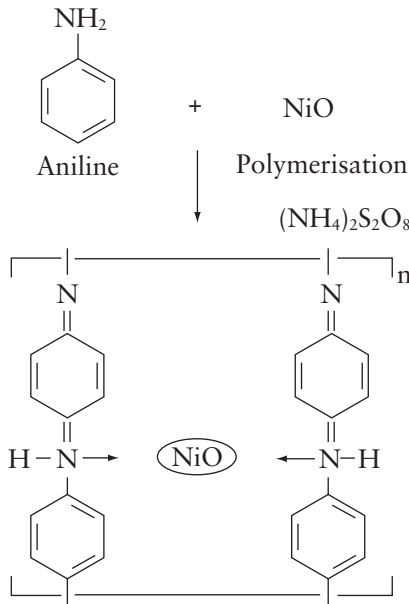


Figure 4.3 PANI–nickel(II) oxide nanocomposite (schematic)

CP binary nanocomposites can also be prepared by the solution route method. Kondawar and co-workers compared a PANI-tin oxide nanocomposite (sample A) prepared by *in situ* polymerisation of aniline in the presence of as-synthesised tin oxide nanoparticles (Figure 4.2) wherein the sol-gel method was used for the synthesis of tin oxide nanoparticles. In a typical method, 0.1 M $\text{SnCl}_4 \cdot 5\text{H}_2\text{O}$ was added to 1 M starch solution and the mixture was stirred for 0.5 h. Then, 0.2 M ammonia was added dropwise into the solution under constant stirring. Stirring was continued for a further 2 h and then the solution was allowed to settle overnight. Supernatant liquid was discarded carefully and the remaining solution centrifuged for 10 min and then filtered. The precipitate of tin oxide was washed completely using distilled water to remove byproducts and excess starch bound to nanoparticles. The product was dried in hot-air oven

at 80 °C overnight. Then, the powder was sintered at 600 °C for 10 h and nanocrystalline tin oxide obtained. Tin oxide-intercalated PANI nanocomposite (sample B) was prepared using tin chloride ($\text{SnCl}_4 \cdot 5\text{H}_2\text{O}$) as a precursor during the polymerisation of aniline.

The solution route method was used to synthesise PANI–tin oxide nanocomposite (sample B). In this method, formation of a nanocomposite proceeded through a reaction at the inorganic–organic interface. First, 2 g of $\text{SnCl}_4 \cdot 5\text{H}_2\text{O}$ in 50 ml of double-distilled water was stirred for 0.5 h and its pH was maintained at ≤ 4 using 0.1 M hydrochloric acid. Then, 10 ml hydrogen peroxide was added in this solution, which oxidised tin ions to tin oxide. The solution turned into a white colour suspension of tin oxide, and this reaction mixture was mixed with 0.1 M aniline and maintained below 4 °C. A 0.1-M ammonium persulfate solution was added in this mixture at room temperature (RT): the colour of the solution turned blue and then green after a few minutes. The precipitate produced in the reaction was removed by filtration, washed repeatedly with 1 M hydrochloric acid, and dried under vacuum for 24 h. The composite powder was a conductive emeraldine salt of PANI–tin oxide nanocomposite (sample B). PANI–tin oxide nanocomposites were found to be good materials for supercapacitor electrodes as compared with those of pure PANI [37]. Formation of the PANI–tin oxide nanocomposite is shown in **Figure 4.4**.

PANI–zinc oxide nanocomposites in various wt% of nanostructure zinc oxide were synthesised by *in situ* polymerisation [38]. Nanostructure zinc oxide was prepared by a microwave-assisted hydrothermal route. In a typical process, 0.5 g of $\text{Zn}(\text{NO}_3)_2 \cdot 4\text{H}_2\text{O}$ was dissolved into 100 ml deionised water under continuous stirring. After 10 min of stirring, 10 ml of 2 M sodium hydroxide aqueous solution was introduced drop-wise into the solution under stirring, resulting in a white aqueous solution that was transferred into a TeflonTM-line SS autoclave. The autoclave was put into a silica carbide chamber and introduced into a microwave irradiation system. The microwave oven had a chamber of dimensions 360 × 210 × 430 mm with a 2.45-GHz frequency multimode source and maximum deliverable power

output of 700 W. Samples were prepared at different conditions of microwave power and irradiation time. Reaction products in the form of a precipitate were filtered and washed with distilled water and ethanol to remove ions remaining in the final products. Finally, products were dried in a hot-air oven at 80 °C. The final (white) products were collected for the preparation of nanocomposites in a PANI matrix. Polymerisation of the monomer (aniline) was initiated by drop-wise addition of oxidising agent (ammonium persulfate) in acidified solution (hydrochloric acid) prepared using double-distilled water under constant stirring at 0–4 °C. During stirring, prepared zinc oxide was added for syntheses of PANI–zinc oxide nanocomposites using *in situ* polymerisation.

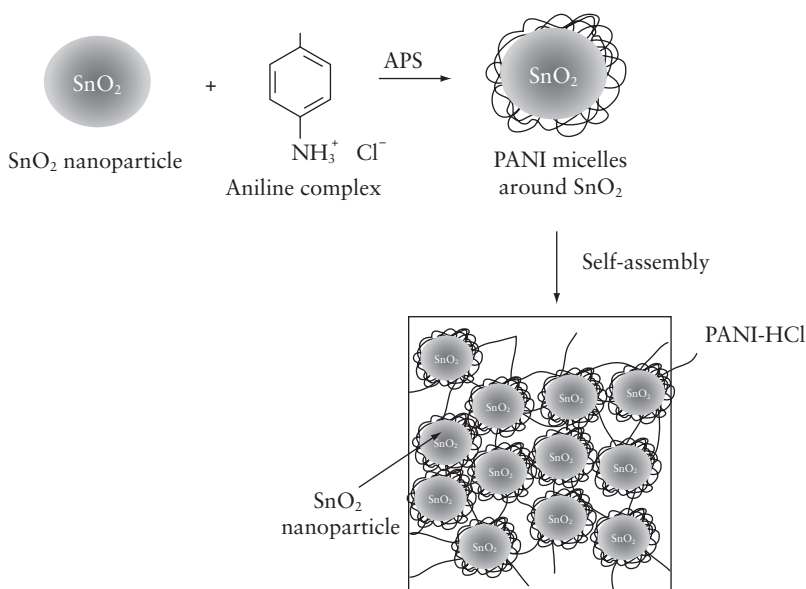


Figure 4.4 PANI–tin oxide nanocomposite (schematic).
APS: Ammonium peroxydisulfate

PANI–nickel ferrite nanocomposites can be prepared in a manner similar to that of *in situ* polymerisation [39]. In a typical process,

0.1 M of aniline monomer is dissolved in 40 ml of 2 M sulfuric acid. As-synthesised nanoparticles of nickel ferrite prepared by the solution combustion method are added and mixed with the monomer solution. Then, 0.125 M of potassium dichromate as an oxidant is dissolved in 50 ml of double-distilled water and added drop-wise into the monomer solution, which is maintained under constant stirring for 2 h. Polymerisation is identified by a change in the colourless solution to a green colour. Loading of nickel ferrite improves the conductive network and electrochemical properties of PANI due to the interaction between the polymer chain and nickel ferrite particles. **Figure 4.5** shows the representative cyclic voltammogram of PANI, nickel ferrite and PANI–nickel ferrite nanocomposite at 20 mV/s measured in the potential window of -0.2 V to 1.0 V *versus* silver/silver chloride. The cyclic voltammetry (CV) curves of PANI and PANI–nickel ferrite show two pairs of redox peaks, suggesting the pseudocapacitive behaviour of these materials. The first pair of redox peaks is due to the redox transition from the leucoemeraldine phase to the polaronic emeraldine phase. The second pair of redox peaks is due to the transition between polaronic emeraldine and bipolaronic pernigraniline [14]. The CV curve of nickel ferrite also shows oxidation and reduction peaks, but the observed peak current is very much lower than that for PANI and PANI–nickel ferrite composites. Also, the area under the CV curve of nickel ferrite is very small compared with other systems. The SC of an electroactive material is directly proportional to the area covered by the CV curve [40]. The CV curve illustrates that the area covered by PANI–nickel ferrite is higher than that for PANI, which may be due to the greater availability of the active sites of PANI and increases in the conducting network by formation of hydrogen bonds [41–43].

Figure 4.6 represents the galvanostatic charge–discharge (GCD) curves of PANI and PANI–nickel ferrite composite measured at a current density of 1 mA/cm². Charge–discharge profiles are quasi-symmetric and enumerate the pseudocapacitive behaviour of the material. The SC of PANI and PANI–nickel ferrite are calculated from the GCD curve using **Equation 2.7** (**Chapter 2**).

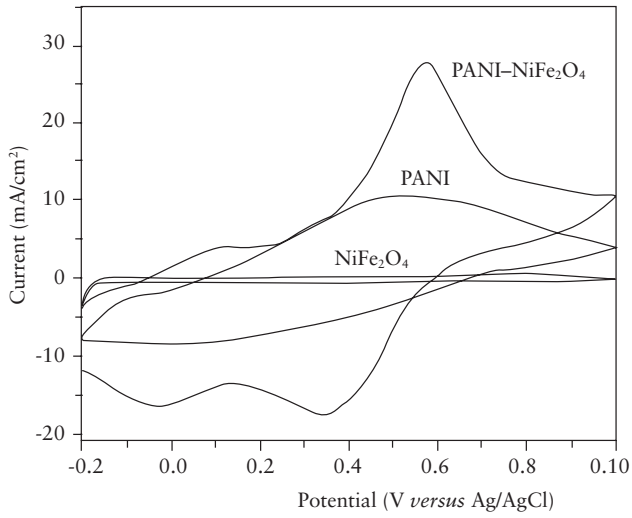


Figure 4.5 CV curves of PANI, nickel ferrite and PANI–nickel ferrite composite

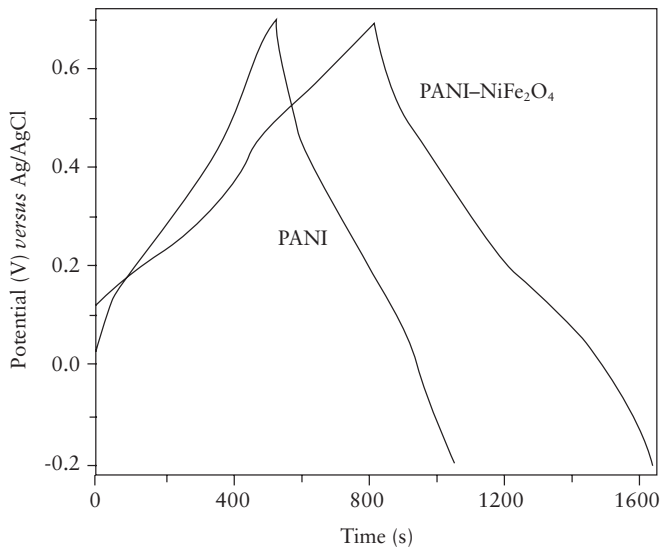


Figure 4.6 GCD curves of PANI and PANI–nickel ferrite

Figure 4.7 represents the variation of SC with respect to the applied current density. PANI–nickel ferrite shows higher SC of 448 F/g when compared with PANI (292 F/g). This observed enhanced SC of PANI–nickel ferrite may be due to the hydrogen bonding between PANI and nickel ferrite. It may also be due to increases in the crystalline nature as well as conducting pathways of PANI, which results in higher SC. It also illustrates that the SC of PANI and PANI–nickel ferrite decreases with increases in current density. It is well known that at low current density, ions in the electrolyte have a long time to diffuse into the inner surface of the electrode material. Hence, at lower current density, the inner and outer surfaces contribute to electrochemical activity, thereby leading to higher SC of the material. In a similar way, at higher current density, only the contribution of the outer surface of the electrode material is higher than that of the inner surface because of the limited access time of ions from the electrolyte. The CV study of pure PANI and PANI–nickel ferrite elucidates good electrochemical performance. The maximum SC of PANI–nickel ferrite compared with that of pure PANI shows that PANI–nickel ferrite is a suitable electrode material for supercapacitor application.

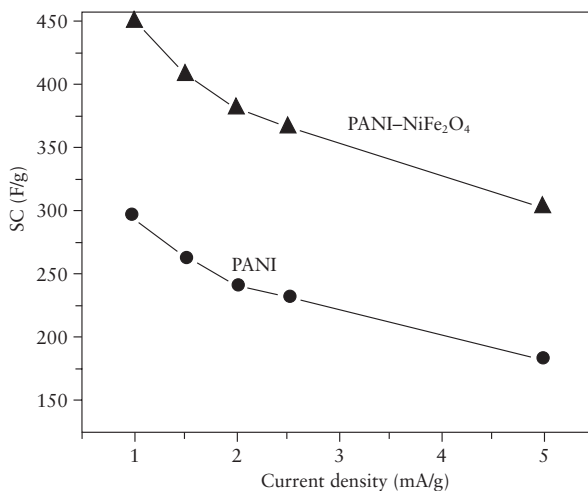


Figure 4.7 SC versus current density of PANI and PANI–nickel ferrite

4.3.2 Flake-reinforced Nanocomposites

Two-dimensional (2D) materials are flakes. Graphene has a 2D ‘honeycomb’ lattice structure of a flake with thickness in the nano-regime. Graphene exhibits unusual and intriguing physical, chemical and mechanical properties [44]. Here, we report on the preparation of graphene reinforced CP-nanocomposites.

Graphene is the basic structural unit of some carbon allotropes, including graphite, CNT and fullerenes. It is believed to be composed of benzene rings stripped of their hydrogen atoms. The ‘rolling up’ of graphene along a given direction can produce a CNT. In 2004, Geim and co-workers at Manchester University (Manchester, UK) successfully identified single layers of graphene. They stated that the promising mechanical, electrical, optical, thermal and magnetic properties of graphene have “led to the creation of a new and exciting ‘laboratory’ for the study of fundamental science.”

Graphene can be prepared using four methods. The first is chemical vapour deposition (CVD) and epitaxial growth, such as the decomposition of ethylene on nickel surfaces. The second is micromechanical exfoliation of graphite, which is also known as the ‘scotch tape’ or ‘peel-off’ method. The third method is epitaxial growth on electrically insulating surfaces, and the fourth is solution-based reduction of graphene oxide (GO) [45].

Graphene is a single-layer of carbon atoms packed densely into a ‘honeycomb’ crystal lattice. The carbon–carbon bond (sp^2) length in graphene is ≈ 0.142 nm and the thickness of the graphene layer is 0.35–1.00 nm. Pristine graphene materials are unsuitable for intercalation by large species such as polymer chains because graphene as a bulk material has a pronounced tendency to agglomerate in a polymer matrix. It is likely that oxidation followed by chemical functionalisation facilitates dispersion and stabilises graphene to prevent agglomeration. Chemical functionalisation of graphene is a particularly attractive target because it can improve the solubility and processability as well as enhance the interactions with organic

polymers [46]. Park and co-workers [47] reported a simple route for the preparation of a homogeneous aqueous suspension of chemically modified graphene with good electrical conductivity. In this method, the precursor GO was first dispersed in water followed by addition of an aqueous potassium hydroxide solution (Figure 4.8).

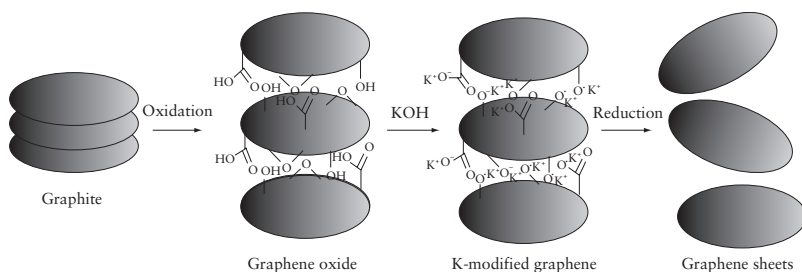


Figure 4.8 A simple route for the preparation of graphene sheets from graphite

The strong base potassium hydroxide can confer a large negative charge through reactions with the reactive hydroxyl, epoxy and carboxylic acid groups on GO sheets, resulting in extensive coating of the sheets with negative charges and K⁺. Addition of hydrazine monohydrate to potassium hydroxide-treated GO can produce a homogeneous suspension of graphene sheets. The mechanism for the interaction in polymer–graphene nanocomposites is dependent upon the polarity, molecular weight, hydrophobicity, and reactive groups present in the polymer, graphene–graphite, and solvent.

A graphene–polyaniline (G–PANI) composite material has been used recently for energy application [48–52]. As the result of the high quality of the sp² carbon lattice, electrons have been found to move ‘ballistically’ into the graphene layer, even at ambient temperatures. Bai and co-workers prepared a G–PANI nanocomposite and discussed

how the graphene could be exploited for energy applications [53]. G-PANI has been synthesised using graphene which has been applied in conjunction with an aniline monomer to produce a highly conductive nanocomposite material [54]. G-PANI nanocomposites can be chemically synthesised by oxidative polymerisation of aniline using ammonium peroxydisulfate (APS) under controlled conditions in an acidic medium (**Figure 4.9**).

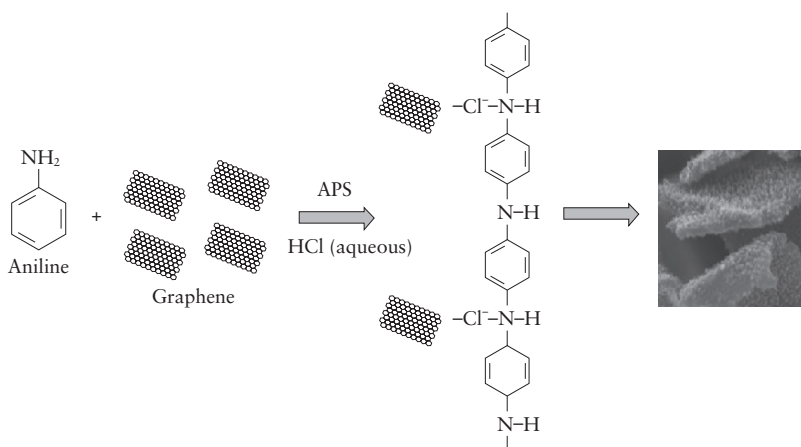


Figure 4.9 Synthesis of a G-PANI nanocomposite (schematic)

Figure 4.10 shows the CV of a G-PANI nanocomposite *versus* silver/silver chloride at a scan rate of 100 mV/s in 0.2 M hydrochloric acid. A reversible redox system with oxidation peaks at 0.3, 0.68 and 0.92 V, and reduction peaks at 0.7, 0.42, and -0.05 V, respectively, can be observed. The peak centred at 0.65 V is attributed to the oxidation of the emeraldine form of PANI, whereas the peak at 0.86 V is due to the pernigraniline form of PANI [55].

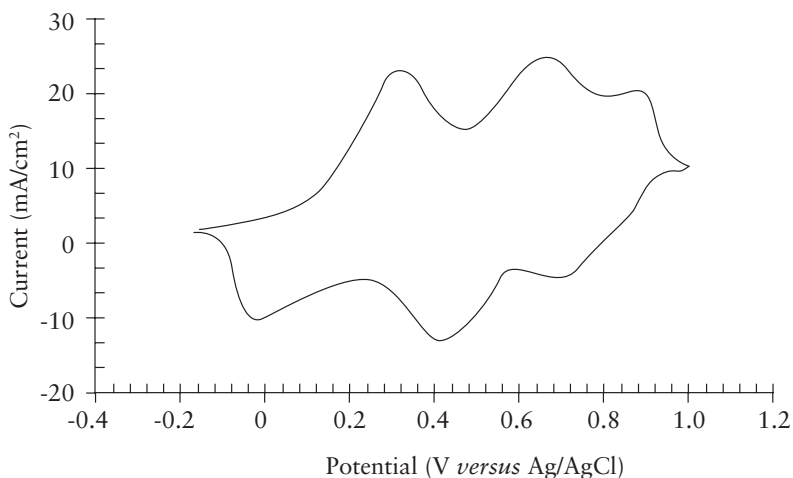


Figure 4.10 CV of a G-PANI nanocomposite in 0.2 M hydrochloric acid

Freestanding and flexible PANI-graphene composite paper (GPCP) has been prepared by *in situ* anodic electropolymerisation (AEP) of aniline on graphene paper (GP) [56]. Briefly, polymerisation was carried out using a three-electrode AEP cell. In this process, a platinum-plate, standard calomel electrode (SCE) and GP were used as the counter, reference and working electrodes, respectively. Aniline (0.05 M) and sulfuric acid (0.5 M) were used as the electrolyte. PANI was electropolymerised *in situ* on GP at a constant potential of 0.75 V *versus* the SCE for different periods (60, 300 and 900 s). CV results of GP and GPCP showed that in the case of GP, only one pair of redox peaks was observed due to the transition between quinone/hydroquinone groups. On the other hand, two redox peaks were observed from GPCP, suggesting the presence of pseudocapacitive PANI.

A high performing PANI-graphene composite electrode was prepared using a spin-coating method [57]. Briefly, an aqueous dispersion

of purified GO films was deposited on a quartz substrate using a deep-coating method followed by thermal reduction to obtain a graphene film. A dark-blue solution of PANI in NMP was then spin-coated on graphene films. The SC of the pure PANI and as-prepared G–PANI composites was a function of scan rates. The SC of G–PANI composites was much higher than that of pure PANI. Enhanced SC was attributed to the synergism between graphene nanosheets and PANI.

Chemically modified graphene and PANI nanofibre composites have been prepared by *in situ* polymerisation of an aniline monomer in the presence of GO under acidic conditions [58]. Resulting PANI–GO composites with different mass ratios were reduced to a graphene composite by hydrazine monohydrate followed by reoxidation and reprotonation of reduced PANI to give PANI–graphene nanocomposites. The electrical conductivity of GO, PANI, PANI–GO and PANI–graphene were reported to be 0.2, 10.6, 231.2 and 168.7 S/m, respectively. Conductivity of PANI–graphene composites was found to be slightly lower than that of PANI–GO composites. This finding was probably due to a decrease in the degree of doping in PANI and a change in the morphology of composites during reduction, reoxidation and reprotonation. CV showed that most of the composites had high SC and good cycling stability, with PANI–graphene composites showing the highest SC of 480 F/g at a current density of 0.1 A/g.

Ppy–GO nanocomposites have been prepared using electrochemical co-deposition for supercapacitors [59]. During deposition, an aqueous solution containing 0.25 M pyrrole monomer and 2 mg GO was dispersed under ultrasonication for ≈ 15 min to form a metastable homogenous colloidal solution that could last for >24 h at RT. Ppy–GO nanocomposites were electrodeposited onto fluorine-doped tin oxide (FTO) conducting glasses in galvanostatic mode in which a current of 1.0 mA/cm^2 was applied from 200 to 2,700 s. After electrodeposition, the composite-coated glasses were washed with enough deionised water to remove unreacted substances, followed by drying at RT in ambient air. During deposition, the cleaned FTO

conducting glasses were fixed in a two-electrode cell with a large-area platinum sheet acting as the counter electrode and pseudo-reference electrode. CV and GCD tests were carried out to investigate the capacitive performance of Ppy-GO nanocomposite electrodes. **Figure 4.11** shows that the CV curve at a scan rate of 200 mV/s does not show obvious redox peaks in the whole potential range. This finding suggests that the electrode was charged and discharged at a pseudo-constant rate over the entire CV process. This is because the capacitor was assembled by two pieces of Ppy-GO-deposited FTO electrodes that were tested by a two-electrode system. During the test, one piece of composite electrode was oxidised whereas the other was reduced, resulting in the non-obvious oxidation/reduction peaks of Ppy and a rectangular CV shape. A rectangular-like CV curve with an almost symmetric I-V response can be observed at a scan rate of 200 mV/s, and exhibits the ideal capacitive behaviour of rapid charge and discharge. Hence, the composites can be candidates for electrochemical capacitors. The charge-discharge test was carried out at a GCD current density of 0.1 mA/cm² and the result is shown in **Figure 4.12**. During charge-discharge, the electrochemical redox reaction between the electrode and electrolyte can be illustrated as **Equation 4.1**:



For a fully charged state of the cells, the anodic process was neutral because the Ppy did not have n-doping ability, the cathodic process was in a fully oxidised state, and charge neutrality was maintained by GO⁻ ions. Upon discharge, Ppy in the cathodic process was reduced and the anode was oxidised to reach the same potential state, and the counter-ions ejected from the cathode were inserted in the anode electrode to maintain charge neutrality [59]. **Figure 4.12** shows that the charging curves are almost symmetrical to their discharging counterparts in the entire potential region, and that the triangular shape demonstrates the high-power performance of Ppy-GO nanocomposites.

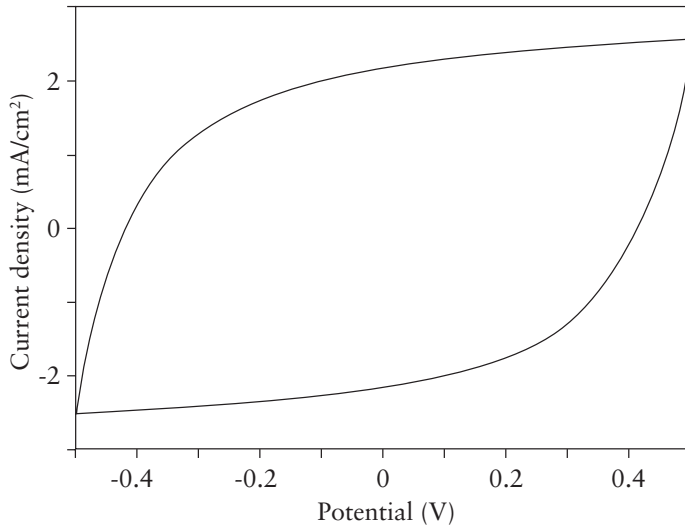


Figure 4.11 CV curve of Ppy-GO at a scan rate of 200 mV/s

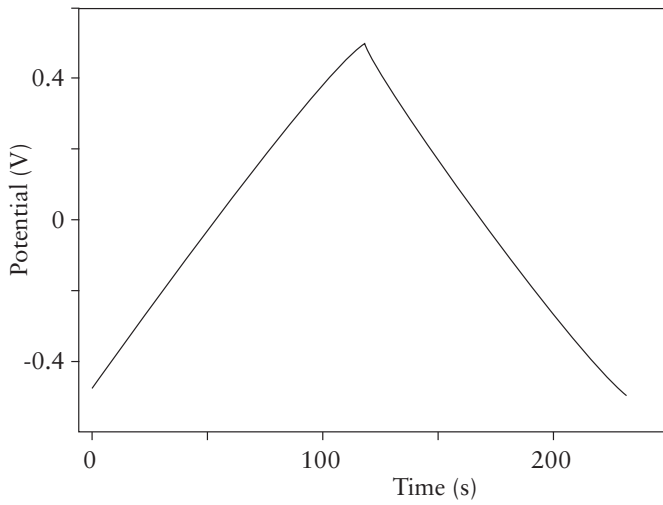


Figure 4.12 GCD curve at a current density of 0.1 mA/cm²

4.3.3 Fibre-reinforced Nanocomposites

Fibres are one-dimensional (1D) materials. Nanotubes, ‘nanorods’, ‘nanowires’, and ‘nanofibres’ are examples of 1D nanomaterials that possess very large aspect ratios compared with their surface area-to-volume ratio. Hence, such materials have a high charge-transfer rate along one direction. Hence, fibre-reinforced CP-nanocomposites can show better electrochemical performance compared with other types of nanocomposites. Here, we report the preparation of CNT-reinforced CP-nanocomposites.

Numerous studies are in progress on CNT in chemistry, physics, materials science and engineering. A CNT is a tubular structure made of carbon atoms having diameter of the order of nanometres but the length of micrometres. CNT have extraordinary properties: many-fold stronger than steel, harder than diamond, electrical conductivity higher than copper, and thermal conductivity higher than diamond. These properties have set-off a ‘goldrush’ in academic and industrial research teams worldwide to find practical uses of CNT. Due to their excellent mechanical characteristics, nanometre size, good electrical conductivity, and extremely accessible surface area, CNT can be used for the preparation of multifunctional composites with outstanding mechanical and electronic properties [60].

Figure 4.13 shows an experimental set-up used for CNT growth by the CVD method in its simplest form. The process involves passing a hydrocarbon vapour (typically for 15–60 min) through a tubular reactor in which a catalyst material is present at sufficiently high temperature (600–1,200 °C) to decompose the hydrocarbon. CNT grow on the catalyst in the reactor, which are collected upon cooling the system to RT. In the case of a liquid hydrocarbon (e.g., benzene, alcohol), the liquid is heated in a flask and an inert gas is purged through it, which in turn carries the hydrocarbon vapour into the reaction zone. If a solid hydrocarbon is to be used as the CNT precursor, it can be kept directly in the low-temperature zone of the reaction tube. Volatile materials (e.g., camphor, naphthalene) turn from solid to vapour directly, and carry out CVD while passing

over the catalyst maintained in the high-temperature zone. Like CNT precursors, the catalyst precursors in CVD can also be used in any form (solid, liquid or gas), which may be placed suitably inside the reactor or fed from outside. Pyrolysis of the catalyst vapour at a suitable temperature liberates metal nanoparticles *in situ* ('floating catalyst method'). Alternatively, catalyst-coated substrates can be placed in the hot zone of the furnace to catalyse CNT growth. If the catalyst–substrate interaction is weak (metal has an acute contact angle with the substrate), the hydrocarbon decomposes on the top surface of the metal, carbon diffuses down through the metal, and CNT precipitate out across the metal bottom, pushing the entire metal particle off the substrate. As long as the top of the metal is available for fresh decomposition of hydrocarbon (a concentration gradient is present in the metal to allow carbon diffusion), CNT continue to grow longer and longer. Once the metal is fully covered with excess carbon, its catalytic activity ceases and CNT growth is stopped. This is known as the 'tip-growth model' (Figure 4.14). In the catalyst–substrate interaction is strong (metal has an obtuse contact angle with the substrate), initial decomposition of the hydrocarbon and carbon diffusion occur similar to that seen in tip-growth, but CNT precipitation fails to push the metal particles upwards. Hence, precipitation is compelled to emerge out from the apex of the metal (farthest from the substrate, having minimum interaction with the substrate). First, carbon crystallises out as a 'hemispherical dome' (the most favourable closed-carbon network on a spherical nanoparticle), which then extends up in the form of a seamless graphitic cylinder. Subsequent deposition of hydrocarbon takes place on the lower peripheral surface of the metal, and as dissolved carbon diffuses upwards. Thus, CNT grow up with the catalyst particle rooted on its base, so this is known as the 'base-growth model' (Figure 4.14). Formation of single-walled carbon nanotubes (SWCNT) or multi-walled carbon nanotubes (MWCNT) is governed by the size of the catalyst particle. Broadly speaking, if the particle size is a few nanometres, SWCNT are formed, whereas if particles are a few tens of nanometres wide, then MWCNT are formed.

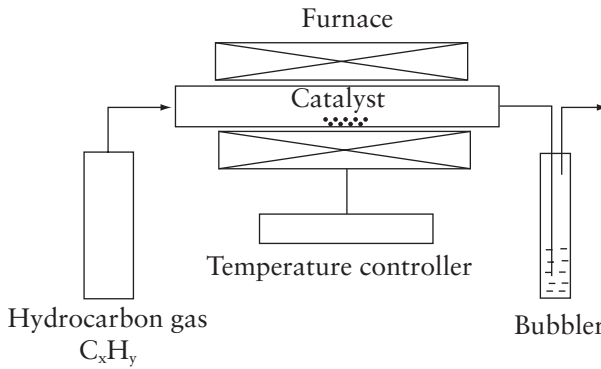


Figure 4.13 CVD setup in its simplest form (schematic)

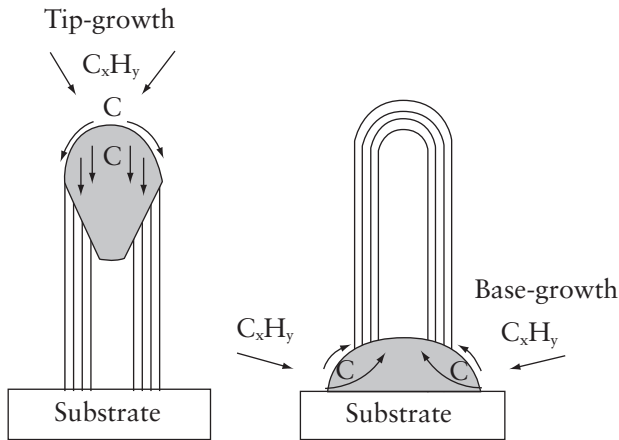


Figure 4.14 Tip-growth and base-growth models (schematic)

Incorporation of SWCNT and MWCNT into polymeric composites enhances electrochemical properties. Such enhancement is due mainly to the superior properties of SWCNT and MWCNT: small

size, high conductivity, high stability and high surface area [61–63]. Use of MWCNT is preferred over SWCNT due to cost. MWCNT have been shown to have excellent electron-transfer kinetics if used in electrochemical applications as compared with SWCNT even though SWCNT show better electrical performance than MWCNT. Introducing CNT into a CP matrix improves the properties of the original CP. Several attempts have been made to synthesise composite materials to compensate for the limitation of each individual material in electrochemical capacitors.

Supercapacitors based on the CNT/CP nanocomposites can be prepared *via* chemical or electrochemical polymerisation. A high SC per gram of 192 F/g has been observed for nanofibres of CNT–Ppy nanocomposites [64]. The SC per area of CNT–Ppy nanocomposites was as $\leq 1.0 \text{ F cm}^{-2}$, much larger than those reported previously for supercapacitors based on similar electrode materials. Capacitance per gram of Ppy-based nanocomposites was enhanced further by construction of an activated carbon nanofibre (ACNF)/CNT/Ppy three-component system [65]. In comparison with ACNF, the nanocomposites had larger specific surface area and higher electrical conductivity. Capacitance of ACNF/CNT/Ppy was 333 F/g, much better than those of ACNF and ACNF–Ppy electrodes. Nanofibres of CNT–PANI and CNT–Ppy composites containing 20 wt% CNT synthesised by *in situ* chemical polymerisation have been employed for supercapacitors [66]. The SC of CNT–Ppy and CNT–PANI nanocomposites were 190 and 360 F/g, respectively, with fairly good cycling life for the supercapacitor.

Gupta and Miura studied the performance of a supercapacitor based on SWCNT–PANI nanocomposites [67]. Their results showed that the SC was strongly dependent on PANI content. When 73 wt% PANI was deposited on the surface of SWCNT, the highest SC of 463 F/g was obtained. Furthermore, the stability of the supercapacitor based on SWCNT–PANI nanocomposites was excellent because capacitance decreased only 5% after 500 cycles and only 1% after the next 1,000 cycles.

Besides PANI and Ppy, CNT–PEDOT composites with 1D core-sheath nanostructures prepared by *in situ* polymerisation under hydrothermal conditions have also been used for the fabrication of supercapacitors [68]. The highest capacitance of 198.2 F/g at a current density of 0.5 A/g was achieved when the content of PEDOT reached 50%. After 2,000 cycles, the capacitance of the supercapacitor decreased by 26.9%. The capacitance and stability of the supercapacitor based on CNT–PEDOT nanocomposites with core-sheath nanostructures were superior to those of pristine PEDOT and CNT–PEDOT composites without core-sheath structures.

In addition to CNT, nanocomposites comprising manganese oxide and CP have also been investigated intensively as building components in supercapacitors. Manganese oxide–PEDOT coaxial nanowires have been prepared by a co-electrodeposition approach [69]. In comparison with manganese oxide nanowires, PEDOT nanowires and even manganese oxide films, the manganese oxide–PEDOT coaxial nanofibres exhibited higher SC. Such high and well-maintained capacitance can be attributed to the inclusion of manganese oxide and the short paths of ion diffusion in nanowires.

Sharma and co-workers prepared solvent-tuned PANI–CNT composites as advanced electrode materials for supercapacitor applications [28]. Composites of PANI and MWCNT were prepared by *in situ* chemical oxidative polymerisation of the aniline monomer in 1 M hydrochloric acid and 1 M hydrochloric acid with 20% ethanol as solvent. In a typical process, a weighed amount (0.2 g) of CNT was dispersed in a solution of 1 M hydrochloric acid and 20% ethanol by ultrasonication for 1 h. Different concentrations of aniline monomer in 1 M hydrochloric acid were added to the dispersed CNT solution and again ultrasonicated for 1 h. To this solution, 1 M of freshly prepared APS in 1 M hydrochloric acid was added drop-wise slowly for ≈ 0.5 h. The mixture was left to polymerise for 6 h at ≈ 0 –5 °C under constant stirring. PANI–CNT composites were obtained by filtering and drying the greenish-black powder. PANI–CNT composites without ethanol were also prepared for comparison. Electrochemical measurements were undertaken using 1 M sulfuric

acid aqueous electrolyte to examine the electrochemical performance of PANI–CNT composite electrodes. CV studies were carried out in the voltage window of 0–0.8 V at scan rates of 2, 5, 10 and 15 mV/s. The SC of PANI–CNT composite using 0.02 M aniline in 1 M hydrochloric acid (20% ethanol) and 1 M hydrochloric acid was reported to be 597.82 and 484.49 F/g, respectively, at a scan rate of 2 mV/s in 1 M sulfuric acid.

A Ppy–CNT composite for electrochemical capacitor applications can be prepared by growing CNT on ceramic fabrics using CVD and subsequently coating Ppy on it by chemical polymerisation [70]. The large surface area and high conductivity of the CNT on porous ceramic fabrics enhances its energy-storage capacity. Ppy provides not only additional capacitance as an active material, but also enhances the adhesion between the CNT and ceramic fabrics. Furthermore, Ppy acts as a conducting binder for connecting every individual CNT to increase capacitance. As-synthesised CNT-ceramic fabric by thermal CVD was immersed in 0.5 M pyrrole solution for 2 h and then in 0.5 M iron(III) chloride aqueous solution for 90 min. After polymerisation, the Ppy–CNT composite on the fabric was washed several times with ethanol and dried in an oven at 50 °C for 24 h. Electrochemical properties of the Ppy–CNT composite electrode were investigated by CV and GCD tests. A Ppy–CNT composite on ceramic fabrics was electrochemically characterised in lithium perchlorate/propylene carbonate (PC) electrolyte solution by CV in the potential range of -1.0 to 1.0 V at a rate of 25 mV/s. The resulting cyclic voltammogram is shown in **Figure 4.15**. In the CV of the Ppy–CNT composite on ceramic fibres, a redox peak corresponding to the charge–discharge of the Ppy was clearly observed. Through the coating of Ppy on the CNT and ceramic fabrics, Ppy provides an electro-conducting path to each CNT, thereby allowing most of the CNT to participate in capacitance behaviour. Ppy provides not only capacitance as an active material, but also electric conductivity among CNT by acting as a type of conducting binder. Ppy have structural uniformity and high conductivity due to strong π – π stacking between the Ppy conjugate backbone and graphitic sidewall of CNT in the composite and provide higher performance.

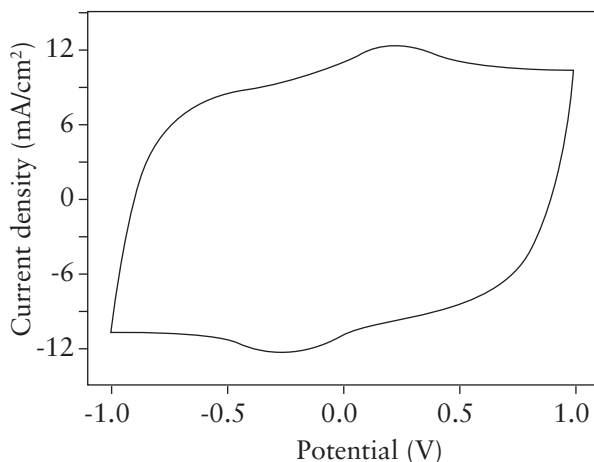


Figure 4.15 CV of a Ppy–CNT composite electrode at a scan rate of 25 mV/s in 1 M lithium perchlorate/PC

Capacitance of a Ppy–CNT composite electrode was tested using GCD in a potential range of 0–2 V. **Figure 4.16** shows the GCD measured at a current density of 1 mA/cm² in 1 M lithium perchlorate/PC solution for a Ppy–CNT composite on ceramic fabrics. Charge–discharge characterisation demonstrates that the cycling performance of Ppy–CNT composite was better than that of pure Ppy. The highly dispersed CNT in the composite may play an important part in improved electrochemical stability. The SC of Ppy–CNT on ceramic fabrics activated in 1 M lithium perchlorate/PC was found to be 152.78 F/g. Ppy provides conducting paths between the CNT, which dramatically enhances the SC.

Ppy has been found to have poor cycling performance mainly due to large volume changes during repeated redox cycles, which can lead to fatal degradation. The thickness of the Ppy layer on the CNT surface is relatively narrow, which causes small changes in volume during the redox cycle. As described above, the strong π – π stacking between the Ppy conjugate backbone and graphitic sidewall of CNT provides enhanced stability to the Ppy–CNT composite.

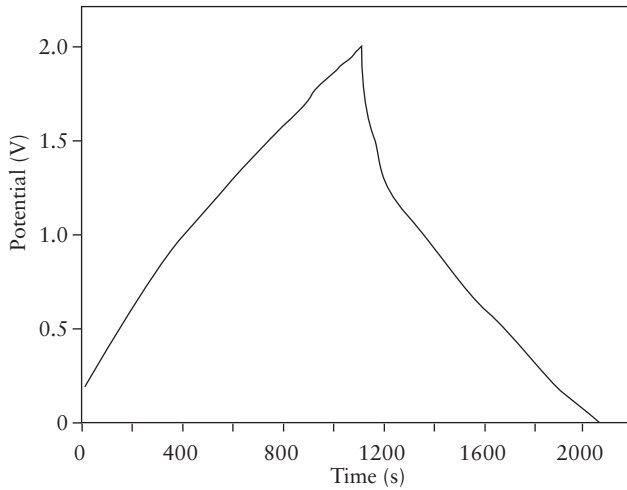


Figure 4.16 GCD of a Ppy-CNT composite electrode on ceramic fabrics at a current density of 1 mA/cm²

References

1. M. Mukhopadhyay in *Mechanics of Composite Materials and Structures*, Universities Press Publisher, Hyderabad, India, 2004.
2. W.L. Song, *Polymer*, 2010, **53**, 3910.
3. O. Jarjees, P.H. Fries and G. Bidan, *Synthetic Metals*, 1995, **69**, 43.
4. C.L. Huang and E. Matijevic, *Journal of Materials Research*, 1995, **10**, 1327.
5. K.H. Wu, M. Shin and C.C. Yang, *Journal of Polymer Science, Part A: Polymer Chemistry Edition*, 2006, **44**, 2657.

Conducting Polymer Nanocomposites for Supercapacitors

6. A. Rudge, J. Davey, I. Raistrick, S. Gottesfeld and J.P. Ferraris, *Journal of Power Sources*, 1994, **47**, 89.
7. D.S. Dhawale, A. Vinu and C.D. Lokhande, *Electrochimica Acta*, 2011, **56**, 9482.
8. S. Palaniappan and S.L. Devi, *Journal of Applied Polymer Science*, 2008, **107**, 1887.
9. S. Palaniappan, S.B. Sydulu and P. Srinivas, *Journal of Applied Polymer Science*, 2010, **115**, 1695.
10. A. Subramania and S.L. Devi, *Polymers for Advanced Technologies*, 2008, **19**, 725.
11. Y. Yan, Q. Cheng, G. Wang and C. Li, *Journal of Power Sources*, 2011, **196**, 7835.
12. H. Mi, X. Zhang, S. Yang, X. Ye and J. Luo, *Materials Chemistry and Physics*, 2008, **112**, 127.
13. L. Shi, X. Wu, L. Lu, X. Yang and X. Wang, *Synthetic Metals*, 2010, **160**, 989.
14. Y. Li, X. Zhao, Q. Xu, Q. Zhang and D. Chen, *Langmuir*, 2011, **27**, 6458.
15. S. Jiao, J. Tu, C. Fan, J. Hou and D.J. Fray, *Journal of Materials Chemistry*, 2011, **21**, 9027.
16. S. Radhakrishnan, C.R.K. Rao and M. Vijayan, *Journal of Applied Polymer Science*, 2009, **114**, 3125.
17. V. Branzoi, F. Branzoi and L. Pilan, *Surface and Interface Analysis*, 2010, **42**, 1266.
18. K. Wang, W. Zou, B. Quan, A. Yu, H. Wu, P. Xiang and Z. Wei, *Advanced Energy Materials*, 2011, **1**, 1068.

19. S.K. Shukla, A. Bharadvaja, A. Tiwari, G.K. Parashar and G.C. Dubey, *Advanced Materials Letters*, 2010, **1**, 2, 129.
20. B.S. Kushwah, S.C. Upadhaya, S. Shukla, A.S. Sikarwar, R.M.S. Sengar and S. Bhadauria, *Advanced Materials Letters*, 2010, **2**, 1, 43.
21. A. Tiwari, R. Kumar, M. Prabhakaran, R.R. Pandey, P. Kumari, A. Chadurvedi and A.K. Mishra, *Polymers for Advanced Technologies*, 2010, **21**, 615.
22. A. Tiwari, V. Sen, S.R. Dhakate, A.P. Mishra and V. Singh, *Polymers for Advanced Technologies*, 2008, **19**, 909.
23. A. Tiwari, *Journal of Polymer Research*, 2008, **15**, 4, 337.
24. A. Tiwari, *Journal of Macromolecular Science, Part A: Pure and Applied Chemistry*, 2007, **44**, 7, 735.
25. S.B. Kondawar, S.R. Thakare, S. Bompilwar and V. Khati, *International Journal of Modern Physics B*, 2009, **23**, 15, 3297.
26. A. Tiwari, M. Prabakaran, R. Pandey and S. Li, *Journal of Inorganic and Organometallic Polymers and Materials*, 2010, **20**, 2, 380.
27. S. Bompilwar and S.B. Kondawar, *Journal of NanoScience, NanoEngineering & Applications*, 2012, **2**, 3, 25.
28. A.K. Sharma, Y. Sharma, R. Malhotra and J.K. Sharma, *Advanced Materials Letters*, 2012, **3**, 2, 82.
29. B. Ziębowicz, M. Drak and L.A. Dobrzański, *Journal of Achieved Materials and Manufacturing Engineering*, 2007, **191**, 352.
30. B.I. Nandapure, S.B. Kondawar, M.Y. Salunkhe and A.I. Nandapure, *Advanced Materials Letters*, 2013, **4**, 2, 134.

31. G.P. Song, J. Han and R. Guo, *Synthetic Metals*, 2007, **157**, 170.
32. G.P. Song, J. Bo and R. Guo, *Colloid Polymer Science*, 2005, **283**, 677.
33. J. Han, G.P. Song and R. Guo, *Journal of Polymer Science, Part A: Polymer Chemistry Edition*, 2006, **44**, 4229.
34. P. Xu-Yuan, L. Xiao-Xia, H. Pei-Jie, D. Dermot and L.J. King-Tong, *Solid State Electrochemistry*, 2009, **14**, 1.
35. Y. Qi, J. Zhang, S. Qiu, L. Sun, F. Xu, M. Zhu, L. Ouyang and D. Sun, *Journal of Thermal Analytical Calorimetry*, 2009, **98**, 2, 533.
36. B. Nandapure, S. Kondawar, M. Salunkhe and A. Nandapure, *Journal of Composite Materials*, 2012, **47**, 5, 559.
37. S.B. Kondawar, S.P. Agrawal, S.H. Nimkar, H.J. Sharma and P.T. Patil, *Advanced Materials Letters*, 2012, **3**, 5, 393.
38. S.B. Kondawar, S.A. Acharya and S.R. Dhakate, *Advanced Materials Letters*, 2011, **2**, 5, 362.
39. B. Senthilkumar, K. Vijaya Sankar, C. Sanjeeviraja and R. Kalai Selvan, *Journal of Alloys and Compounds*, 2013, **553**, 350.
40. B. Senthilkumar, P. Thenamirtham and R. Kalai Selvan, *Applied Surface Science*, 2011, **257**, 9063.
41. L. Chena, L-J. Suna, F. Luana, Y. Lianga, Y. Li and X.X. Liua, *Journal of Power Sources*, 2010, **195**, 3742.
42. K. Vijaya Sankar, S.T. Senthilkumar, L. John Berchmans, C. Sanjeeviraja and R. Kalai Selvan, *Applied Surface Science*, 2012, **259**, 624.

43. D. Zhang, X. Zhang, Y. Chen, P. Yu, C. Wang and Y. Ma, *Journal of Power Sources*, 2011, **196**, 5990.
44. G. Wang, X. Shena, J. Yao and J. Park, *Carbon*, 2009, **47**, 8.
45. D. Li, M.B. Muller, S. Gilje, R.B. Kaner and G.G. Wallace, *Nanotechnology*, 2007, **3**, 101
46. K.A. Worsley, P. Ramesh, S.K. Mandal, S. Niyogi, M.S. Itkis and R.C. Haddon, *Chemical Physics Letters*, 2007, **445**, 51.
47. S. Park, J. An, R.D. Piner, I. Jung, D. Yang and A. Velamakanni, *Chemical Materials*, 2008, **20**, 6592.
48. D.W. Wang, F. Li, J. Zhao, W. Ren, Z.G. Chen, J. Tan, Z-S. Wu, I. G, G.Q. Lu and H.M. Cheng, *ACS Nanotechnology*, 2009, **3**, 7.
49. H. Wang, Q. Hao, X. Yang, L. Lu and X. Wang, *Electrochemical Communication*, 2009, **11**, 6.
50. Y. Zhu, S. Murali, W. Cai, X. Li, J.W. Suk, J.R. Potts and R.S. Ruoff, *Advanced Materials*, 2010, **22**, 35.
51. M. Srivastava, M. Kumar, R. Singh, U.C. Agrawal and M.O. Garg, *Journal of Science Industrial Research*, 2009, **68**, 93.
52. M. Baibarac and P. Gómez-Romero, *Journal of Nanoscience and Nanotechnology*, 2006, **1**, 5.
53. C. Bai, J. Wang, S. Jia and Y. Yang, *Applied Physics Letters*, 2010, **96**, 1.
54. H. Gomez, M.K. Ram, F. Alvi, E. Stefanakos and A. Kumar, *Journal of Physical Chemistry C*, 2010, **114**, 18797.
55. H. Gómez, M.K. Ram, F. Alvi, P. Villal, E. Stefanakosc and A. Kumar, *Journal of Power Sources*, 2011, **196**, 4102.

Conducting Polymer Nanocomposites for Supercapacitors

56. L. Peponi, A. Tercjak, R. Verdejo, M.A. Lopez-Manchado, I. Mondragon and J.M. Kenny, *Journal of Physical Chemistry*, 2009, **113**, 17973.
57. D.W. Wang, F. Li, J. Zhao, W. Ren, Z.G. Chen and J. Tan, *ACS Nano*, 2009, **7**, 1745.
58. K. Zhang, L.L. Zhang, X.S. Zhao and X. Wu, *Journal of Chemical Materials*, 2010, **22**, 1392.
59. H. Zhou, G. Han, Y. Xiao, Y. Chang and H.J. Zhai, *Journal of Power Sources*, 2014, **263**, 259.
60. M.A. Salam and R. Burk, *Analytical Bioanalytical Chemistry*, 2008, **390**, 2159.
61. C.S. Du, J. Yeh and N. Pan, *Nanotechnology*, 2005, **16**, 350.
62. H.T. Ham, Y.S. Choi, N. Jeong and I.J. Chung, *Polymer*, 2005, **46**, 6308.
63. M. Hughes, M.S.P. Shaffer, A.C. Renouf, C. Singh, G.Z. Chen, J. Fray and A.H. Windle, *Advanced Materials*, 2002, **14**, 382.
64. M. Hughes, G.Z. Chen, M.S.P. Shaffer, D.J. Fray and A.H. Windle, *Chemical Materials*, 2002, **14**, 1610.
65. Y.W. Ju, G.R. Choi, H.R. Jung and W.J. Lee, *Electrochimica Acta*, 2008, **53**, 5796.
66. V. Khomenko, E. Frackowiak and F. Beguin, *Electrochimica Acta*, 2005, **50**, 2499.
67. V. Gupta and N. Miura, *Electrochimica Acta*, 2006, **52**, 1721.
68. L. Chen, C.Z. Yuan, H. Dou, B. Gao, S. Chen and X. Zhang, *Electrochimica Acta*, 2009, **54**, 2335.

69. R. Liu and S.B. Lee, *Journal of American Chemical Society*, 2008, **130**, 2942.
70. H. Lee, H. Kim, M.S. Cho, J. Choi and Y. Lee, *Electrochimica Acta*, 2011, **56**, 7460.

Conducting Polymer Nanocomposites for Supercapacitors

5 Ternary Nanocomposites for Supercapacitors

5.1 Metal Oxide-based Ternary Nanocomposites

According to the energy-storage mechanism, supercapacitors are, in general, classified into electrochemical double-layer capacitors (EDLC), using carbon-active materials [e.g., carbon nanotubes (CNT), graphene] based on the surface area of electrode materials, and ‘pseudocapacitors’, using redox-active materials based on fast and reversible Faradic reactions.

The specific capacitance (SC) just from the electrical charges at the electrode–electrolyte interface of EDLC is lower than ‘pseudocapacitance’ based on conducting polymers (CP) [e.g., polyaniline (PANI), polypyrrole (Ppy) and polythiophene] and transition metal oxides (e.g., ruthenium(IV) oxide, cobalt(II,III) oxide, manganese dioxide, titanium dioxide).

Poor cycling due to structural degradation through the redox process limits the applications of pseudocapacitors. However, combining the advantages of EDLC and pseudocapacitors has attracted considerable interest due to synergistic effects. On this basis, it is apparent that electrochemical performances can be enhanced by incorporation of carbon materials with pseudocapacitive materials. However, the electrochemical properties of electrodes play a crucial part in determination of supercapacitor performance. To overcome this obstacle, studies are needed to develop excellent electrode materials for supercapacitors.

5.1.1 Manganese Dioxide/Carbon Nanotube/Polyaniline and Manganese Dioxide/Carbon Nanotube/Polypyrrole Nanocomposites

Composites of CNT and CP are even more interesting and promising because they combine two relatively inexpensive materials to benefit from the large pseudocapacitance of the CP coupled with the conductivity and mechanical strength of the CNT [1–8]. Several studies have been done on CP/CNT nanocomposites, but the electron conduction and stability of the nanocomposites are not known.

Recently, manganese dioxide has been considered to be a prospective material of pseudocapacitors with respect to its high SC, cost-effectiveness and environmental compatibility. However, the poor electrical conductivity of manganese dioxide and instability in high proton-conducting medium greatly diminish the SC of manganese dioxide, which restricts its application in supercapacitors [9–11]. To improve the electrochemical performance of electrode materials for supercapacitors, binary composites of carbon-based materials/manganese dioxide [12, 13] and CP/manganese dioxide [14, 15] have been studied. Such binary composites have demonstrated improvement in electrochemical stability, but significant reinforcement for practical applications has not been shown. To overcome the cycle degradation caused by volumetric change, the design and development of hierarchical ternary composite materials have been explored [16].

CP-based ternary nanocomposites have been synthesised by *in situ* polymerisation of aniline/pyrrole monomer in the presence of functionalised CNT using potassium permanganate as an oxidising agent. A comparative study of the electrochemical performance of two types of ternary nanocomposites, PANI/CNT/manganese dioxide and Ppy/CNT/manganese dioxide, is reported here. Among the synthetic methods adopted for the synthesis of ternary composites, the most suitable and effective method is believed to be *in situ* chemical oxidation. Potassium permanganate is a strong oxidising agent. Hence, if potassium permanganate solution is added to the monomer solution, the monomer is oxidatively polymerised, manganese in

potassium permanganate is reduced to a lower valence state of +4, and hydrous manganese dioxide is precipitated. Hydrous manganese dioxide and PANI/Ppy are formed *in situ*, so the dispersion of the manganese dioxide in the polymer must be effective and should be distributed in a three-dimensional (3D) manner.

Ternary nanocomposites of CP PANI/Ppy with CNT and manganese dioxide were synthesised by our one of the groups Mahore and co-workers [17]. Preparation of PANI/CNT/manganese dioxide and Ppy/CNT/manganese dioxide ternary nanocomposites by *in situ* chemical oxidation polymerisation is shown in **Figure 5.1**. To prepare PANI/CNT/manganese dioxide ternary nanocomposites, the monomer aniline 0.75 M was added to an aqueous solution containing 0.25 M sodium dodecyl sulfate (SDS). Then, 1% (*w/w*) functionalised CNT were suspended in this monomer solution. The solution containing CNT and monomer was sonicated for 30 min to facilitate CNT dispersion and for greater absorbance of the monomer on the walls of CNT so that when the oxidant was added drop-wise it would enable better polymerisation and growth of polymer on the walls of CNT. To this solution while stirring, 0.75 M potassium permanganate was added drop-wise as an oxidant as well as to 'embed' manganese dioxide into the polymer matrix along with CNT. Stirring was continued for 3 h to complete polymerisation and then the solution was stored overnight. A precipitate of the ternary nanocomposite PANI/CNT/manganese dioxide was obtained by filtration and washed repeatedly using deionised water until the filtrate became colourless, and was vacuum-dried at 80 °C. To prepare the ternary nanocomposite Ppy/CNT/manganese dioxide, an identical process was adopted using pyrrole as the monomer instead of aniline under the same conditions, and the results compared.

Conducting Polymer Nanocomposites for Supercapacitors

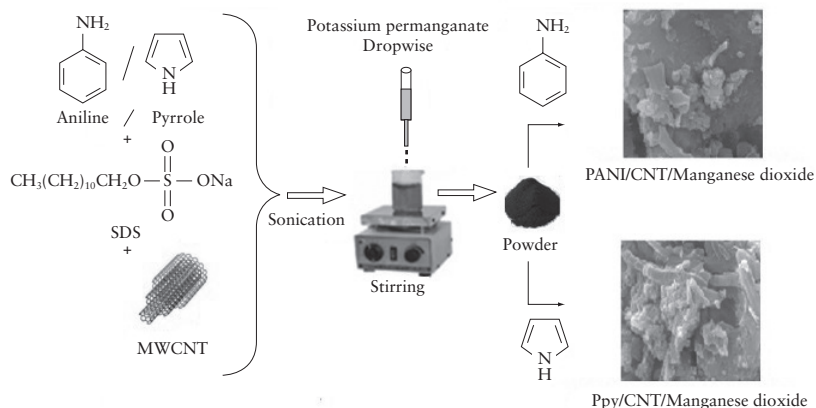


Figure 5.1 Preparation of PANI/CNT/manganese dioxide and Ppy/CNT/manganese dioxide ternary nanocomposites (schematic)

Electrochemical performance of ternary nanocomposites was studied by cyclic voltammetric analyses in a three-electrode cell. The ‘working’ electrode was one of the ternary nanocomposites, a platinum wire was the ‘counter’ electrode, and silver/silver chloride was used as the ‘reference’ electrode. The working electrode was in the form of a pellet obtained by pressing nanocomposites at 5,000 kg/cm², and pellet diameter was 1.2 cm. Electrochemical performance was measured in 1.0 M sodium sulfate electrolyte solution in the voltage range 0.1–0.9 V at scan rates 0.5 and 1 V/s. Cyclic voltammograms recorded for ternary composites at various scan rates are shown in **Figure 5.2a** and **5.2b**, respectively, for PANI/CNT/manganese dioxide and Ppy/CNT/manganese dioxide. Interestingly, the cyclic voltammograms for ternary nanocomposites resembled an ideal rectangular shape, suggesting that charge and discharge occur reversibly at the electrode–electrolyte interface. Visible redox peaks were not observed, implying the stability of the electrolyte. The shape of the cyclic voltammetry (CV) curves was symmetric in both cases, suggesting high efficiency of capacitive characteristics at the electrode–electrolyte interface [3].

During the reaction of the polymer with potassium permanganate, concurrent growth of manganese dioxide with polymer generates uniform and ordered structures that lead to efficient charge storage. During redox cycling, mass insertion/ejection takes place in the polymer chains, and repetitive swelling/shrinkage causes chain defects in the polymer matrix, thereby causing deterioration in the mechanical stability of the electrode. Such deterioration in CV performance at high scan rates supports the notion that molecular-level dispersion of manganese dioxide in the polymer matrix is important [18]. The SC of the ternary nanocomposites PANI/CNT/manganese dioxide and Ppy/CNT/manganese dioxide determined using Equation 5.1 were (in F/cm²) 11.50 and 5.57 at a scan rate of 0.5 V/s, and 16.81 and 7.07 F/cm² at a scan rate of 1 V/s, respectively.

$$C = \frac{I}{vA} \quad (5.1)$$

Where:

I is the current;

v is the scan rate; and

A is the surface area of loaded sample.

Figure 5.2 reveals that the shape of the CV curve seemed to be more rectangular for Ppy/CNT/manganese dioxide. In comparison, Ppy/CNT/manganese dioxide showed good electrochemical performance for supercapacitors compared with that of PANI/CNT/manganese dioxide.

Conducting Polymer Nanocomposites for Supercapacitors

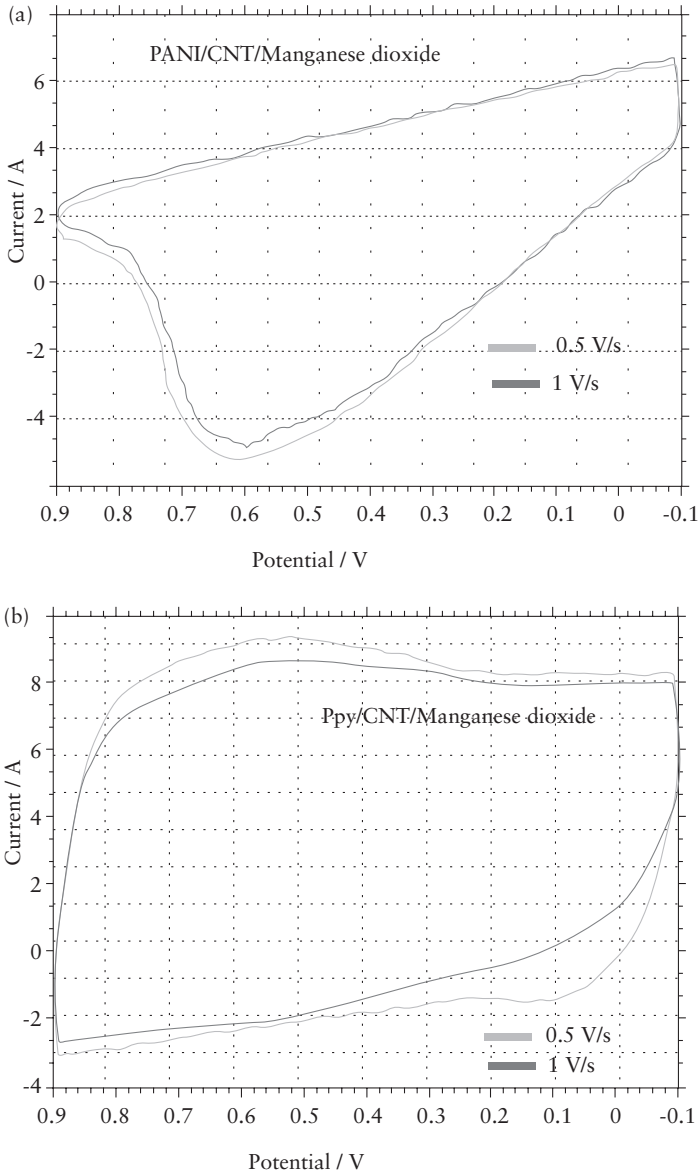


Figure 5.2 a) CV of PANI/CNT/manganese dioxide and b) CV of Ppy/CNT/manganese dioxide

5.1.2 Titanium Dioxide/Graphene/Polyaniline Ternary Nanocomposites

Polyaniline/graphene/titanium dioxide nanotubes (PGTN) ternary nanocomposites fabricated by *in situ* polymerisation have been found to be good supercapacitor electrodes [19] compared with polyaniline/titanium dioxide nanotubes (PTN) composites because titanium dioxide nanotubes have high accessible surface area, good chemical/thermal stability, ordered and controllable pore structure, and are relatively inexpensive [20, 21]. The PGTN possessed a novel 3D, highly ordered, hybrid nanostructure comprising coaxial PTN arrays and graphene coated with PANI on the surface of titanium dioxide.

Titanium dioxide nanotubes on titanium foils ($1.0 \times 0.05 \times 5.0$ cm) were fabricated *via* potentiostatic anodisation in a two-electrode electrochemical cell. Before anodisation, titanium foils were first degreased by ultrasonication in cold acetone, ethanol and deionised water, followed by drying in a stream of pure nitrogen. Samples were anodised in 0.15 M hydrofluoric acid aqueous electrolyte using platinum as the cathode at 20 V for 2 h. After anodisation, titanium dioxide nanotubes were rinsed immediately with distilled water and dried in air. Then, anodised samples were annealed at 450 °C for 1 h to form the anatase phase in a muffle furnace. The modified titanium dioxide/titanium electrode was immersed in an aqueous solution containing 0.2 M aniline and 1.25 M hydrochloric acid by stirring under a vacuum for 1 h. Besides, 0.5 mL aniline monomers were dispersed in 4 mL graphene suspension in another reaction vessel and sonicated for 30 min. After ultrasonication, the mixture was dispersed in 25 mL of 1.25 M hydrochloric acid to form a uniform solution by magnetic string in an ice–water bath (0–5 °C) for 20 min. Then, treated titanium dioxide nanotubes were transferred into the solution described above. Subsequently, 25 mL of 0.09 M ammonium peroxydisulfate (APS)/KH(IO₃)₂ (molar ratio, 8:1) composite oxidant solution was poured rapidly into the mixture described above. Continuous stirring for 30 min and polymerisation for a further 4 h without stirring was undertaken. The reaction product was washed

with hydrochloric acid solution to remove oligomers and dried at 60 °C for 2 h to obtain a green film on a titanium dioxide substrate. Aniline concentration in the first step is higher to ensure that the aniline in the tube polymerised first. **Figure 5.3** details the preparation required for a 3D architecture for PGTN.

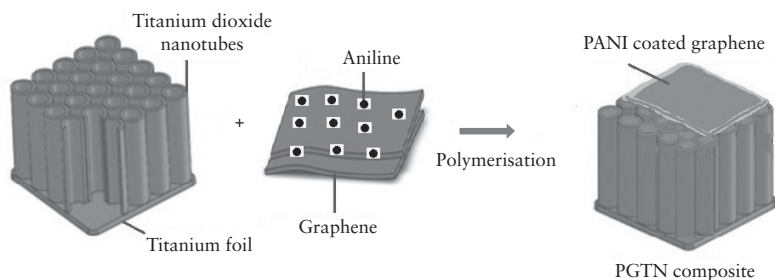


Figure 5.3 Preparation of PGTN (schematic)

To evaluate the electrochemical properties of electrode materials, CV tests and galvanostatic charge–discharge (GCD) are employed to characterise capacitance performances. **Figure 5.4** shows the CV curve of PGTN at a scan rate of 5 mV/s. The curve of PGTN exhibits a typical pseudocapacitive characteristic of PANI [20]. In addition, the area surrounded by the CV curve for PGTN is larger, suggesting an improved SC. Only a few percent of graphene is present in the ternary composites, so such high capacitance may originate from the synergistic effect between PANI and graphene. The CV curve area corresponds directly to the SC, so the capacitance of individual components is smaller than that of the PGTN composite [21]. Capacitance of a supercapacitor is proportional to the accessible surface area. The larger capacitance of ternary composites probably results from the higher surface area of PGTN and enhanced accessibility by electrolyte ions [22–25].

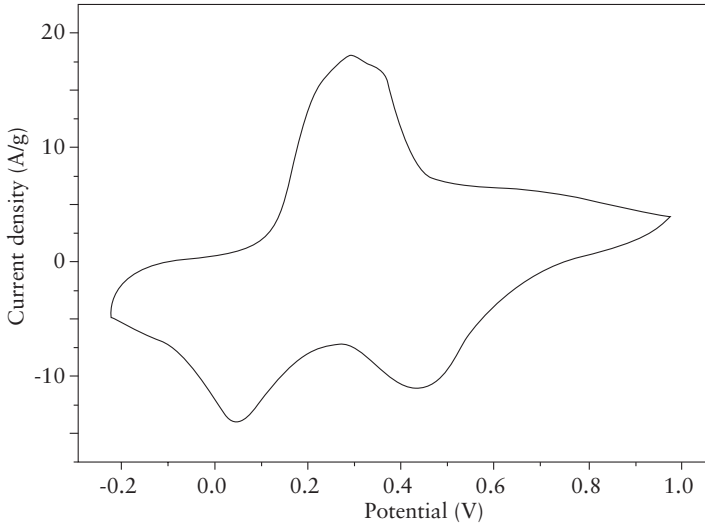


Figure 5.4 CV curve of PGTN at a scan rate of 5 mV/s

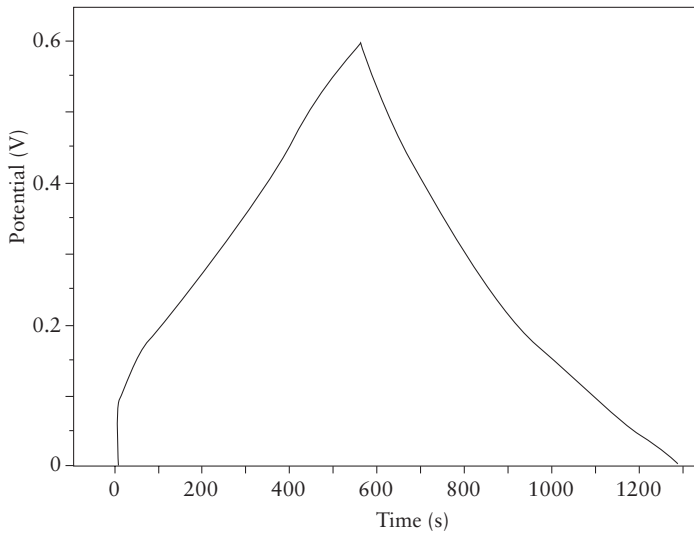


Figure 5.5 GCD curve of PGTN

GCD is a reliable method for evaluation of the electrochemical capacitance of materials under controlled current conditions. **Figure 5.5** shows the GCD curve of PGTN in the potential range 0–0.6 V at a current density of 1.5 A/g. PGTN composites present capacitive behaviour with almost symmetric charge–discharge curves. Moreover, slight deviation to linearity is typical of a pseudocapacitive contribution. The calculated SC at a current density of 1.5 A/g was 930 F/g, which is much higher than that of binary composites [26]. At a power density of 450 W/kg, the energy density was 93.3 Wh/kg. Notably, when the power density was increased to 9,000 W/kg, an energy density of 71 Wh/kg was retained, suggesting that the PGTN electrode could be operated with high energy and power densities at high charge–discharge rates. Power density and energy density, as important parameters for the investigation of electrochemical performance, have been found to be much higher than those of nickel ferrite/graphene/PANI [27] and manganese ferrite/graphene/polyaniline (MGP) ternary nanocomposites [28].

5.2 Ferrite-based Ternary Nanocomposites

To improve further the electrochemical performance of CP-based binary nanocomposites, ternary nanocomposites have been developed in which noble metal-CP or metal oxide-CP is hybridised with graphene or CNT to combine their advantages. Transition metal oxides possess multiple oxidation states/structures that enable rich redox reactions for pseudocapacitance generation. Ruthenium(IV) oxide is one of the most prominent transition metal oxides due to its ultra-high pseudocapacitance but its extraordinarily high cost has greatly limited its commercial applications. Therefore, exploration of alternative and inexpensive electrode materials with high performance is an active research area in supercapacitor electrode materials.

Much attention has been paid to inexpensive metal oxides, such as oxides of manganese, nickel, cobalt, and iron, owing to their low cost and environmental compatibility. Unfortunately, these simple metal oxides exhibit a low SC, particularly at higher charge–discharge rates.

Design of complex metal oxide-based systems having a high SC and low cost is of interest. If such designs can be accomplished, obtaining much more effective and cheaper supercapacitors should be possible. Spinel ferrites (MFe_2O_4 , where $M = Fe, Co, Ni, Cu, \text{ or } Mn$) have been conceived as a promising cost-effective and scalable alternatives for supercapacitors due to their greater electronic conductivity and electrochemical activity than single-component metal oxides.

5.2.1 Nickel ferrite/Graphene/Polyaniline Nanocomposites

The electrochemical property of graphene can be enhanced significantly due to incorporation of heteroatoms into graphene. Here, we report the preparation of ternary nitrogen-doped graphene/nickel ferrite/polyaniline (NGNP) nanocomposites by a facile two-step approach and its electrochemical properties as electrodes for supercapacitors. Spinel transition metal oxides (AB_2O_4) with two metal elements provide the feasibility to tune the energy density and working voltage by varying metal content [29]. Spinel nickel composites are also an attractive candidate in supercapacitor applications due to a high theoretical SC, well-defined redox behaviour, low cost, and environmental friendliness. For example, nickel ferrite is an ‘inverse spinel’ in which Ni^{2+} occupies the octahedral site and half of the Fe^{3+} ions occupy tetrahedral sites [30]. If applied as anode material for lithium-ion batteries, excellent electrochemical properties result [31–33]. Nickel ferrite as a pseudocapacitive candidate can improve the electrochemical properties of nickel ferrite if combined with a carbon nanostructure and CP. Hence, a composite of nitrogen-doped graphene (N-GE), PANI and nickel ferrite could be a promising electrode for high-performance supercapacitors.

Various methods have been proposed to prepare nitrogen-doped carbon materials: spray deposition [34], hydrothermal carbonisation [35], pyrolysis [36] and the hydrothermal method [37]. However, the latter has the merits of mild conditions and simple synthetic procedures, lower production costs, and easy scale-up. Reduction and doping of graphene oxide (GO) can be achieved simultaneously by

introduction of urea (reducing agent), a doping agent, and a donor of the hydroxyl ion in the hydrothermal method. NiFe_2O_4 nanoparticles simultaneously grow on N-GE, leading to formation of nitrogen-doped graphene/nickel ferrite (NGN) composites. Subsequently, the thin PANI films coat on NGN nanosheets *via in situ* chemical polymerisation of aniline in the presence of NGN sheets (Figure 5.6). In a typical procedure, NGN was placed in absolute ethanol with violent stirring for 1 h to obtain a uniform suspension. Then, an amount of aniline was added slowly to the suspension, followed by stirring in an ice–water bath for 2 h. While maintaining vigorous stirring, the oxidant ammonium persulfate in an acidic medium was added to the solution and stirred in an ice–water bath for 12 h. The prepared composite was centrifuged and washed with ethanol and distilled water repeatedly to obtain NGNP. The ternary hybrid NGNP may utilise the advantages of three types of components and avoid the drawbacks of each one, leading to a high SC (≤ 667.0 F/g at 0.1 A/g) and excellent cycling life at a high current density of 5 A/g. The ternary hybrid NGNP has potential applications in renewable energy technologies and energy-intensive industries.

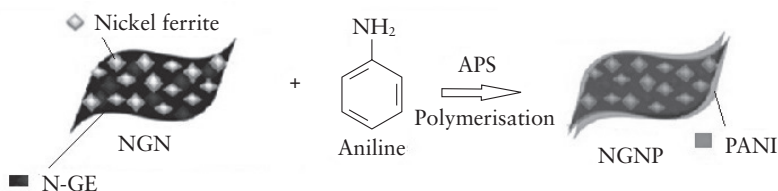


Figure 5.6 Preparation of ternary NGNP (schematic)

Electrochemical experiments of electrode materials of ternary NGNP were carried out using a three-electrode system. Platinum foils were used as counter electrodes, whereas saturated calomel electrodes

or mercury/mercury(II) oxide electrodes were used as reference electrodes. CV and electrochemical impedance spectroscopy (EIS) measurements were undertaken on a potentiostat. Electrochemical measurements were made with a three-electrode system from 0.3 V to -0.8 V in 1 M potassium hydroxide solution to evaluate the electrochemical performance as supercapacitor electrode materials. The electrode of graphene exhibits a nearly rectangular shape with no peaks corresponding to lower capacitances, which is a characteristic of the EDLC of carbon-based materials. However, for N-GE, the capacitive response arises from a combination of EDLC and redox reactions related to the functionalities of heteroatom N-doping [38]. Presence of N in the N-GE matrix can enhance the hydrophilicity between the electrolyte and electrode materials, thereby introducing extra pseudocapacitance and enhancing EDLC [39]. Moreover, it also demonstrates that N-GE has better electron-transfer efficiency than graphene, boosting its potential use for electrochemical supercapacitors.

Figure 5.7 shows the CV curve of NGNP recorded at 10 mV/s, revealing that the ternary NGNP electrode has the best electrochemical properties because of the largest current-density response. The electrochemical behaviour of NGNP is improved distinctly owing to the combined effects between EDLC and pseudocapacitive performance arising from PANI and nickel ferrite. Therefore, the roles of nickel ferrite and PANI are to enhance the SC (especially pseudocapacitance), whereas that of nickel ferrite can also prevent the stacking of N-GE sheets and create ultra-thin PANI film coats on the surface of NGN. This result implies that the synergetic effect among the three components leads to additional capacitance. The SC of NGNP was found to be ≤ 335.0 F/g at 10 mV/s, suggesting the superiority of NGNP as a supercapacitor compared with binary nanocomposites, as well as the individual components used in NGNP ternary nanocomposites.

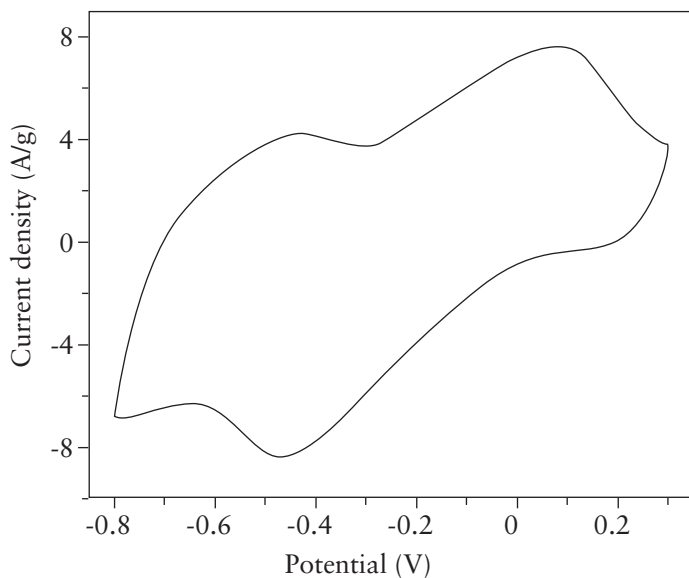


Figure 5.7 CV curve of NGNP in 1 M potassium hydroxide at a scan rate of 10 mV/s

GCD measurement is considered as a more accurate method, especially for pseudo-capacitances. Therefore, the electrochemical behaviour of an as-fabricated NGNP composite electrode was investigated in a two-electrode system by GCD. To evaluate the capacitance and rate capability of electrodes for symmetric supercapacitors, the GCD curve for NGNP at 0.1 A/g is displayed as **Figure 5.8**. This charge–discharge curve shows good symmetry and fairly linear slopes, demonstrating ideal electrochemical capacitance behaviour, fast Faraday redox reaction, and good capacitive behaviour of the ternary NGNP.

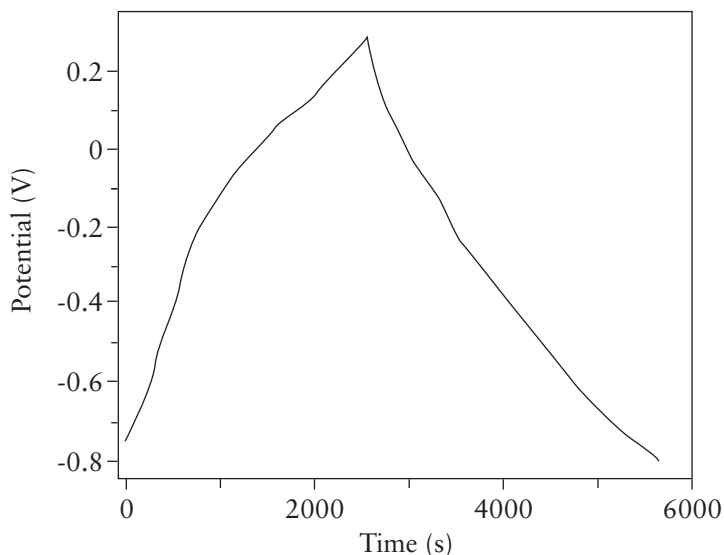


Figure 5.8 GCD curve of NGNP at a current density of 0.1 A/g

5.2.2 Manganese Ferrite/Graphene/Polyaniline Nanocomposites

A MGP ternary nanocomposite has been synthesised *via* a facile two-step approach and exhibited outstanding electrochemical performance in the form of a high SC and good cycling stability superior to those of its individual components (manganese ferrite, reduced-GO, PANI) and corresponding binary hybrids [manganese ferrite/graphene (MG), manganese ferrite/PANI and graphene/PANI]. The high electrochemical performance of ternary MGP can be attributed to its well-designed nanostructure and the synergistic effect of its individual components.

Graphite oxide was prepared from purified natural graphite by a modified Hummers method, as described previously [40]. Binary

MG was prepared by a hydrothermal method [41]. Graphite oxide (50 mg), $\text{MnCl}_2 \cdot 4\text{H}_2\text{O}$ (0.65 mmol), and $\text{FeCl}_3 \cdot 6\text{H}_2\text{O}$ (1.30 mmol) were well-dispersed and mixed together in 70 mL of ethylene glycol. A stable homogeneous emulsion was obtained after adjustment of the pH to 10 with sodium hydroxide solution. The resulting mixture was transferred into a 100 mL TeflonTM-lined stainless steel (SS) autoclave and heated to 180 °C for 24 h. The precipitate was filtered, washed with ethanol and distilled water, and dried in a vacuum oven at 60 °C. Ternary MGP was synthesised *via in situ* polymerisation of aniline monomers in the presence of binary MG [42] (Figure 5.9). Then, 400 mg of MG and APS (0.75 g) were dispersed in 100 mL of 0.1 mol/L *p*-toluene sulfonic acid aqueous solution with ultrasonic vibration for 30 min to obtain a uniform suspension. Aniline (0.3 mL) was added to this mixture drop-wise under vigorous stirring in an ice-water bath, after which the resulting mixture was allowed to polymerise under stirring for 24 h in the ice-water bath. Finally, the ternary MGP hybrid was filtered and washed with a large amount of deionised water.

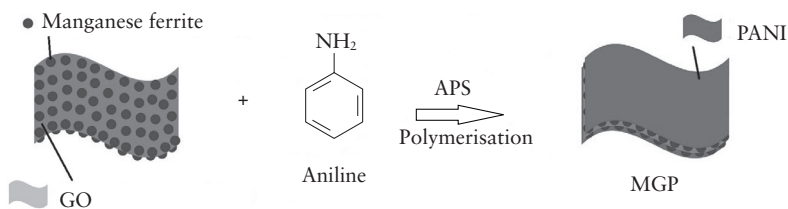


Figure 5.9 Formation of MGP ternary nanocomposite (schematic)

To evaluate the electrochemical performance of as-obtained ternary MGP composites, CV and GCD measurements in a 1 M potassium hydroxide aqueous solution using a three-electrode system were carried out. Figure 5.10 presents the CV curve of a ternary MGP nanocomposite. A pair of redox peaks is shown in the CV curve of

ternary MGP. Two pairs of redox peaks indicate the pseudocapacitance behaviour of MnFe_2O_4 . Reduced GO exhibited a nearly rectangular shape with no obvious peaks for oxidation and reduction, suggesting a characteristic of the electric double-layer capacitance behaviour of carbon-based materials, whereas PANI showed a pair of redox peaks due to the redox transition between a semiconducting state (leucoemeraldine form) and conducting state (polaronic emeraldine form) [43]. Moreover, the ternary MGP nanocomposite showed the highest current density compared with individual and binary composites, implying the best capacitive performance. **Figure 5.11** reveals that ternary MGP exhibited the longest discharge time, suggesting the best electrochemical performance. The ternary MGP showed a high SC of 454.8 F/g at 0.2 A/g, illustrating the high capacity of the ternary MGP. The ternary MGP electrode exhibited much higher capacitive performance than that of binary composites. Remarkably, a high energy density of 216.74 Wh/kg at a power density of 351.47 W/kg was attained with ternary MGP.

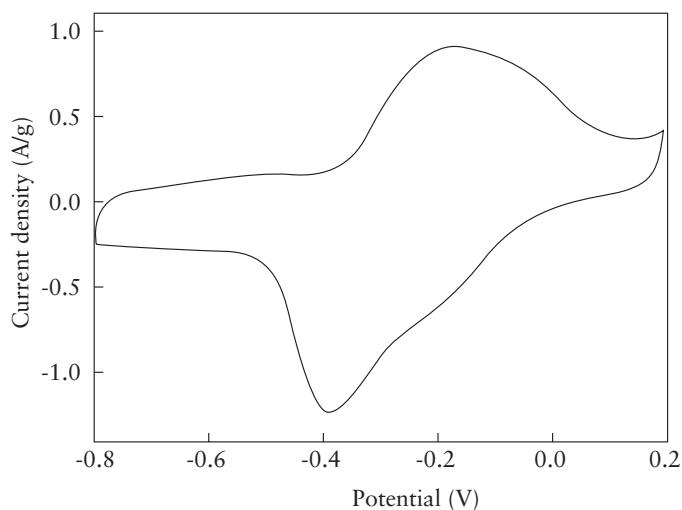


Figure 5.10 CV curve of ternary MGP at 1 mV/s

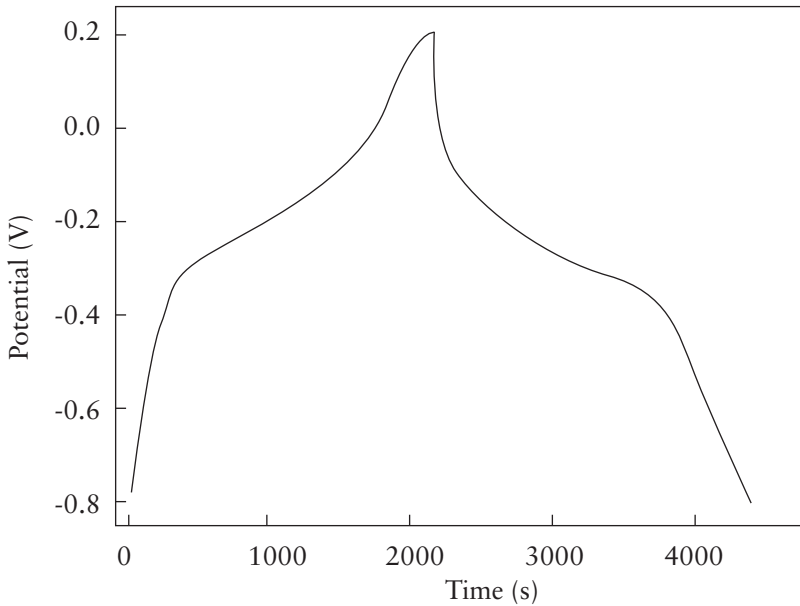


Figure 5.11 GCD of ternary MGP

5.3 Graphene/Carbon Nanotubes/Polyaniline Ternary Nanocomposites

New types of ternary nanocomposites can be prepared for supercapacitor electrodes by making use of graphene nanosheets (GNS) as support materials for deposition of PANI particles and CNT as conductive wires interconnected among GNS/PANI particles. CNT can not only provide highly conductive paths resulting in the improvement of conductivity of composites, it can also maintain mechanical strength.

GNS/CNT/PANI ternary nanocomposites have been prepared by *in situ* polymerisation [43]. In a typical procedure, CNT were functionalised by a mixture (3:1, *v/v*) of concentrated sulfuric acid

(98 wt%) and nitric acid (65 wt%) for 2 h to remove the catalyst particles and other impurities. GNS was prepared by reduction of graphite oxide. Then, 0.165 g GNS and CNT (mass ratio of GNS to CNT was 99:1) were added to 135 mL of water and sonicated for 2 h. Then, 0.25 M aniline monomers (40 mL, solvent: 1 M hydrochloric acid) were added to the GNS/CNT suspension and sonicated for 30 min. Afterwards, an equal volume of 0.25 M APS solution was added into the mixture described above and stored at 0–4 °C for 4 h. Finally, the GNS/CNT/PANI composite was washed with distilled water and ethanol, and dried in a vacuum oven at 80 °C for 12 h. For the preparation of electrodes, the electroactive materials carbon black and polytetrafluoroethylene were mixed in a mass ratio of 75:20:5 and dispersed in ethanol. Then, the resulting mixture was coated onto a nickel foam substrate (1 × 1 cm) with a spatula, followed by drying at 100 °C for 12 h in a vacuum oven. Mass of each electrode was ≈4 mg (including the conducting agent and binder). PANI particles on GNS could interconnect with each other due to a CNT conductive network as well due to an improvement in mechanical strength. Therefore, this unique structure was favourable for the enhancement of electrochemical performance.

CV tests were done between -0.7 V and 0.3 V [*versus* mercury/mercury(II) oxide] at a scan rate of 10 mV/s. The GCD curve was measured at current densities of 2, 10, 20 and 50 mA/cm². **Figure 5.12** shows the CV curves of as-prepared samples in which the current has been transferred onto a specific current per unit mass of electroactive material. Positive currents in **Figure 5.12** denote oxidation processes and negative currents denote reduction processes. In **Figure 5.12**, a couple of redox peaks in CV curves of pure PANI and as-prepared composites can be attributed to the redox transition of PANI between a semiconducting state (leucoemeraldine form) and conducting state (polaronic emeraldine form), which results in redox capacitance. Values of 0.18, 0.29 and 0.37 V were obtained for the redox reactions of PANI with GNS and/or CNT incorporation, suggesting that redox reactions were more reversible after addition of GNS and/or CNT. Also, the larger current-density response of the GNS/PANI composite electrode denotes a higher SC than that

of CNT/PANI and GNS/CNT/PANI composites. Dispersion of nanoscale PANI particles on GNS reduces the diffusion and migration length of electrolyte ions during fast charge–discharge processes and increases the electrochemical utilisation of PANI.

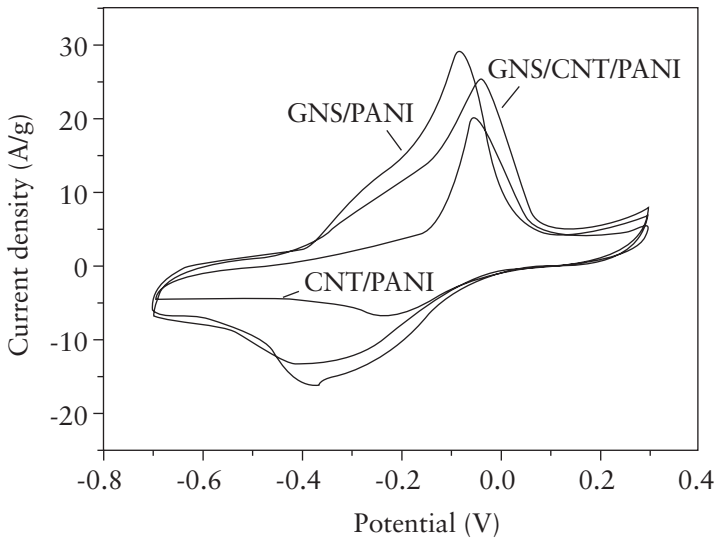


Figure 5.12 CV curve of CNT/PANI, GNS/PANI binary and GNS/CNT/PANI ternary nanocomposites at a scan rate of 10 mV/s

Figure 5.13 shows the GCD curves of binary and ternary nanocomposites. The charge voltage becomes lower and discharge voltage becomes higher after GNS and/or CNT are incorporated in PANI. This finding suggests that the energy consumed by internal resistance is reduced and, therefore, effective energy-storage is improved. This improvement could be because the inner resistance of the electrode is reduced if GNS and/or CNT are present.

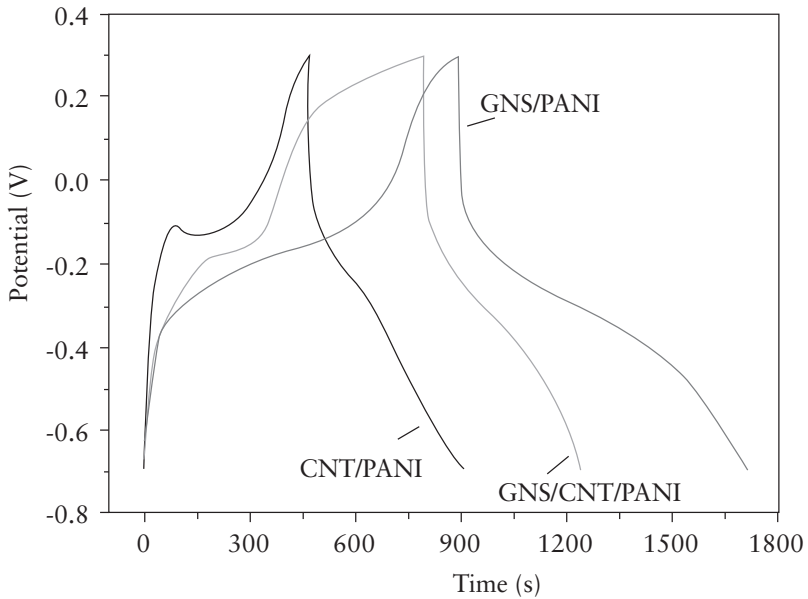


Figure 5.13 GCD of GNS/PANI, CNT/PANI binary and GNS/CNT/PANI ternary nanocomposites at 2 mA/cm^{-2}

Two obvious voltage stages are in the curves: -0.2 to 0.3 and -0.7 to -0.2 V. During the former, the short duration of charge–discharge can be ascribed purely to the electric double-layer capacitance of the electrode. During the latter, the combination of electric double-layer capacitance and Faradaic capacitance is responsible for the longer charge–discharge duration due to Faradaic charge transfer accompanied by the double-layer charging–discharging process. These results are in accordance with those deduced from CV tests. The SC of GNS/CNT/PANI was found to be much higher than that of the CNT/PANI composite but lower than that of the GNS/PANI composite at the same scan rate. A maximum SC of $1,035 \text{ F/g}$ was obtained at a scan rate of 1 mV/s for the GNS/CNT/PANI composite compared with 780 and $1,046 \text{ F/g}$ for CNT/PANI and GNS/PANI, respectively. This greatly enhanced SC is due to the synergistic effect

between GNS and PANI. In addition, the small nanometre-sized PANI can exhibit enhanced electrode–electrolyte interface areas, providing high electroactive regions and short diffusion lengths [44], which can ensure high utilisation of PANI. The SC of GNS/CNT/PANI composite is much larger than that of single-walled CNT/PANI (350–485 F/g) [45], porous carbon/PANI (160–180 F/g) [46], multi-walled carbon nanotubes (MWCNT)/PANI (322–606 F/g) [6, 47], and activated carbon/PANI (380–500 F/g) [48, 49]. The GNS/CNT/PANI electrode is found to exhibit excellent stability over the entire cycle numbers. After the first cycle, the SC increases by 11% and the electrode thereafter reaches a stable state. After 1,000 cycles, the capacitance decreases only 6% of initial capacitance compared with 52 and 67% for GNS/PANI and CNT/PANI composites, demonstrating that the GNS/CNT/PANI electrode exhibits excellent cycle stability. The decrease in SC could be attributed to swelling and shrinkage during long-term charge–discharge processes [50].

With this new type of ternary nanocomposites, the maximum SC was found to be 1,035 F/g at a scan rate of 1 mV/s in 6 M potassium hydroxide. After 1,000 cycles, only 6% of the initial capacitance was decreased compared with 52 and 67% for GNS/PANI and CNT/PANI composites, respectively, thereby demonstrating that the GNS/CNT/PANI electrode has excellent cycle stability. Therefore, the intriguing GNS/CNT/PANI composite is quite a suitable and promising electrode material for supercapacitors compared with GNS/PANI and CNT/PANI binary nanocomposites.

5.4 Polyaniline/Polypyrrole/Carbon Nanotubes Ternary Nanocomposites

CP are widely investigated polymers for electrochemical supercapacitors. Among CP, PANI and Ppy are considered to be the most important materials due to their easy synthesis, low cost, high electrical conductivity, favourable physiochemical properties, and environmental stability. These two CP have individually shown enormous potential for application in the construction of electrodes

for supercapacitors, so a combination of the two could display superior performance.

Several reports are available on the synthesis of copolymer-based on PANI and Ppy *via* different synthetic methods, and researchers have investigated their various properties (e.g., morphological, thermal, electrochemical). Zhang and co-workers prepared a composite of PANI and Ppy by two-step electrochemical polymerisation and investigated its electrochemical performance [51]. Xu and co-workers investigated the morphological and electrochemical reactivity of poly(aniline-*co*-pyrrole) prepared by chemical oxidative copolymerisation [52]. Mavundla and co-workers reported the morphological evolution as well as optical and structural properties of poly(aniline-*co*-pyrrole) synthesised by chemical oxidative copolymerisation [53]. Qin and co-workers prepared poly(aniline-*co*-pyrrole) by chemical oxidative polymerisation using cetyltrimethylammonium chloride as a template and investigated its electrochemical performances [54]. Palaniappan and co-workers synthesised poly(aniline-*co*-pyrrole) by inverted emulsion polymerisation and checked its electrochemical properties [55]. Javadian and co-workers synthesised PANI–Ppy copolymer by *in situ* chemical polymerisation and investigated its capacity for the removal of Co(II) from aqueous solutions [56]. Bhaumik and co-workers prepared PANI–Ppy nanofibres *via in situ* chemical polymerisation and examined their adsorption efficiency towards the dye Congo red [57]. Nawaz and co-workers synthesised a multi-layered PANI/Ppy/MWCNT nanocomposite *via* layer-by-layer oxidative polymerisation and checked its morphological and thermal properties [58]. Li and co-workers synthesised a sodium molybdate-doped PANI–Ppy copolymer on SS by CV and studied its corrosion prevention properties [59]. Deng and co-workers prepared a Ppy–PANI/titanium dioxide nanocomposite by *in situ* oxidative polymerisation and investigated its morphology, structure, optical and photoelectrochemical properties [60]. Dubal and co-workers synthesised a PANI–Ppy nanocomposite by simplest oxidative chemical polymerisation and studied its electrochemical properties [61]. Furthermore, the doping of CP by transition metal ions such

as Cu^{2+} , Co^{2+} , Mn^{2+} , Zn^{2+} , and Fe^{3+} (work as redox-active materials) improves capacitance and thus enhances energy density [62–64].

Copper-doped copolymer of PANI and Ppy/MWCNT ternary nanocomposites have been prepared by a simple and inexpensive *in situ* chemical oxidative polymerisation method using APS as an oxidant and hydrochloric acid as a dopant, and have been investigated as high-performance supercapacitor electrode materials [65]. The synthesis of poly(aniline-*co*-pyrrole) copper/CNT nanocomposite is shown in **Figure 5.14**. In a typical process, 1.24 g of Cetyltrimethylammonium bromide (CTAB) and 60 mg of MWCNT were added to 150 ml of 1.5 M hydrochloric acid solution and sonicated for 30 min at room temperature (RT). In another beaker, 0.67 ml of aniline and 0.33 ml of pyrrole were dissolved in 1.5 M hydrochloric acid (60 ml) solution. Into this solution was added (drop-wise) copper(II) chloride solution followed by stirring for 15 min. Then, copper(II) chloride-doped monomer solution was added in a well-dispersed suspension of MWCNT solution. Subsequently, 60 ml of deionised water containing 2 g of APS was added drop-wise to the solution described above and stirred at constant speed for 5 h at RT. After complete polymerisation, the entire solution was maintained at 1–5 °C for 12 h. The resultant precipitate was filtered and washed with deionised water and ethanol several times, and dried at 70 °C for 12 h to obtain the poly(aniline-*co*-pyrrole) copper/CNT nanocomposite. Scanning electron microscopy clearly revealed the formation of nanocomposites.

Electrochemical characterisations for ternary nanocomposites were compared with other binary nanocomposites. CV and GCD were carried out to identify the oxidation and reduction potentials as well as the effect of Cu^{2+} on the electrochemical performance of the nanocomposite. CV curves of poly(aniline-*co*-pyrrole) copper/CNT electrode material at scan rates of 10, 20, 50, 100, 200 mV/s in 1 M potassium chloride solution within the applied voltage range (-0.8 to +0.8 V) are shown in **Figure 5.15**. In the CV curves, the negative and the positive current region denotes cathodic reduction and anodic oxidation, respectively. The non-rectangular shape of CV curves

implies redox behaviour because of functional groups. Two pairs of redox peaks at potentials of -0.53 V/-0.35 V and -0.13 V/0.55 V were obtained for poly(aniline-co-pyrrole) copper/CNT nanocomposite, and the peaks were found to be shifted with reductions in scan rate.

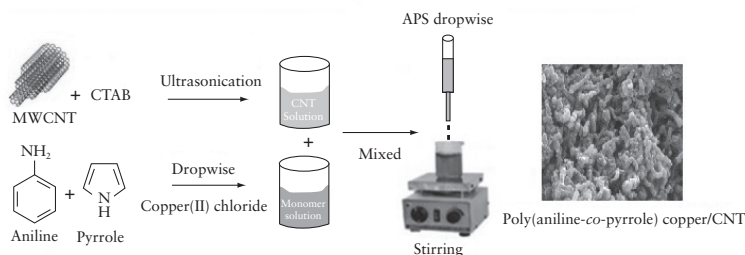


Figure 5.14 The synthesis of poly(aniline-co-pyrrole) copper/CNT nanocomposite (schematic)

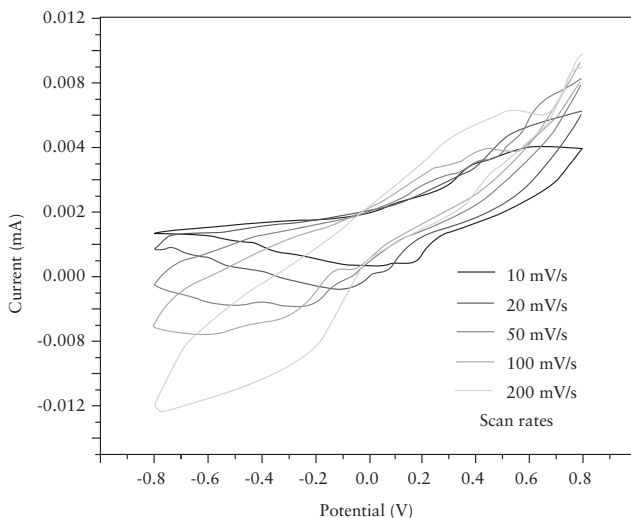


Figure 5.15 CV of poly(aniline-co-pyrrole) copper/CNT nanocomposite at different scan rates

Poly(aniline-*co*-pyrrole) copper/CNT nanocomposite achieved a maximum SC of 411 F/g at a scan rate of 10 mV/s compared with those of binary composites. Achievement of the highest SC of the poly(aniline-*co*-pyrrole) copper/CNT nanocomposite could have been due to: (i) doping of transition metal ions; (ii) highly accessible surface area of MWCNT in poly(aniline-*co*-pyrrole) copper/CNT nanocomposites enhances the SC; (iii) strong interactions among the π -bonded MWCNT surface with the conjugated structure of the copolymer improve the SC; and (iv) uniform coating of copper(II) chloride-doped poly(aniline-*co*-pyrrole) over the MWCNT surface increases the SC.

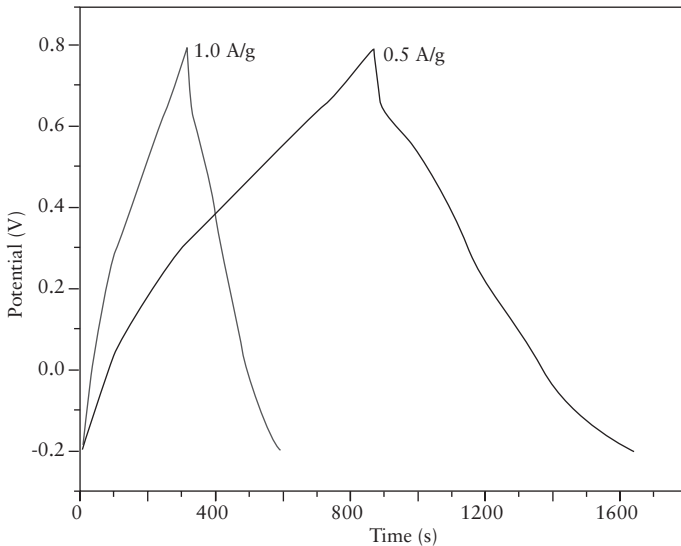


Figure 5.16 GCD of poly(aniline-*co*-pyrrole) copper/CNT nanocomposite

GCD plots of poly(aniline-*co*-pyrrole) copper/CNT nanocomposite at current densities of 0.5 and 1.0 A/g within the potential window of -0.2 V to 0.8 V are shown in Figure 5.16. The second voltage

drop had a longer duration of discharge. The quick discharge in the 0.8–0.64 V potential region was associated with electrochemical double-layer (EDL) capacitance, whereas the second voltage drop at 0.64 V to -0.1 V had a longer duration of discharge, signifying a combination of EDL capacitance and pseudocapacitance. With an increase in the current density, the discharge time decreased. Based on their superior electrochemical performance, as-prepared poly(aniline-*co*-pyrrole) copper/CNT ternary nanocomposites can be used for high-performance supercapacitor electrode materials.

EIS is helpful for analyses of the behaviour of the electrochemical frequency of supercapacitor electrodes. The ideal Nyquist impedance plot displays a semicircle at high frequency and straight line at low frequency. Nyquist plots are usually interpreted by fitting the experimental spectra to equivalent electrical circuits. **Figure 5.17** shows the Nyquist plot of poly(aniline-*co*-pyrrole) copper/CNT nanocomposite at 0 V.

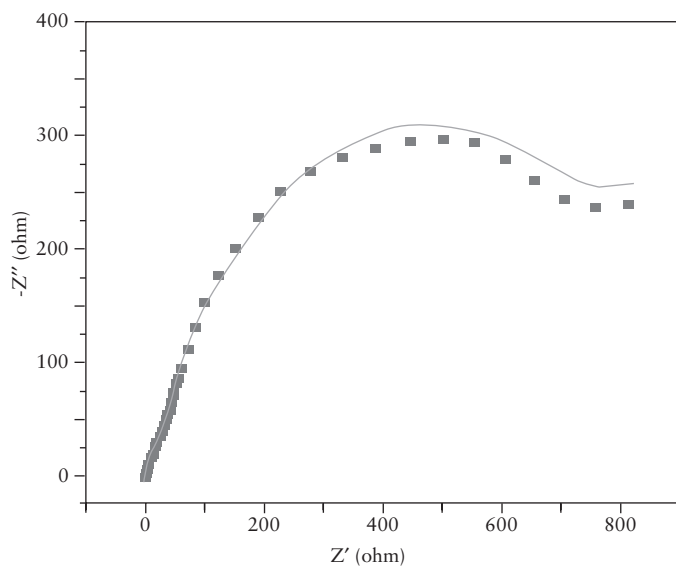


Figure 5.17 Nyquist plot of poly(aniline-*co*-pyrrole) copper/CNT nanocomposite

The area at higher frequency denotes electrolyte properties, and the area at the middle frequency is associated with processes at the electrode–electrolyte interface. The resultant relaxation effect is represented by a semicircle whose intercept at a higher frequency with a real axis corresponds to solution resistance, and at the middle frequency with a real axis corresponds to charge transfer resistance. The linear part is due mainly to the diffusion-limited processes that result from Warburg behaviour. The solution resistance and charge transfer resistance of poly(aniline-*co*-pyrrole) copper/CNT nanocomposites determined from an equivalent circuit stimulated by fitting data from the experimental curve were found to be 1.276 and 950 Ω . The low solution resistance of poly(aniline-*co*-pyrrole) copper/CNT nanocomposite corresponds to higher conductivity and higher capacitance, which are important parameters for redox supercapacitors. This phenomenon arises due to maximum charge delocalisation of Cu^{2+} ions in poly(aniline-*co*-pyrrole) copper/CNT nanocomposite.

References

1. A.G. Porras-Gutiérrez, B.A. Frontana-Uribeb, S. Gutiérrez-Granados, S. Griveaud and F. Bedioud, *Electrochimica Acta*, 2013, **89**, 840.
2. C. Peng, S. Zhang, D. Jewell and G.Z. Chen, *Progress in Natural Science*, 2008, **18**, 777.
3. V. Gupta and N. Miura, *Electrochimica Acta*, 2006, **52**, 1721.
4. T.I.W. Schnoor, G. Smith, D. Eder, K.K. Koziol, G. Tim and K. Schulte, *Carbon*, 2013, **60**, 229.
5. B. Dong, B. He, C. Xu and H. Li, *Materials Science and Engineering B*, 2007, **143**, 7.

6. H. Mi, X. Zhang, S. An, X. Ye and S. Yang, *Electrochemistry Communications*, 2007, **9**, 2859.
7. T.M. Wu, H.L. Chang and Y.W. Lin, *Composites Science and Technology*, 2009, **69**, 639.
8. H. Lee, H. Kim, M.S. Cho, J. Choi and Y. Lee, *Electrochimica Acta*, 2011, **56**, 7460.
9. M. Lu, L. Guo, S. Kharkwal, H. Wu, H.Y. Ng and S.F. Li, *Journal of Power Sources*, 2013, **221**, 381.
10. A. Cormie and A. Cross, *Electrochimica Acta*, 2010, **55**, 7478.
11. Y. Zhang and G. Li, *International Journal of Hydrogen Energy*, 2011, **36**, 11760.
12. H. Wang and C. Peng, *Materials Science and Engineering B*, 2011, **176**, 1073.
13. X. Zhao and L. Zhang, *American Chemical Society*, 2012, **6**, 5404.
14. S. Razak, A. Ahmad and S.H. Zein, *Journal of Physical Science*, 2009, **20**, 27.
15. R.K. Sharma, A.C. Rastogi and S.B. Desu, *Electrochimica Acta*, 2008, **53**, 7690.
16. X. Lu, H. Dou, C. Yuan, S. Yang, L. Hao, F. Zhang, L. Shen, L. Zhang and Z. Zhang, *Journal of Power Sources*, 2012, **197**, 319.
17. R.P. Mahore, S.B. Kondawar, D.K. Burghate and B.H. Meshram, *Journal of the Chinese Advanced Materials Society*, 2015, **3**, 45.

18. R. K. Sharma, A. Karakotic, S. Seala and L. Zhaia, *Journal of Power Sources*, 2010, **195**, 1256.
19. H. Huang, M. Gan, L. Ma, L. Yu, H. Hu, F. Yang, Y. Li and C. Ge, *Journal of Alloys and Compounds*, 2015, **630**, 214.
20. K. Xie, J. Li, Y. Lai, Z.a. Zhang, Y. Liu, G. Zhang and H. Huang, *Nanoscale*, 2011, **3**, 2202.
21. F. Gobal and M. Faraji, *Journal of Electroanalytical Chemistry*, 2013, **691**, 51.
22. Z.F. Li, H. Zhang, Q. Liu, L. Sun, L. Stanciu and J. Xie, *Applied Materials Interface*, 2013, **5**, 2685.
23. J. Yan, T. Wei, B. Shao, Z. Fan, W. Qian, M. Zhang and F. Wei, *Carbon*, 2010, **48**, 487.
24. J. Li, H. Xie, Y. Li, J. Liu and Z. Li, *Journal of Power Sources*, 2011, **196**, 10775.
25. X. Li, Y. Chai, H. Zhang, G. Wang and X. Feng, *Electrochimica Acta*, 2012, **85**, 9.
26. L.L. Zhang, S. Zhao, X.N. Tian and X.S. Zhao, *Langmuir*, 2010, **26**, 17624.
27. W. Wang, Q. Hao, W. Lei, X. Xia and X. Wang, *Journal of Power Sources*, 2014, **269**, 250.
28. P. Xiong, C. Hu, Y. Fan, W. Zhang, J. Zhu and X. Wang, *Journal of Power Sources*, 2014, **266**, 384.
29. X. Wang, L. Yu, X. Wu, F. Yuan, Y. Guo, Y. Ma and J. Yao, *Journal of Physical Chemistry C*, 2009, **113**, 15553.
30. S. Anwar, K.S. Muthu, V. Ganesh and N. Lakshminarasimhan, *Journal of Electrochemistry Society*, 2011, **158**, 976.

31. Y. Fu, Y. Wan, H. Xia and X. Wang, *Journal of Power Sources*, 2012, **213**, 338.
32. C. Vidal-Abarca, P. Lavela and J.L. Tirado, *Journal of Physical Chemistry C*, 2010, **114**, 12828.
33. C.T. Cherian, J. Sundaramurthy, M.V. Reddy, P. Suresh Kumar, K. Mani, D. Pliszka, C.H. Sow, S. Ramakrishna and B.V.R. Chowdari, *ACS Applied Materials Interface*, 2013, **5**, 9957.
34. N.A. Kumar, H. Nolan, N. McEvoy, E. Rezvani, R.L. Doyle, M.E.G. Lyons and G.S. Duesberg, *Journal of Materials Chemistry A*, 2013, **1**, 4431.
35. L. Chen, X. Zhang, H. Liang, M. Kong, Q. Guan, P. Chen, Z. Wu and S. Yu, *ACS Nano*, 2012, **6**, 7092.
36. S. Wang, E. Iyyamperumal, A. Roy, Y. Xue, D. Yu and L. Dai, *Angewandte Chemie International Edition*, 2011, **50**, 11756.
37. P. Chen, T. Xiao, Y. Qian, S. Li and S. Yu, *Advanced Materials*, 2013, **25**, 3192.
38. Y. Lee, K. Chang and C. Hu, *Journal of Power Sources*, 2013, **227**, 300.
39. E. Iyyamperumal, S. Wang and L. Dai, *ACS Nano*, 2012, **6**, 5259.
40. H. Wang, Q. Hao, X. Yang, L. Lu and X. Wang, *Applied Materials Interface*, 2010, **2**, 821.
41. Y. Fu, P. Xiong, H. Chen, X. Sun and X. Wang, *Industrial Engineering Chemistry Research*, 2012, **51**, 725.
42. P. Xiong, H. Huang and X. Wang, *Journal of Power Sources*, 2014, **245**, 937.

43. J. Yan, T. Wei, Z. Fan, W. Qian, M. Zhang, X. Shen and F. Wei, *Journal of Power Sources*, 2013, **195**, 3041.
44. H. Zhang, G.P. Cao, W.K. Wang, K.G. Yuan, B. Xu, W.F. Zhang, J. Cheng and Y.S. Yang, *Electrochimica Acta*, 2009, **54**, 1153.
45. Y.K. Zhou, B.L. He, W.J. Zhou and H.L. Li, *Journal of Electrochemical Society*, 2004, **151**, A1052.
46. W.C. Chen and T.C. Wen, *Journal of Power Sources*, 2003, **117**, 273.
47. S.R. Sivakkumar, W.J. Kim, J.A. Choi, D.R. MacFarlane, M. Forsyth and D.W. Kim, *Journal of Power Sources*, 2007, **171**, 1062.
48. J.H. Park and O.O. Park, *Journal of Power Sources*, 2002, **111**, 185.
49. M.J. Bleda-Martinez, C. Peng, S.G. Zhang, G.Z. Chen, E. Morallon and D. Cazorla-Amoros, *Journal of Electrochemical Society*, 2008, **155**, A672.
50. V. Khomenko, E. Frackowiak and F. Beguin, *Electrochimica Acta*, 2005, **50**, 2499.
51. A.Q. Zhang, Y. Zhang, L.Z. Wang and X.F. Li, *Polymer Composites*, 2011, **32**, 1.
52. P. Xu, X.J. Han, C. Wang, B. Zhang and H.L. Wang, *Synthetic Metals*, 2009, **159**, 430.
53. S.E. Mavundla, G.F. Malgas, D.E. Motaung and E.I. Iwuoho, *Journal of Materials Science*, 2010, **45**, 3330.
54. L. Qiu, S. Zhang, L. Zhang, M. Sun and W. Wang, *Electrochimica Acta*, 2010, **55**, 4632.

55. S. Palaniappan, S.B. Sydulu and P. Srinivas, *Journal of Applied Polymer Science*, 2010, **115**, 1695.
56. H. Javadian, *Journal of Industrial Engineering Chemistry*, 2014, **20**, 4233.
57. M. Bhaumik, R. McCrindle and A. Maity, *Chemical Engineering Journal*, 2013, **228**, 506.
58. S. Nawaz, M. Siddiq, A. Kausar, S.T. Hussain and F. Abbas, *Polymer Plastic Technology Engineering*, 2014, **53**, 661.
59. F. Li, G. Li, J. Zeng and G. Gao, *Journal of Applied Polymer Science*, 2014, **131**, 40602.
60. F. Deng, L. Min, X. Luo, S. Wu and S. Luo, *Nanoscale*, 2013, **5**, 8703.
61. D.P. Dubal, S.V. Patil, G.S. Gund and C.D. Lokhande, *Journal of Alloys and Compounds*, 2013, **552**, 240.
62. J. Li, M. Cui, Y. Lai, Z. Zhang, H. Lu, J. Fang and Y. Liu, *Synthetic Metals*, 2010, **160**, 1228.
63. S. Dhibar, P. Bhattacharya, G. Hatui, S. Sahoo and C.K. Das, *ACS Sustainable Chemical Engineering*, 2014, **2**, 1114.
64. G. Karthikeyan, S. Sahoo, G.C. Nayak and C.K. Das, *Macromolecule Research*, 2012, **20**, 351.
65. S. Dhibar, P. Bhattacharya, G. Hatui and C.K. Das, *Journal of Alloys and Compounds*, 2015, **625**, 64.

Conducting Polymer Nanocomposites for Supercapacitors

A**bbreviations**

0D	Zero-dimensional
1D	One-dimensional
2D	Two-dimensional
3D	Three-dimensional
AC	Alternating current
ACNF	Activated carbon nanofibres(s)
AEP	Anodic electropolymerisation
APS	Ammonium peroxydisulfate
CNT	Carbon nanotube(s)
CP	Conducting polymer(s)
CTAB	Cetyltrimethylammonium bromide
CV	Cyclic voltammetry
CVD	Chemical vapour deposition
EDL	Electrochemical double-layer
EDLC	Electrochemical double-layer capacitors
EIS	Electrochemical impedance spectroscopy

Conducting Polymer Nanocomposites for Supercapacitors

EMI	Electromagnetic interference
ESR	Equivalent series resistance
FTO	Fluorine-doped tin oxide
GCD	Galvanostatic charge–discharge
GNS	Graphene nanosheet(s)
GO	Graphene oxide
GP	Graphene paper
G–PANI	Graphene–polyaniline
GPCP	Graphene composite paper
HEV	Hybrid electric vehicle(s)
LED	Light-emitting diode
LRV	Light-rail vehicle(s)
MG	Manganese ferrite/graphene
MGP	Manganese ferrite/graphene/polyaniline
MWCNT	Multi-walled carbon nanotube(s)
N-GE	Nitrogen-doped graphene
NGN	Nitrogen-doped graphene/nickel ferrite
NGNP	Nitrogen-doped graphene/nickel ferrite/polyaniline
NMP	N-methyl pyrrolidone
PA	Polyacetylene
PANI	Polyaniline

Abbreviations

PC	Propylene carbonate
PEDOT	Poly(3,4-ethylenedioxythiophene)
PGTN	Polyaniline/graphene/titanium dioxide nanotube(s)
Ppy	Polypyrrole
PTH	Polythiophene
PTN	Polyaniline/titanium dioxide nanotube(s)
RF	Radio frequency
RT	Room temperature
SC	Specific capacitance(s)
SCE	Standard calomel electrode
SDS	Sodium dodecyl sulfate
SS	Stainless steel
SWCNT	Single-walled carbon nanotube(s)
UPS	Uninterruptible power supply(ies)
VRH	Variable range hopping

Conducting Polymer Nanocomposites for Supercapacitors

Index

A

- Absorbance, 111
 - Absorption, 25
- Acceleration, 21
- Acetonitrile, 11, 18
 - electrolyte, 18
- Acid, 11, 19-20, 55, 59-60, 65, 77, 82-84, 88-90, 98-99, 115-116, 124, 126-127, 132
 - base chemistry, 55
 - Acidic, 76, 79, 89, 91, 120
- Activated carbon nanofibre(s) (ACNF), 97
- Activation energy, 62
- Adetel Group, 23
- Adhesion, 76, 99
- Adsorption, 32, 131
- Aerogel, 6, 77
- Agent, 83, 110, 120, 127
- Agglomerate, 87
 - Agglomeration, 66, 75, 87
- Airbus™, 17
- Alstom, 22
- Alternating current (AC), 25, 45
- Aluminium, 44
- Ambient air, 91
- Ammeter, 30-31
- Ammonium peroxydisulfate (APS), 80, 83, 89, 115, 120, 124, 127, 132-133
- Ammonium persulfate, 76, 79, 82-83, 120

Amorphous, 63
Amperometry, 31
Analyte, 29-32, 34, 41-44
 concentration, 29
 solution, 30-31
Anatase phase, 115
Aniline, 59, 80-84, 89-91, 98-99, 110-112, 115-116, 120, 124,
 127, 131-136
Anion, 34
Anode, 92, 119
Anodic, 39, 41, 90, 92, 132
 electropolymerisation (AEP), 90
 Anodisation, 115
Aqueous, 11-12, 38-39, 59, 82, 88-91, 99, 111, 115, 124, 131
 solution, 82, 91, 99, 111, 115, 124
Aromatic, 57-58
Arrhenius, 61-62
Asymmetric, 8, 13-14
 hybrid, 14
Autoclave, 82, 124
Auxiliary electrode, 29-31, 35, 43

B

Backbone, 13, 52, 54-55, 57, 60, 74, 99-100
Base-growth model, 95
Battery(ies), 1, 4-5, 7-8, 11, 13-21, 24-25, 59-60, 119
 conventional, 8, 11, 16
 electrode, 14
 size, 17
Benzene, 87, 94
Binary, 74-75, 77-81, 110, 118, 121, 123-125, 128-130, 132, 134
Binder, 99, 127
 Binding, 57
Biomaterial, 77
Bipolaron, 57-61
 Bipolaronic, 84
Blend, 65

Blending, 52, 74
Bombardier Transportation, 21
Bond, 56, 87
 Bonding, 58, 66, 86
Braking energy, 18, 21-23
Buffer, 18-20
Bus, 18, 23-24

C

Calibration, 44
Calomel electrode, 35, 37-38, 90
Calorimetry, 104
Camphor, 94
Capabus™, 18, 23-24
Capacitor, 1-4, 8-9, 16-17, 24, 92, 99
 Conventional, 1, 3, 8, 16, 24
Capacity, 2, 8, 52, 99, 125, 131
Carbon, 2, 6, 10, 12-14, 16, 18, 20-21, 23-24, 26, 35, 38, 43-45, 56, 76-77, 87-88, 94-95, 97, 105, 109-110, 119, 121, 125-127, 130, 136, 138
 aerogel, 77
 -based material, 13
 black, 127
 -carbon, 56, 87
 diffusion, 95
 dioxide, 21, 23, 132
 electrode, 12, 14, 18, 24
 nanofibre(s), 97
 nanotube(s), 6, 12-13, 77-78, 87, 94-95, 97-101, 109-114, 118, 126-130, 132-136
 -negative electrode, 14
Carboxylic acid, 88
Carrier, 61
Catalyst, 94-96, 127
 activity, 95
Catenary voltage, 21
Cathode, 8, 92, 115

Conducting Polymer Nanocomposites for Supercapacitors

- Cathodic, 39, 41, 92, 132
 - current, 39, 41
 - voltage, 39
- Cation, 34, 57-58, 69
- Cell, 19-20, 25, 29-31, 34-37, 42, 45, 90, 92, 112, 115
- Cellulose, 6
- Ceramic, 73-75, 99-101
- Cetyltrimethylammonium bromide (CTAB), 77, 132-133
- Cetyltrimethylammonium chloride, 131
- Charge, 1-3, 5, 7-13, 15-17, 20, 23-25, 32, 34-35, 38-39, 43-44, 46, 53, 55-57, 60-63, 66, 77, 79, 84, 88, 92, 94, 99, 112-113, 116, 118, 122, 128-130, 136
 - carrier, 61
 - discharge, 7-8, 11, 38-39, 44, 79, 84, 92, 99, 116, 118, 122, 128-130
 - storage, 12, 16, 56
 - time, 15
 - transfer, 46, 55, 129, 136
- Charged, 2, 11, 14, 18, 22-23, 34, 53, 56, 58, 92
- Charging, 1, 5, 16, 25, 61, 92, 129
- Chemical, 13, 25-27, 32, 42, 46, 51-53, 55, 58-59, 64, 66-67, 70, 76, 87, 97-99, 105-107, 110-111, 115, 120, 131-132, 137, 141
 - composition, 58
 - reaction, 32, 42
 - structure, 51
 - vapour deposition (CVD), 87, 94-96, 99
- Chemistry, 20, 34, 43, 47-48, 52-53, 55, 72, 94, 101-106, 138-139, 141
- Circuit, 4, 8, 19, 21, 29, 37, 45-46, 136
- Co-electrodeposition, 98
- Co-polymers, 74
- Coated, 46, 67, 76, 79, 91, 95, 115-116, 127
 - metal, 46
 - Coating, 13, 70, 76, 88, 90-91, 99, 134
- Cobalt(II,III) oxide, 109
- Coefficient, 34, 44
- Colloid, 104

- Colloidal, 67-68, 76, 91
 - solution, 91
- Colour, 82, 84
 - Colourless, 84, 111
- Combustion, 84
- Commercialisation, 15-16, 78
- Composite, 13, 46, 61, 65, 73, 75-76, 80, 82, 84-85, 88, 90-92, 97, 99-101, 104, 110, 115-116, 119-120, 122, 127, 129-131
 - electrode, 13, 90, 92, 99-101, 122, 127
- Composition, 10, 30, 32, 42, 58
- Concentration, 29, 33-35, 41, 44, 75, 95, 116
- Conducting polymer(s) (CP), 2, 4, 6, 8, 10, 12-14, 16, 18, 20, 22, 24, 26, 28, 30, 32, 34, 36, 38, 40, 42, 44-46, 48, 50-62, 64-70, 72, 74-82, 84, 86-88, 90, 92, 94, 96-98, 100, 102, 104, 106, 108-112, 114, 116, 118-120, 122, 124, 126, 128, 130-132, 134, 136, 138, 140, 142
- Conduction, 5, 7, 55, 62-64, 110
- Conductive, 5, 8, 11, 51-53, 59, 61, 64, 75, 82, 84, 89, 126-127
 - Conductivity, 5, 42, 51-54, 56, 60-65, 73-75, 77-78, 80, 88, 91, 94, 97, 99, 110, 119, 126, 130, 136
- Congo red, 131
- Conjugated, 52-57, 59, 72, 134
 - polymer, 53, 59
 - Conjugation, 52
- Construction, 19, 45, 97, 130
- Consumer, 16, 18
- Consumption, 20-23
- Contact angle, 95
- Convection, 33-35
- Conventional battery(ies), 8, 11, 16
- Conventional capacitor, 1, 3, 8, 16, 24
- Cooling, 94
- Copolymerisation, 131
- Copper, 53, 94, 132-136
- Corrosion, 73, 131
 - resistance, 73
- Cost, 12, 15, 19, 24, 31, 65, 78-79, 97, 118-119, 130

Conducting Polymer Nanocomposites for Supercapacitors

- Coulometry, 31
- Counter electrode, 29, 36, 38, 41-43, 92
- Coupling, 2, 14
- Crystal, 71, 87
 - Crystalline, 63, 71, 86
- Curling, 66
- Current, 2, 4-6, 11, 15, 18, 20-21, 25-26, 29-36, 38-41, 43-46, 61, 67, 84-86, 90-93, 98, 100-101, 113-114, 117-118, 120-123, 125, 127-128, 132-135
 - collector, 6
 - density, 38, 44-45, 67, 84, 86, 91-93, 98, 100-101, 117-118, 120, 122-123, 125, 128, 135
- Cyclic, 38-40, 59, 78, 84, 99, 112
 - stability, 78
 - voltammetry (CV), 38-43, 46, 59, 84-86, 89-93, 99-100, 112-114, 116-117, 121-122, 124-125, 127-129, 131-133
- Cycling, 10-15, 20, 78, 91, 97, 100, 109, 113, 120, 123
 - stability, 11-14, 78, 91, 123

D

- Damage, 25
- Decomposition, 87, 95
- Dedoping, 64-65, 76, 78
- Degradation, 100, 109-110
- Degree of polymerisation, 51
- Deionised, 82, 91, 111, 115, 124, 132
 - water, 82, 91, 111, 115, 124, 132
- Density, 1-2, 4-9, 11, 15-16, 20, 24-25, 38-39, 44-45, 56, 61, 63, 67, 77-78, 84, 86, 91-93, 98, 100-101, 117-123, 125, 127-128, 132, 135
- Deposition, 80, 87, 91, 95, 119, 126
- Deterioration, 8, 113
- Dielectric, 2-5, 9-11, 61
 - block, 5
 - constant, 3
 - material, 2, 4
- Diesel, 18, 20-21, 23-24

Diffusion, 33-35, 41-44, 46, 95, 98, 128, 130, 136
 layer, 33, 35
Dilute, 76
Diode, 18
Discharge(d), 2, 4-5, 7-8, 11, 20, 23, 25, 38-39, 44, 78-79, 84, 92,
 99, 112, 116, 118, 122, 125, 128-130, 135
 Discharging, 15, 25, 92, 129
Dispersant, 75
Dispersed phase, 75
Dispersion, 51, 61, 74, 87, 90, 111, 113, 128
Distilled water, 81-84, 115, 120, 124, 127
Dodecyl benzenesulfonic acid, 77
Dodecyl(trimethyl)azanium bromide, 77
Dopant, 52, 67, 69, 74, 132
Doped, 52-54, 59, 64, 78, 119, 131-132, 134
 state, 54, 78
Doping, 52-56, 58-61, 64-65, 74, 76, 91-92, 119-121, 131, 134
Double-layer, 2, 5, 9-11, 13, 20, 45, 77, 109, 125, 129, 135
 capacitance, 10, 13, 20, 45, 125, 129
Drying, 91, 98, 115, 127
 separator, 2
 Dried, 81-83, 99, 111, 115-116, 124, 127, 132
Dynamic(s), 30-31, 35

E

Electric, 1-2, 11, 15, 18, 21-24, 99, 125, 129
 bus, 18, 23-24
 double-layer, 2, 11, 125, 129
 field, 2
Electrical, 4-5, 7, 13, 19-20, 29, 31, 45, 51-54, 61-62, 64-65, 74,
 76-77, 87-88, 91, 94, 97, 109-110, 130, 135
 circuit, 29
 conductivity, 51, 54, 61-62, 65, 74, 88, 91, 94, 97, 110, 130
 properties, 52, 64
Electricity, 24, 32
Electroactive material, 84, 127
Electroanalytical, 32, 43, 138

Conducting Polymer Nanocomposites for Supercapacitors

- Electrochemical, 1-2, 4-5, 8, 10-11, 18, 26-27, 29-31, 33, 35-41, 43-49, 52, 55, 59, 64, 66-67, 76, 78-80, 84, 86, 91-92, 94, 96-100, 105, 109-110, 112-113, 115-116, 118-125, 127-128, 130-132, 135, 140
 - bath, 29
 - batteries, 4-5, 11
 - cell, 29-31, 36-37, 45, 115
 - characterisation, 38, 79
 - doping, 55
 - double-layer (EDL), 2, 10-11, 77-78, 109, 135
 - capacitor(s) (EDLC), 2, 5, 10-14, 16-18, 24-25, 109, 121
 - impedance spectroscopy (EIS), 38, 44-46, 121, 135
 - instrumentation, 29
 - measurements, 29, 98, 121
 - polymerisation, 29, 67, 97, 131
 - property(ies), 40, 64, 84, 96, 99, 109, 116, 119, 121, 131
 - reaction, 1, 33
 - stability, 36, 80, 100, 110
- Electrochemistry, 34, 46-47, 70, 104, 137-138
- Electrode, 2-3, 5-10, 12-16, 18, 20, 24, 29-46, 78, 86, 90, 92, 97-101, 109-110, 112-113, 115-116, 118-122, 124-125, 127-130, 132, 135-136
 - area, 5, 32
 - bulk, 7
 - electrolyte, 109, 112, 130, 136
 - layer, 15
 - solution interface, 32
 - structure, 15
 - surface, 7, 33-35, 41, 43
- Electrodeposition, 91, 98
- Electrolyte, 5-6, 8, 10-13, 18, 20, 29, 35-36, 38-39, 42-43, 46, 86, 90, 92, 99, 109, 112, 115-116, 121, 128, 130, 136
 - conductance, 6
- Electrolytic capacitor, 2
- Electromagnetic interference (EMI), 60, 64
- Electron, 32-33, 35, 39, 41-42, 44, 52, 56-58, 63, 97, 110, 121, 132

- acceptor, 57
- transfer, 32-33, 35, 39, 41-42, 97, 121
- Electronic, 1, 5, 15, 29-30, 36, 46, 53, 56, 60, 64, 75, 78, 94, 119
- device, 36
- Electrosorption, 12
- Electrostatic, 2, 11, 60, 65
 - capacitor, 2
 - charge, 60
- Electrostatically, 9-10, 12
- Emeraldine, 53-54, 59, 82, 89, 125, 127
 - base, 53, 59
 - salt, 59, 82
- Emirates Air Line™, 24
- Emulsion, 124, 131
 - polymerisation, 131
- Encapsulation, 76
- Energy, 1-2, 4-12, 14-25, 39, 52, 56-58, 62-63, 72, 77-78, 88-89, 99, 102, 109, 118-120, 125, 128, 132, 137
 - consumption, 21-22
 - density(ies), 2, 4, 6-12, 15-16, 24, 39, 77-78, 118-119, 125, 132
 - generation, 16
 - source, 15
 - storage, 1-2, 5-6, 16, 19-20, 22, 24, 99, 109, 128
 - device, 19
- Energy Saver™ system, 21
- Engine, 17, 20-21, 23
- Engineering, 27, 71-72, 94, 103, 136-137, 139, 141
- Environment, 22
 - Environmental, 1, 8, 65, 76-78, 110, 118-119, 130
 - stability, 65, 76-78, 130
- Epoxy, 73, 88
- Equilibrium, 35, 70
- Equivalent series resistance (ESR), 4-5, 11-12, 25, 45
- Ethanol, 83, 98-99, 115, 120, 124, 127, 132
- Ethylene, 87, 124
- Evans Capacitor Company, 17
- Excitation, 33, 35, 45, 56

External circuit, 8

F

Facile doping, 76

Farad, 5

Faradaic, 10, 12-14, 32-33, 35, 129

current, 33, 35

process(es), 10, 12, 14, 32

pseudocapacitance, 10

Faradaically, 10, 12

Faraday's law, 32-34

Ferrite, 77, 83-86, 118-121, 123-124

Fibre, 6, 51, 73-74, 78, 94

Fick's first law, 34

Filled, 61

Filler, 74-75, 77, 79

Film(s), 46, 60, 67, 76, 91, 98, 116, 120-121

Filter, 2, 80

Filtering, 2, 98

Filtrate, 111

Filtration 82, 111

Flake, 73-74, 78, 87

Flask, 94

Flexibility, 64, 77

Flexible, 1, 90

Floating catalyst method, 95

Flow, 5, 11, 30-32, 34-36, 79-80

rate, 34

Fluid, 35

Fluorine-doped tin oxide (FTO), 91-92

Flux, 34

Foam, 127

Free energy, 58

Free space, 3

Frequency, 19-20, 25, 45-46, 82, 135-136

Fuel, 4-5, 7, 15, 19, 23-24

cell, 19

consumption, 23
efficiency, 15
Functionalisation, 87
Furnace, 95-96, 115

G

Galvanostat, 30
Galvanostatic, 31, 38, 44, 84, 91, 116
charge-discharge (GCD), 38-39, 44, 84-85, 92-93, 99-101,
116-118, 122-124, 126-129, 132, 134
Gas, 33, 77, 94-96
Gel, 81
Generator, 17
Geneva Public Transport, 22
Geometry, 42, 73, 75
Glass, 36, 80
transition temperature, 80
Glassy, 38, 43-44, 77
carbon, 38, 43-44, 77
Gold, 35, 38, 43-44, 76-77
Gradient, 95
Graphene, 6, 77-78, 87-91, 109, 115-116, 118-121, 123, 126
composite paper (GPCP), 90
-graphite, 88
nanosheet(s) (GNS), 91, 126-130
oxide, 87-88, 119
paper (GP), 90
-polyaniline (G-PANI), 88-91
Graphite, 38, 44, 73, 87-88, 123-124, 127
oxide, 123-124, 127
Green energy, 16
Green product, 16
Grid, 19, 22
voltage, 19

H

- Handling, 20
- Heat, 11, 15
- Heteroatom, 121
- Heterogeneous, 75
- High-energy, 16
- High-impedence potentiometer, 31
- High-molecular weight, 51
- High-power, 15-17, 92
- High-speed, 23
- High-temperature, 94
- High-throughput, 65
- Homogeneous, 13, 88, 124
- Hot-air oven, 81, 83
- Hybrid, 9-10, 12-19, 23-24, 77-79, 115, 120, 124
 - bus, 18, 23
 - electric vehicle(s) (HEV), 15
 - system, 16
- Hydrazine monohydrate, 88, 91
- Hydrocarbon, 94-96
 - vapour, 94
- Hydrochloric acid, 59, 82-83, 89-90, 98-99, 115-116, 127, 132
- Hydrogen bonding, 66, 86
- Hydrogen peroxide, 82
- Hydrophilicity, 121
- Hydrophobic, 70
 - Hydrophobicity, 88
- Hydroquinone, 90
- Hydrothermal carbonisation, 119
- Hydrothermal method, 119-120, 124
- Hydroxyl, 88, 120
- Hysteresis, 42

I

- Ice, 115, 120, 124
 - water, 115, 120, 124

- bath, 115, 120, 124
 - Impedance, 4, 30, 38, 44-46, 121, 135
 - Impurity(ies), 127
 - In situ*, 76, 79, 81-83, 90-91, 95, 97-98, 110-111, 115, 120, 124, 126, 131-132
 - Indicator electrode, 29
 - Indium tin oxide, 44, 77
 - Inert, 35, 43, 94
 - Inhomogeneous, 61
 - Inorganic, 51, 74, 76, 82, 103
 - organic, 82
 - Instability, 110
 - Insulate, 43
 - Insulation, 5
 - Insulator, 10, 43, 64
 - Integrated circuit, 19
 - Intercalated, 82
 - Intercalation, 12, 87
 - processes, 12
 - Interface, 2, 5, 11, 32, 82, 102, 109, 112, 130, 136, 138-139
 - Intermolecular charge, 60
 - Intramolecular charge, 60
 - Ion, 7, 10, 15, 24, 33, 79, 98, 119-120
 - Ionic, 5, 7, 16, 36, 46, 78
 - liquid, 16
 - Ionisation, 58
 - Iron(II) chloride, 76
 - Iron(III) chloride, 76, 99
 - Iron(III) nitrate, 76
 - Iron(III) oxide, 77
 - Irradiation, 82-83
 - time, 83
 - Isomeric, 56
 - Isomerisation, 56
- K**
- Kinetic, 46

Kinetically, 32

L

Lattice, 87-88

structure, 87

Layer, 2, 5, 9-11, 13, 15, 20, 33, 35, 45-46, 77, 87-88, 100, 109, 125, 129, 131, 135

Lead-acid battery, 19-20

Lead dioxide, 14

Leucoemeraldine, 54, 59, 125, 127

Life-cycle, 1, 5, 8, 14-15, 17, 20, 77

Light, 18-19, 21-23

-emitting diode, 18

-rail, 18, 22-23

vehicle(s) (LRV), 18, 21-23

Linear, 31, 40, 46, 51, 59-60, 122, 136

Linearity, 118

Liquid, 11, 16, 71, 81, 94-95

Lithium-ion, 7, 10, 15, 24, 119

battery(ies), 7, 15, 24, 119

Los Alamos National Laboratory, 17

Low-energy, 18

Low-power, 18

Low-temperature, 25, 62, 94

M

Macromolecular, 55, 103

Macromolecule, 141

Magnetic, 53, 76-77, 87, 115

Manchester University, 87

Manganese dioxide, 109-114

Manganese ferrite/graphene (MG), 91, 118, 123-124, 127, 132

Manganese ferrite/graphene/polyaniline (MGP), 118, 123-126

Manganese oxide, 6, 77, 98

Mannheim Stadtbahn, 18

Manufacture, 8, 18

- Manufacturing, 45, 103
- Mass, 4, 33-35, 39, 44-45, 67, 91, 113, 127
 - loading, 39
 - ratio, 127
 - transfer, 34
 - transport, 33-35
- Mat structure, 13
- Matrix, 56, 61, 73-75, 77, 83, 87, 97, 111, 113, 121
 - phase, 73-74
- Maxwell Technologies, 17
- Mechanical behaviour, 51
- Mechanical properties, 51, 87
- Mechanical strength, 110, 126-127
- Mechanical stress, 13
- Membrane, 66-67
- Mercury, 35, 38, 121, 127
 - Mercury(II) oxide, 121, 127
- Metal, 6, 8, 10, 12-13, 16, 42, 45-46, 61, 63-64, 66-68, 73-75, 77-79, 95, 109, 118-119, 131, 134
 - oxide, 6, 13, 79, 109, 118-119
 - plate, 8
 - ruthenium, 78
 - Metallic, 52-53, 61, 63-64, 74
- Metastable, 91
- Metro train, 22
- Micelle, 66
 - theory, 66
- Michael Faraday, 5
- Microscopic, 61, 78
 - Microscopy, 132
- Microsphere, 69
- Microwave, 82-83
 - irradiation system, 82
 - power, 83
- Migrating, 35
 - Migration, 33-35, 128
- Mixed, 33, 80, 82, 84, 124, 127, 133

Conducting Polymer Nanocomposites for Supercapacitors

- Mixing, 75-76
- Mixture, 81-82, 98, 115, 124, 126-127
- Model, 46, 66, 95
 - Modelling, 16, 79
- Modification, 75
 - Modified, 54, 88, 91, 115, 123
- Moist separator, 2
- Molar ratio, 115
- Molecular weight, 51, 88
- Monitor, 30
 - Monitoring, 32
- Monomer, 29, 51, 65, 67, 69, 78, 83-84, 89, 91, 98, 110-111, 132
 - solution, 84, 110-111, 132
- Morphological, 75, 131
 - Morphologies, 64, 66, 76
 - Morphology, 64, 66, 70, 91, 131
- Multi-walled carbon nanotube(s) (MWCNT), 95-98, 112, 130-134

N

- N-doping, 92, 121
- N-methyl pyrrolidone (NMP), 76, 91
- N-type doping, 56
- Nanocomposite, 16, 37, 73-75, 77, 79-84, 88-90, 92, 111, 123-125, 131-136
- Nanocrystalline, 82
- Nanofibre, 65, 67, 91, 97
- Nanomaterial, 75
- Nanometre, 5, 75, 94, 130
- Nanoparticle, 66, 73, 79, 83, 95
- Nanoporous, 67
- Nanoscience, 64, 103, 105
- Nanosheet, 66
 - curling, 66
- Nanostructure, 64-66, 77, 82, 115, 119, 123
- Nanotechnology, 64, 72, 74, 105-106
- Nanotube, 69, 110

Nanowire, 69
Naphthalene, 94
Negative charge, 88
NeoGreen, 23
Nernst equation, 32, 35
 Nernstian, 38, 44
 system, 44
Nickel, 14, 44, 77, 79-81, 83-87, 118-121, 127
 ferrite, 77, 83-86, 118-121
 hydroxide, 14
Nickel(II) oxide, 77, 79-81
Nitrogen, 58, 115, 119
Nitrogen-doped graphene (N-GE), 119-121
Nitrogen-doped graphene/nickel ferrite (NGN), 120-121
Nitrogen-doped graphene/nickel ferrite/polyaniline (NGNP), 119-123
Non-Faradaic, 10, 14, 32
 process(es), 10, 14, 32
 Non-Faradaically, 10
Non-linear, 59-60
Nucleation, 42, 67
Nyquist impedance plot, 135
Nyquist plot, 45-46, 135

O

One-dimensional (1D), 63, 94, 98
Operating voltage, 16
Optical, 53, 60, 64-65, 87, 131
 properties, 64-65
Organic, 11-12, 39, 51, 56, 62, 82, 87
 electrolyte, 11-12
Output, 36-37, 83
Oven, 81-83, 99, 124, 127
Oxidant, 65, 67, 79, 84, 111, 115, 120, 132
Oxidation, 12, 32-34, 36, 41-43, 57, 59, 62, 78, 84, 87-89, 92, 110-111, 118, 125, 127, 132
 peak, 41-42

Conducting Polymer Nanocomposites for Supercapacitors

- state, 33
 - Oxidative, 58-60, 89, 98, 131-132
- Oxidise, 43
 - agent, 83, 110
- P**
- Packaging, 60
 - Packing, 11
- Panasonic, 18, 27
- Paper, 90
- Particle(s), 2, 5, 34, 61, 67-68, 73, 75, 77, 84, 95, 126-128
 - size, 95
- Particulate, 73-74, 78-79
- Peak anodic, 39
- Peak current, 21, 41, 84
- Peroxide, 82
- Phenazine theory, 66
- Photodoping, 55
- Physical properties, 51-52, 75
- Physical separation, 11
- Physics, 5, 11, 26, 52-53, 56, 71, 94, 102-103, 105
- Physiochemical, 130
- Plastic, 51, 141
- Platinum, 35, 38, 43-44, 77, 90, 92, 112, 115, 120
 - wire, 35, 38, 112
- Polarisation, 5, 42
 - Polarised, 8
- Polarity, 8, 41, 88
- Polaron, 57, 59-61
 - Polaronic, 84, 125, 127
- Poly(3,4-ethylenedioxythiophene) (PEDOT), 77, 98
- Poly(aniline-*co*-pyrrole), 131-136
- Poly(aniline-*co*-pyrrole) copper, 132-136
- Polyacetylene (PA), 53-54, 56, 58, 65
- Polyaniline (PANI), 6, 44, 53-55, 57-61, 63, 65-66, 76-86, 88-91, 97-99, 109-116, 118-121, 123, 125-132
- Polyaniline/graphene/titanium dioxide nanotube(s) (PGTN), 115-

- 118
- Polyaniline/titanium dioxide nanotube(s) (PTN), 115
- Polyconjugated system, 53
- Polyethylene, 36, 76
terephthalate, 76
- Polymer, 2, 4, 6, 8, 10, 12-14, 16, 18, 20, 22, 24, 26, 28, 30, 32,
34, 36, 38, 40, 42, 44, 46-48, 50-56, 58-60, 62-80, 82, 84, 86-
88, 90, 92, 94, 96, 98, 100-104, 106, 108, 110-114, 116, 118,
120, 122, 124, 126, 128, 130, 132, 134, 136, 138, 140-142
backbone, 52, 55, 60, 74
-based electrode, 13
chain, 51-53, 58, 84
matrix, 56, 73, 77, 87, 111, 113
nanocomposite, 73
Polymeric, 46, 64-65, 75, 96
Polymerisation, 29, 51, 66-69, 76, 79, 81-84, 89-91, 97-99,
110-111, 115-116, 120, 124, 126, 131-132
Polymerise, 98, 124
- Polypropylene, 6
- Polypyrrole (Ppy), 6, 13, 44, 53, 57-58, 65, 76-79, 91-93, 97-101,
109-114, 130-132
- Polytetrafluoroethylene, 76, 127
- Polythiophene (PTH), 6, 53, 55, 57-58, 65, 76-78,
- Polyvinylidene fluoride, 76
- Pore, 11, 16, 115
size, 11
- Porosity, 5-6, 11, 15
Porous, 2, 6, 24, 67-68, 99, 130
- Positioning, 20
- Positive and negative, 1-2
- Positive charge, 34, 53
- Potassium dichromate, 76, 84
- Potassium hydroxide (KOH), 11, 88, 121-122, 124, 130
- Potassium permanganate, 76, 110-113
- Potentiometer, 30-31
- Potentiostat circuit, 37
- Powder, 82, 98, 112

Conducting Polymer Nanocomposites for Supercapacitors

- Power, 1-2, 4-8, 11-12, 14-20, 22-23, 25-27, 31, 39, 45, 47-48, 77, 79, 82-83, 92, 102, 104-106, 118, 125, 137-140
 - charger, 23
 - density(ies), 1, 4-8, 11-12, 14, 16, 20, 25, 39, 77, 79, 118, 125
 - factor, 6
 - source, 17-18, 20
 - supply, 18, 31
- PowerBurst®, 25
- Precipitate, 43, 81-83, 95, 111, 124, 132
 - Precipitated, 111
- Precursor, 82, 88, 94
- Procedure, 16, 120, 126
- Process, 32-33, 42, 46, 52, 61, 64-65, 67, 82-83, 90, 92, 94, 98, 109, 111, 129, 132
 - Processability, 51, 64, 75, 87
 - Processing, 64-65
- Product, 3, 16-17, 45, 51, 81, 115
 - Production, 16-17, 67, 119
- Propylene, 99
 - carbonate (PC), 99-100
- Proton, 110
 - Protonated, 59
 - Protonation, 59, 66
 - Protonic acid, 55, 60
 - Protonic doping, 59
- Prototype, 21-22
- Pseudocapacitor, 14
- Pulse, 17
 - power, 17
- Purified, 91, 123
- Pyrolysis, 95, 119
- Pyrrole, 57, 91, 99, 110-112, 131-136

Q

- Quality, 45, 52, 88
 - assurance, 45
- Quinoid section, 58

Quinone, 59, 90

R

Radio frequency, 2, 19

antenna, 19

Ragone plot, 6-7

Rail, 18, 22-23

Reactor, 94-95

Recharge, 15, 17, 23-24, 46

time, 17

Rechargeable, 8, 18-19

batteries, 8, 18

Recharged, 18, 23

Recharging, 14, 22-24

Rectifier circuit, 19

Recyclability, 16

Redox, 8, 16, 32-33, 35, 41-43, 46, 52-53, 55, 64, 77-79, 84, 89-90, 92, 99-100, 109, 112-113, 118-119, 121-122, 124-125, 127, 132-133, 136

couple, 32, 41-42

peak, 99

process, 32, 109

reaction, 32-33, 35, 92, 122

system, 89

Reduction, 12, 23, 32-34, 36, 41-44, 58-59, 62, 84, 87-89, 91-92, 119, 125, 127, 132

peak, 41

Reference electrode, 29-31, 35-38, 41-42, 92

Reoxidation, 91

Reprotonation, 91

Research, 12-14, 16, 44, 48, 53, 64-66, 70, 78, 94, 101, 103, 105, 118, 139, 141

Resonance, 58-59

Room temperature (RT), 53, 82, 91, 94, 132

Rutenium oxide, 6

Ruthenium(IV) oxide, 77-78, 109, 118

S

- Safety, 8
- Saturated, 120
- Scan cycle, 42
- Scan rate, 38-41, 89, 92-93, 99-100, 113, 116-117, 122, 127-130, 133-134
- Scanning electron microscopy, 132
- Second electrode, 8, 29, 43
- Self-discharging, 15
- Sensor, 36, 77
- Separator, 2, 5-6, 10
- Shelf-life, 5
- Shrinkage, 78, 113, 130
- Siemens, 22
- Silver, 35, 38, 77, 84, 89, 112
 - chloride, 35, 38, 84, 89, 112
- Single-walled carbon nanotube(s) (SWCNT), 95-97, 130
- Slide-wire resistor, 30-31
- Sodium dodecyl sulfate (SDS), 77, 111-112
- Sodium hydroxide, 82, 124
- Solar batteries, 60
- Solar-cell, 20
- Solar smoothing, 20
- Solid state, 26, 104
- Solubility, 43, 65, 87
- Solution, 10, 30-35, 40, 42-44, 46, 67, 69-70, 80-84, 88, 91, 98-100, 110-112, 115-116, 120-121, 124, 127, 132-133, 136
- Solvent, 29, 36, 42-43, 88, 98, 127
- Sonication, 112
- Specific capacitance(s) (SC), 12, 2, 38-39, 44-45, 78, 84, 86, 91, 97-100, 109-110, 113, 116, 18-121, 123, 125, 127, 129-130, 134
- Specific power, 7-8
- Specific surface, 97
- Spectra, 46, 135
- Spectroscopic, 53, 78

- Spectroscopy, 38, 44, 121
- Speed, 11, 23, 132
- Spin-coating, 90
- Spray deposition, 119
- Stabilisation, 21
 - Stabilise, 18-19
 - Stabiliser, 19
 - Stability, 11-14, 16, 36, 39, 43, 65, 76-78, 80, 91, 97-98, 100, 110, 112-113, 115, 123, 130
- Stacking, 66, 68, 99-100, 121
- Stainless steel (SS), 44, 77, 82, 124, 131
- Standard calomel electrode (SCE), 35, 90
- Stirring, 33, 35, 43, 80-84, 98, 111-112, 115, 120, 124, 132-133
- Stoichiometry, 44
- Stop-and-go power, 15
- Storage, 1-2, 5-6, 9-10, 12-13, 16, 19-20, 22, 24, 56, 77, 99, 109, 113, 128
 - capacity, 2, 99
- Substrate, 10, 69, 91, 95-96, 116, 127
- Sulfation, 20
- Sulfuric acid, 11, 20, 84, 90, 99, 126
 - electrolyte, 20
- Supercapacitor, 1-2, 5-6, 8, 12, 14-15, 17, 19-22, 24, 38-39, 78, 82, 86, 97-98, 109, 115-116, 118-119, 121, 126, 132, 135
- Surface, 2-5, 7, 10-13, 24, 33-35, 41, 43, 67, 69-70, 78, 86, 94-95, 97, 99-100, 102, 104, 109, 113, 115-116, 121, 134
 - area, 2-3, 5, 10-12, 24, 43, 94, 97, 99, 109, 113, 115-116, 134
- Surfactant, 69-70
- Sustainable, 1, 141
- Symmetric, 8, 18, 92, 112, 118, 122
 - Symmetry, 122
- Synergistic, 38, 78, 109, 116, 123, 129
- Synthesis, 66-69, 72, 76, 79-81, 89, 110, 130-133
- Synthetic, 47-48, 51, 65, 70-71, 101-102, 104, 110, 119, 131, 140-141
- SYTRAL, 23

T

- Tantalum, 77
- Tecate Group, 25
- Teflon™, 36, 82, 124
- Temperature, 25, 33, 53, 61-63, 80, 82, 94-96, 132
- Thames Cable Car™, 24
- Thermal conductivity, 73, 75, 94
- Thermal properties, 131
- Thermal reduction, 91
- Thermal stability, 80, 115
- Thermodynamic, 42
 - Thermodynamically, 32, 56, 69
- Thermoplastic, 51
- Thermosetting, 51
- Three-dimensional (3D), 13, 51, 63, 68, 111, 115-116
- Tin chloride, 82
- Tin oxide, 44, 77, 81-83, 91
- Tip-growth model, 95
- Titanium, 6, 14, 44, 77, 109, 115-116, 131
 - dioxide, 6, 109, 115-116, 131
- Tohyco-Rider™, 23
- Train, 21-22
- Tram, 22-23
- Transmission, 21, 46
- Transportation, 21, 23
- Tribrid™, 24
- Two-dimensional (2D), 87

U

- UltraBattery, 19-20
- Ultracapbus™, 23
- Ultracap™, 23
- Ultrasonic, 124
 - Ultrasonicated, 98
 - Ultrasonication, 80, 91, 98, 115, 133
- Undoped, 53-54

Uninterruptible power supply(ies) (UPS), 1, 19
University of Glamorgan, 24

V

Vacuum, 82, 111, 115, 124, 127
 oven, 124, 127
van der Waals, 68
Vanadium(V) oxide, 77
Vapour, 87, 94-95
Variable range hopping (VRH), 62-63
Vibration, 23, 124
Volatile, 94
Voltage, 1-6, 9-12, 16, 19, 21, 25, 37, 39-40, 99, 112, 119, 128-129, 132, 134-135
Voltammetry, 31, 35, 38-40, 59, 84, 112
Voltammogram, 33, 40, 84, 99

W

Water, 81-84, 88, 91, 111, 115, 120, 124, 127, 132
 bath, 115, 120, 124
Wind, 19-20
 smoothing, 20
Wood, 75
Working electrode, 29-31, 33, 35-37, 40-43, 112

Y

Yield, 45, 59
 Yielding, 64

Z

Zero-dimensional (0D), 79
Zhuzhou Electric Locomotive Corporation, 22
Zinc oxide, 77, 82-83

π -conjugation of the polymer, 52
 π -system, 54, 56, 58

Conducting Polymer Nanocomposites for Supercapacitors



Published by Smithers Rapra Technology Ltd, 2015

Supercapacitors have attracted considerable attention owing to their high power density, long cycle-life, short charging time, and safe operation for promising applications to overcome limited supplies of energy and environmental problems. Supercapacitors are designed to bridge the gap between batteries and capacitors, and to form fast-charging energy-storage devices for intermediate, specific energy. The supercapacitor is an important device in energy-storage and energy-conversion systems, and is used in electric vehicles, uninterruptible power supplies, as well as memory protection for computer electronics and mobile phones.

This book aids understanding of the basic technology and nanostructure of conducting polymers and their composites, which are emerging as novel fields of research and development for 'smart' materials (especially supercapacitors).

Concepts of supercapacitors are explained clearly and concisely. This book is oriented around chemical engineering, so professionals involved in polymer science may find this book suitable for their advanced and applied field of research. This book will provide such professionals the opportunity to learn about conducting polymers and nanocomposites, as well as their production and processing technology for supercapacitors. Attention is focused mainly on the preparation of conducting polymer-based binary and ternary nanocomposites and their electrochemical performances for supercapacitor application. Nevertheless, this book will be a valuable reference for scientists, engineers, and students interested in the investigation and exploitation of a fascinating new class of conducting polymer nanocomposites.



Shawbury, Shrewsbury, Shropshire, SY4 4NR, UK
Telephone: +44 (0)1939 250383
Fax: +44 (0)1939 251118
Web: www.polymer-books.com